Universidade do Minho
Escola de Medicina

Ruth Victoria Esho

Novel Phenotypic features of the malaria parasite through time-domain Nuclear Magnetic Resonance

Outubro de 2022

Novel phenotypic features of the malaria parasite through time-domain Nuclear Magnetic Resonance

Ruth Victoria Esho

UMinho | 2022

Universidade do Minho
Escola de Medicina

Ruth Victoria Esho

Novel Phenotypic features of the malaria parasite through time-domain Nuclear Magnetic Resonance

Dissertação de Mestrado
Mestrado em Ciências da Saúde

Trabalho efetuado sob a orientação de
Doutora Maria Isabel Mendes Veiga

e de

Doutor Weng Kung Peng

Outubro de 2022

ACKNOWLEDGEMENTS

In the first place, I would like to thank God, for his help and guidance through each step of this master's program. His love and ever abiding presence have contributed to who I am today. I am thankful to him for bringing wonderful people to my path. My friends at the residence, Ronisio, Patricia, Shayanne and Adelino, were there through thick and thin, and I am grateful for your love. My appreciation goes to the wonderful people at ICVS who I worked with. Vitoria, a teacher, turned colleague and then friend. I am thankful for your support through different phases of this master's program. To Isabel, my supervisor, I would like to give my appreciation for your supportive care and corrections through my masters. Thanks to Peng, my co-supervisor, for your timely insights and innovative tutoring.

Finally, I would like to thank my family, Joshua Esho, Elizabeth Esho, Deborah Esho, Esther Esho, Andronicus Akinyelu, Samuel Esho, and Mary Esho, for their calls, prayers, and wise counsel at one point or the other in this journey. Words cannot express how I feel about you guys. Thanks once again.

FINANCIAL SUPPORT

The work presented in this dissertation was performed at the Life and Health Sciences Research Institute (ICVS), Minho University. This work has been funded by ICVS Scientific Microscopy Platform, member of the national infrastructure PPBI - Portuguese Platform of Bioimaging (PPBI-POCI-01-0145-FEDER-022122; by National funds, through the Foundation for Science and Technology (FCT) - project UIDB/50026/2020 and UIDP/50026/2020 and by a Research Grant 2021 of the European Society of Clinical Microbiology and Infectious Diseases (ESCMID) to MIV.

STATEMENT OF INTEGRITY

I hereby declare having conducted this academic work with integrity. I confirm that I have not used plagiarism or any form of excessive use of information or falsification of results along the process leading to its elaboration.

I further declare that I have fully acknowledged the Code of Ethical Conduct of the University of Minho.

RESUMO

As infeções de malária continuam a ser um flagelo em regiões endémicas de todo o mundo, atrasando o crescimento económico e reduzindo a esperança de vida das crianças. O caminho para o controlo e eliminação da malária tem sido dificultado pela resistência aos medicamentos e ferramentas de diagnóstico ineficazes para detetar infeções de baixa densidade e assintomáticas. Com a carteira limitada de medicamentos disponíveis para tratar a malária, é fundamental melhorar a compreensão dos mecanismos de resistência e avaliar a biologia e patogénese das células parasitárias. Nesta dissertação, visamos explorar a tecnologia espectroscópica de Ressonância Magnética Nuclear de baixo campo (RMN), juntamente com abordagens genéticas inversas para estudar a *haemozoin*, um biomarcador natural de parasitas da malária com propriedades magnéticas únicas e cuja via biológica para a sua formação, está de alguma forma relacionada com a maioria dos medicamentos antimaláricos conhecidos.

Caracterizámos o parasita em diferentes fases morfológicas utilizando a RMN de baixo campo para definir as interações paramagnéticas e a dinâmica de troca de estirpes resistentes a parasitas. A partir destas medições, caracterizámos com sucesso todo o ciclo intra eritrócito do parasita *Plasmodium falciparum*, ligando alguns padrões de RMN de domínio temporal a alterações fisiológicas específicas, tais como os parasitas específicos de ponto temporal que se deslocam para uma nova fase de desenvolvimento. Para explorar a capacidade de detetar características distintas de RMN relacionadados com perturbações na via de desintoxicação da hemoglobina, concentrámo-nos no estudo do *Pf*MDR2, um transportador de metais pesados e nas plasmepsinas, protéases aspárticas que degradam a hemoglobina dentro do vacúolo alimentar do parasita. Concebemos uma estratégia para o KO *pf*mdr2 na estirpe *P. falciparum* Dd2 e realizámos um ensaio de fracionamento da hemoglobina em parasitas geneticamente modificados, sobre expressores de plasmepsinas.

Os dados de RMN de baixo campo obtidas a partir deste estudo foram capazes de distinguir as fases de parasitas e parasitemia tão baixo quanto 0,01% e revelaram um elevado potencial para explorar ainda mais o equilíbrio magnético entre espécies de hemorragia e a sua possível correlação com a suscetibilidade dos parasitas aos fármacos. São necessários estudos futuros para explorar melhor o papel deste transportador e das enzimas no equilíbrio das espécies de hemorragia e a sua capacidade de fornecer impressões digitais fenotípicas distintas de NMR. Dadas as características de portabilidade de um dispositivo de RMN de baixo campo, a captura de dados específicos de RMN poderia fornecer um protótipo para a potencial distribuição de medicamentos com precisão contra a malária no futuro, aos pacientes.

Palavras-chave: malária, Ressonância Magnética Nuclear, PfMDR2, hemozoína, plasmepsina.

ABSTRACT

Malaria infections remain a scourge in endemic regions worldwide, stalling economic growth and reducing life expectancy in children. The path towards malaria control and elimination has been hindered by drug resistance and ineffective diagnostic tools to detect low density and asymptomatic infections. With the limited portfolio of drugs available to treat malaria, it is fundamental to improve the understanding of resistance mechanisms and appraise parasite cell biology and pathogenesis. In this dissertation, we aimed to exploit low-field Nuclear Magnetic Resonance (NMR) spectroscopic technology, along with reverse genetics approaches to study hemozoin, a natural malaria parasite biomarker with unique magnetic properties and which biological pathway to its formation, is somehow related with most of the known antimalarial drugs.

We have characterized the parasite at different morphological stages using low-field NMR in order to define the paramagnetic interactions and the exchange dynamics of parasite-resistant strains. From these measurements, we successfully characterized the entire intraerythrocytic cycle of the *Plasmodium falciparum* parasite linking some behavioral time-domain NMR patterns to specific physiological changes such as the specific time-point parasites move to a new stage development. To explore the capability of detecting distinct NMR features related with disturbance in haem detoxification pathway, we focused on the study of *Pf*MDR2, a heavy metal transporter and on plasmepsins, aspartic proteases that degrade haemoglobin inside the parasite food vacuole. We designed a strategy to KO *pf*mdr2 into *P. falciparum* Dd2 strain and performed a haem fractionation assay on previously genetic engineered parasites over-expressing plasmepsins.

The low-field NMR fingerprints obtained from this study was capable to distinguish parasite stage and parasitaemia as low as 0.01% and revealed high potential to further exploit the magnetic balance between haem species and its possible correlation with parasite susceptibility to drugs. Future studies are needed to explore better the role of this transporter and enzymes in the balance of the haem species and their ability to deliver distinct phenotypic NMR fingerprints. Given the portability characteristics of a low-field NMR device, the capture of specific NMR fingerprint could provide a proof-of-concept towards potential delivery of future precision malaria medicine, at the patients side.

Keywords: Malaria, Nuclear Magnetic Resonance, *Pf*MDR2, haemozoin, plasmepsin.

TABLE OF CONTENTS

RESUMO v

ABSTRACT vi

LIST OF ABBREVIATIONS ix

LIST OF FIGURES xi

TABLE OF CONTENTS xiv

CHAPTER 1 1

INTRODUCTION 1

1.1 Malaria Epidemiology 2

1.2 Malaria Infection and Parasite biology 2

1.3 Parasite Life Cycle 3

1.3.1 Human Host 3

1.3.2 Hepatic stage 4

1.3.3 Intra-erythrocytic stage 4

1.3.4 Insect Vector 5

1.3.5 Clinical Manifestations of Malaria 5

1.4 Parasite Haemoglobin Metabolic Pathway 6

1.4.1 Haemoglobin 6

1.4.2 Haem 6

1.4.3 Hemozoin biocrystallization 7

1.5 Antimalarial Drug Treatment 9

1.5.1 Artemisinin and its derivatives 9

1.5.2 Quinolines 10

1.5.3 Antimalarial Drug resistance 12

1.6 Antimalarial Drug Mediating Transporters 14

1.6.1 *P. falciparum* MDR2 15

1.7 Current Tools for Malaria Diagnosis 16

1.7.1 Properties of Haemozoin that Makes It an Attractive Target for Malaria Diagnosis 17

1.7.2 Principle of the Nuclear Magnetic Resonance 19

1.7.3 Deep phenotyping using low-field NMR 21

CHAPTER 2 23

CHAPTER 3 25

3.1 Study 1: Time-domain NMR characterization of wild type parasites 26

3.1.1 *P. falciparum* culture 26
3.1.2 Synchronization of *P. falciparum* culture 26
3.1.3 *P. falciparum* growth analysis 27
3.1.4 Dilution of *P. falciparum* culture 28
3.1.5 *P. falciparum* sample preparation for time-domain NMR detection 28
3.1.6 NMR measurement 29
3.1.7 NMR phenotypic assay 29
3.1.8 Statistical Analysis 30
3.2 Study 2: Phenotypic features of the *P. falciparum* MDR2 transporter 30
3.2.1 Genomic DNA Isolation 31
3.2.2 Genotyping *of P. falciparum Pf*MDR2 KO parasites 32
3.2.3 Construction of *Pf*MDR2 KO parasites 33
3.2.4 *P. falciparum* transfection 34
3.2.5 *P. falciparum* selection 35
3.2.6 Drug susceptibility assays 35
3.3 Study 3: Phenotypic features of the *P. falciparum* plasmepsins 36
3.3.1 Haem Fractionation Assay 36
CHAPTER 4 38
4.1 Phenotyping infected red blood cells through relaxometry spectroscopy 39
4.2 Time-domain iRBC characterization of slack synchronized parasites 39
4.3 Time-domain iRBC characterization of tight synchronized parasites 44
4.3.1 Early intra-erythrocytic stage 45
4.3.2 Later intra-erythrocytic stages 45
CHAPTER 5 56
5.1 Phenotyping infected red blood cells through relaxometry spectroscopy 57
5.2 Understanding the role *Pf*MDR2 in the physiology of *P. falciparum* parasites 61
5.3 Plasmepsins impact into the balance of the haem species 61
CHAPTER 6 64
CHAPTER 7 67

LIST OF ABBREVIATIONS

ABC	ATP-binding cassette
ACT	Artemisinin-based combination therapy
AQ	Amodiaquine
ART	Artemisinin
bp	Base pair
CPMG	Carr-Purcell-Meiboom-Gill
CQ	Chloroquine
DHA	Dihydroartemisinin
DHA-PPQ	Dihydroartemisinin-piperaquine
DNA	Deoxyribonucleic acid
DV	Digestive vacuole
gDNA	Genomic DNA
GFP	Green fluorescent protein
hDHFR	Human dihydrofolate reductase
HF	Halofantrine
HZ	Hemozoin
IC_{50}	Half-maximal inhibitory concentration
IDC	Intra-erythrocytic development cycle
INL	International Iberian Institute of Nanotechnology
iRBCs	Infected red blood cells
ITNs	Insecticide-treated mosquito nets
kDa	Kilodalton
K13	Kelch 13
KO	Knockout
LB	Lysogeny-broth
LUM	Lumefantrine
MCM	Malaria culture medium
MQ	Mefloquine

MRP	Multidrug resistance protein
MRR	Magnetic resonance relaxometry
NBD	Nucleotide binding domain
NMR	Nuclear magnetic resonance
PBS	Phosphate-buffered saline
PCR	Polymerase chain reaction
pDNA	Plasmid DNA
PfCRT	*P. falciparum* chloroquine resistance transporter
Pfhap	*P. falciparum histoaspartic proteases*
PfMDR1	*P. falciparum* multidrug resistance protein 1
PfMDR2	*P. falciparum* multidrug resistance transporter 2
PfMRP1	*P. falciparum* multidrug resistance-associated protein 1
PfPM2	*P. falciparum* plasmepsin 2
PfPM3-1	*P. falciparum* plasmepsin 3-1
PMQ	Primaquine
POC	Point of care
PPQ	Piperaquine
QN	Quinine
R_1	Longitudinal water relaxation rate constant
R_2	Transverse water relaxation rate constant
rpm	Rotations per minute
RBCs	Red blood cells
RDT	Rapid diagnostic test
RNA	Ribonucleic acid
SDS	Sodium dodecyl sulphate
SLI	Selection linked integrase
T_1	Longitudinal relaxation time
T_2	Transverse relaxation time
TAE	Tri-acetate EDTA (Ethylenediaminetetraacetic acid)

WHO	World Health Organization
WT	Wild type

LIST OF FIGURES

Figure 1: Malaria endemicity in 2000 and 2021. Adapted from world malaria report, WHO 2021 [1]. 3

Figure 2: Schematic diagram representing the life cycle of the malaria parasite across human and mosquito hosts. Adapted from Baptista et al. [26]..... 4

Figure 3: Chemical structure of HZ showing iron attached to four nitrogen atoms. Adapted from Carney et al. [57]. 7

Figure 4: A reconstructed tomographic section of HZ crystals lying side by side at the inner membrane wall of the digestive vacuole of an early stage trophozoite. © 2021 The Authors. ChemMedChem published by Wiley-VCH GmbH (Adapted from Kapishnikov et al.) [53]. 9

Figure 5: Schematic diagram of the chemical structure of DHA and PPQ tetraphosphate. 12

Figure 6: Schematic demonstration of the photoacoustic method for malaria detection. The technique adopts an incident laser, photodetectors for recognition of the optical spectra and an ultrasound transducer that identifies waves generated by the high temperature in the sample. The image is not to scale. Adapted from Vitoria et al. [115]. 18

Figure 7: Schematic diagram demonstrating ions in their equilibrium state and highly aligned ions when excited by a magnetic field. Created with BioRender.com. 20

Figure 8: Bench-top setup NMR system, with a PCB (printed circuit board) probe, a micro coil for sample detection. Capillaries are placed into the coil with the end containing concentrated iRBCs. Adapted from Peng et al. INL laboratory protocol, NMR setup with a capillary tube containing concentrated blood at one end. 27

Figure 9: Schematic diagram of sample preparation and NMR measurement process. (A) Slack synchronized cultures of rings, different parasitaemia (e.g., 1% as shown above) collected into three capillaries on different occasions. (B) Tight synchronized cultures of rings collected into nine capillaries, three capillaries for each diluent Created by Biorender. 30

Figure 10: PCR strategy of primers used for verifying mutant and WT parasites. 32

Figure 11: Gene editing strategy used in the construction of PfMDR2 mutant parasites. pSLI-TGD containing pfmdr2 gene (which is the homologous sequence) was constructed and inserted into the parasite genome along with a green fluorescence protein (GFP) FP, a skip peptide (2A) and Neomycin-R (which confers resistance to G418). The resistant marker – hDHFR incorporated into mutated parasites were selected with WR99210.Adapted from Addgene, Created with BioRender.com. 35

Figure 12: Schematic diagram representing sample preparation and characterization of rings collected in three capillaries. The three capillaries were read at time points T0 to T12 corresponding to 0h to 12h,respectively. This procedure was performed for rings at 0.01%, 0.1%, and 1% and for trophs and schizonts as well. Created by BioRender.com..... 39

Figure 13: Time tracking T_1, T_2, and A-ratio readings of asynchronous rings across varying parasite concentration (0.01, 0.1, 1 %). **** (P < 0.0001), ** (P < 0.05), bars with no astericks represent non-significant P values. ... 40

Figure 14: Image of Time tracking T_1-T_2 and A-ratio measurements of asynchronized Trophozoite stages across 0.01,0.1 and 1 % parasitemia. **** ((P > 0.0001), bars with no asterick represent non-significance). 41

Figure 15: Time tracking T_1, T_2 and A-ratio readings of asynchronous schizonts stages at 0.01 and 1% parasite concentration. **** (P < 0.0001), * (P < 0.05). 42

Figure 16: A-ratio values showing the behavioral pattern of the intra-erythrocytic stage at 1% parasitemia. **** (P < 0.0001), ** (P < 0.005). 43

Figure 17: Reflects the progression of the intra-erythrocytic cycle over time. Starting from A-ratio readings of iRBCs at ring stage to schizonts and back to early rings. 44

Figure 18: Rings across parasitemia (0.01, 0.1, 1 %) showing (a) Transverse and (b) Longitudinal relaxation time and (c) A-ratio Synchronized cultures. * (P < 0.05), ** (P < 0.005), bars with no asterick represents non-significant P value). 46

Figure 19: Image of T_1-T_2 and A-ratio measurements of Trophozoite stages across 0.01,0.1 and 1 % parasitemia. * (P < 0.05), bars with no asterick represents with non-significant P value. 47

Figure 20: T_1, T_2, and A-ratio readings of Schizonts across different parasitemia (0.01, 0.1, and 1 %). * (P < 0.05), bars with no asterick represents with non-significant P value. 48

Figure 21: T_1, T_2 and A-ratio readings across P.falciparum intra-erythrocytic stages at 0.01% parasitemia.*** (P < 0.0005), ** (P < 0.005), bars with no asterick represents with non-significant P value..... 49

Figure 22: T_1, T_2 and A-ratio readings across P.falciparum intra-erythrocytic stages at 0.1% parasitemia. *** (P < 0.0005), bars with no asterick represents with non-significant P value..... 50

Figure 23: T_1, T_2 and A-ratio readings across P.falciparum intra-erythrocytic stages at 1% parasitemia. Bars with no asterick represents with non-significant P value..... 51

Figure 24: Graphical representation of in vitro IC50 assays carried out on pfmdr2 KO parasites. Mean±SEM IC50 values are represented for chloroquine, dihydroartemisinin, piperaquine, pyrimethamine, pyronaridine, desethylamodiaquine, mefloquine, lumefantrine. At least three assays were performed for each drug. 53

Figure 25: PCR results for confirmation of pfmdr2 KO. Gel electrophoresis results indicating no amplification of the 5' nor 3' reactions at the constructed Dd2 pfmdr2 KO line, while a correct band was observed for the WT reaction and in the edited line in another gene and in the negative controls for integration. 54

Figure 26: Graphical Analysis of Haem fractionation assay showing ratio of haemoglobin, free haem and HZ between different parasite lines at 32 hours. 55

LIST OF TABLES

Table 1: Primer sequence and PCR strategy for mutant and WT parasites confirmation...... 33

Table 2: Reaction condition used in the confirmation PCR. 33

CHAPTER 1

INTRODUCTION

1.1 Malaria Epidemiology

Malaria is an infectious disease predominant in tropical and subtropical regions worldwide (Figure 1). In 2020, an estimated 241 million new clinical cases were recorded by the World Health Organization (WHO), in association with 627,000 deaths [1). Most fatal cases reported were among children aged five and below. The burden of malaria rests in the African region by 95% due to the tropical climate and poverty prevalent in this region [1]. These underlying conditions provide optimal breeding conditions for the parasite vector that spreads the disease from person to person.

In the last two decades, however, there has been a decline in new cases (238 million in 2000 to 229 million in 2019), and a 56% decrease in mortality [2]. The three key players that have helped in surmounting these milestones are insecticide-treated mosquito nets (ITNs), rapid diagnostic test (RDT) strips, and artemisinin combination therapies (ACTs) [3–7]. Studies performed over the years showed that the effective use of ITNs has helped reduce new malaria infections by 41% [3]. Furthermore, the introduction of RDTs facilitated the massive diagnosis of malaria infections in endemic regions because they were favourable, and user-friendly for point of care (POC) testing [6]. However, in the last two years, a 12% increase in malaria deaths has been documented due to the disruption of malaria control interventions during the COVID-19 pandemic [1]. Resistance to ACTs has been reported in some parts of Asia and rising cases of partial resistance have been recently observed in the WHO African region [8–10]. These problems have impaired malarial control and elimination interventions in the endemic regions. In 2019 alone, an estimate of US$3.0 billion went into funding these interventions [1]. The impact of this disease has not only affected the quality of living in these countries but has played a significant role in stalling the health sector and economic growth of these countries. This is due to reoccurring cases, frequent doctor visits, and absenteeism from school and the place of work. To address these problems, there is an urgent need for effective malaria control mediation at all levels [11–15].

1.2 Malaria Infection and Parasite biology

Malaria is caused by the protozoan parasite-*Plasmodium,* of the phylum Apicomplexa [16]. It thrives in warm tropical climates, predominantly transmitted by the female *Anopheles gambiae* mosquito [17]. The *Plasmodium* species, carried by a vector, infect many vertebrates from mammals, birds, amphibians, and humans [18]. It consists of six species that cause infection in humans. These are *Plasmodium falciparum*, *Plasmodium malariae*, *Plasmodium ovale,*

Plasmodium vivax, and the zoonotic *Plasmodium knowlesi* and *Plasmodium cynomolgi* [19–21]. *P. falciparum* is the most deadly and prevalent among these species [2].

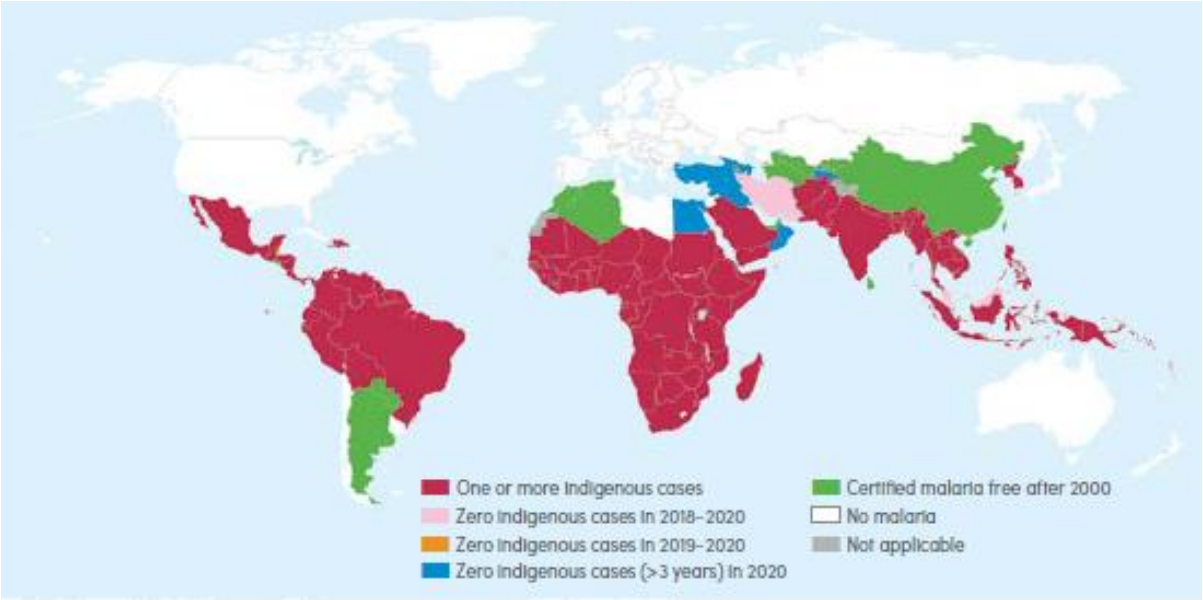

***Figure 1*:** Malaria endemicity in 2000 and 2021. Adapted from world malaria report, WHO 2021 [1].

1.3 Parasite Life Cycle

P. falciparum remains the highest contributor to the mortality rate of malaria and is the focus of this thesis. The malaria parasite life cycle consists of two interrelated phases (Figure 2). In the first phase, the parasite infects a human host during the hepatic and intra-erythrocytic stages. In the second phase, it is transmitted through a bite from the human host to an uninfected mosquito [18].

1.3.1 Human Host

The *P. falciparum* life cycle begins when parasites, in an elongated crescent shape form called sporozoites, are released from a mosquito during a blood meal and, enter the human dermis through vessels [22]. The sporozoites leave the dermis [23] and migrate quickly to the liver through vessels of the body [24,25].

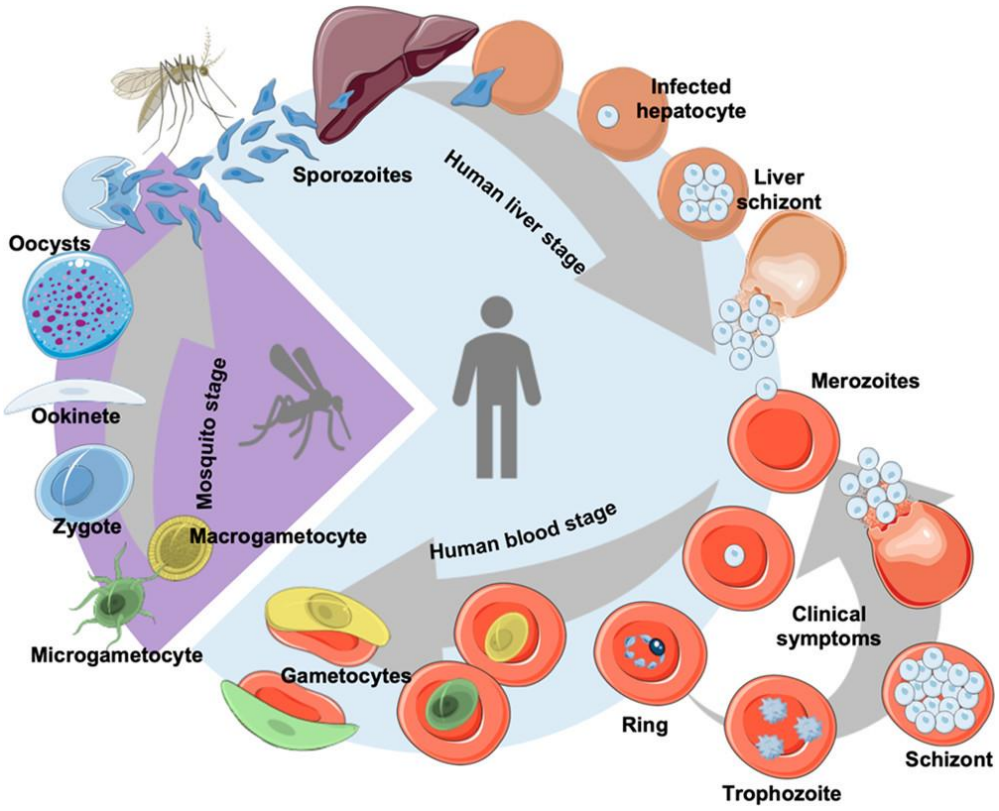

Figure 2: Schematic diagram representing the life cycle of the malaria parasite across human and mosquito hosts. Adapted from Baptista *et al.* [26].

1.3.2 Hepatic stage

In the liver, the sporozoites invade hepatocytes and multiply exponentially, in a replicative process known as schizogony [24]. Sporozoites mature to form schizonts containing thousands of merozoites. These merozoites multiply in the hepatocytes and are released back into the bloodstream [24,27].

1.3.3 Intra-erythrocytic stage

The merozoites invade red blood cells (RBCs) and multiply by asexual reproduction in the blood stream. A single merozoite invades an RBC and multiplies asexually by schizogony forming about 32 merozoites [28]. These newly formed merozoites each invade new-uninfected RBCs and differentiate into several morphological stages [29]. The first developmental stage is known as rings due to its ring-like structure. This early intra-erythrocytic stage persists for about 24 hours (*P. falciparum)* and develops to trophozoites [12-16 hours) and finally schizonts (8 hours), the most mature intra-erythrocytic stage in the *Plasmodium* species. Each intra-erythrocytic cycle takes about 48 hours [18]. Once a cycle is about to be completed, the mature schizont containing

merozoites enlarges, the RBC lyse, and a new cycle begins [28]. However, some merozoites released from the schizont do not undergo this asexual replication in erythrocytes, but rather differentiate into sexual erythrocytic forms, the gametocytes [29,30]. These gametocytes distinguish into males (microgamete) and females (macrogamete) [31].

1.3.4 Insect Vector

The gametocytes roaming in the vessel are picked up by an insect vector while taking a blood meal from an infected person. They move to the lumen of the vector's mid-gut, where the environment is optimal to activate males into microgametes and females into macrogametes [32,33]. The microgamete fertilizes the macrogamete to form a zygote. Meiosis occurs, and the zygote distinguishes into a motile form known as an ookinete [34]. The ookinete enters the wall of the mid-gut and comes out as an oocyst [35]. In the oocyst, a series of mitotic divisions occur to produce sporozoites (sporogony) [32,36,37]. The oocyst matures and ruptures, releasing the sporozoites into the haemolymph, where it passes to the salivary gland and gains the ability to infect [38]. These parasites complete their cycle in the insect vector and are prepared to infect a human host in 10-18 days.

The pregnant female *Anopheles* mosquito nourishes her eggs before hatching by ingesting blood [39]. When the mosquito bites an uninfected person, gametocytes are released through its proboscis and move into the bloodstream of the uninfected individual. Therefore, early diagnosis and treatment are paramount to prevent further transmission. This calls for effective diagnostic tools that can detect low-density infections and, distinguish the intra-erythrocytic morphological stages, on which lies the importance of this research.

1.3.5 Clinical Manifestations of Malaria

The manifestation of clinical signs and symptoms of malaria begins in the intra-erythrocytic stage. Mature schizonts form merozoites and cause RBC lysis, marking the onset of fever, a characteristic presenting sign of malaria infection [40]. This may also lead to other complications, such as severe malaria and anaemia, especially in children due to the rupture of lots of RBCs [41]. Other symptoms are chills, headache, and vomiting, which are characteristic symptoms of other febrile infections. Therefore, it is important to utilize effective diagnostic tools to detect and treat malaria infection even at low densities and in asymptomatic patients, as this represents a reservoir of parasites capable to progress with the disease transmission.

1.4 Parasite Haemoglobin Metabolic Pathway

In the blood stage of infection, the parasite invades RBCs and feeds on haemoglobin as the source of amino acids. As the parasite degrades haemoglobin, a toxic by-product is generated known as haem. For the parasites to survive beyond a 48-hour intra-erythrocytic life cycle it detoxifies haem by converting it to an inert crystal-haemozoin (HZ) [42,43].

1.4.1 Haemoglobin

The major component of the RBC is haemoglobin and comprises about 95% of the RBC cytosolic protein [43]. In the intra-erythrocytic stage of infection, about 80% of the host's cytoplasm is consumed. In this process, 75% of haemoglobin is absorbed through the cytostome and transferred to the digestive vacuole (DV) [43]. Few amounts of haemoglobin are consumed in the ring stage in comparison to later stages where more metabolic activities are carried out [43].

Haemoglobin degradation occurs inside the DV of the malaria parasite. The DV has an acidic environment with an estimated pH of 5.0 to 5.4. It is maintained by a proton gradient activated by an ATPase pump [44,45]. The malaria parasite not only degrades haemoglobin as the source of amino acids, but also frees up space to grow inside the RBC [43]. As the parasite matures in the RBC, the cell becomes more permeable to lysis [46]. Therefore, the parasite degrades and absorbs haemoglobin in a process called colloid osmosis to prevent early lysis of RBC that may take place with an increase in cell volume [47,48].

The enzymes involved in the haemoglobin degradation pathway consist of four aspartic proteases (plasmepsin I-IV) and a cysteine protease (falcipain) contained in the DV of *P. falciparum* [49]. In the ring stage, only plasmepsin I is expressed and persists in other stages of the parasite. Plasmepsin II (PM2) is majorly expressed in trophozoites, the most metabolically active stage and in which most of the host cytoplasm is consumed [50,51]. Falcipain is the last enzyme involved in haemoglobin degradation and only further cleaves haemoglobin after it has been denatured by the plasmepsins [52].

1.4.2 Haem

After haemoglobin is enzymatically cleaved to smaller peptides it releases free haem (Fe^{III}-protophyrin IX) [53]. Free haem is a toxic by-product because it is produced from the oxidation of Fe (II) protorphyrin IX (Fe^{II}PPIX) to Fe (III) protoporphyrin IX (Fe^{III}PPIX). This change in redox state constitutes oxidative stress to the parasite environment. This is due to the reactive nature of iron

and the presence of unpaired electrons which combine with oxygen to form reactive oxygen species. Since malaria parasites do not have the enzyme (haem oxygenase) responsible for degrading haem monomers, it detoxifies haem by converting it to an inert crystal known as HZ [43]. Thus, the HZ crystallization process is crucial for the parasite's survival as it is its defensive mechanism against haem toxicity [54].

1.4.3 Hemozoin biocrystallization

Biocrystallization can be defined as the formation of crystals from molecular weight organic materials by living organisms [55]. The first stage in HZ formation is removing water from aqua-ferriprotoporphyrin IX [56]. This occurs when the parasites oxidize Fe^{II} PPIX to Fe^{III} PPIX in the DV. Fe^{III} PPIX units combine (dimerization) and sequester into insoluble micro-crystallites known as HZ. As the parasite matures, there is an increasing deposit of HZ crystals, whose unique structure consists of an iron atom attached by ionic bonds to four adjacent nitrogen atoms of porphyrin [55].

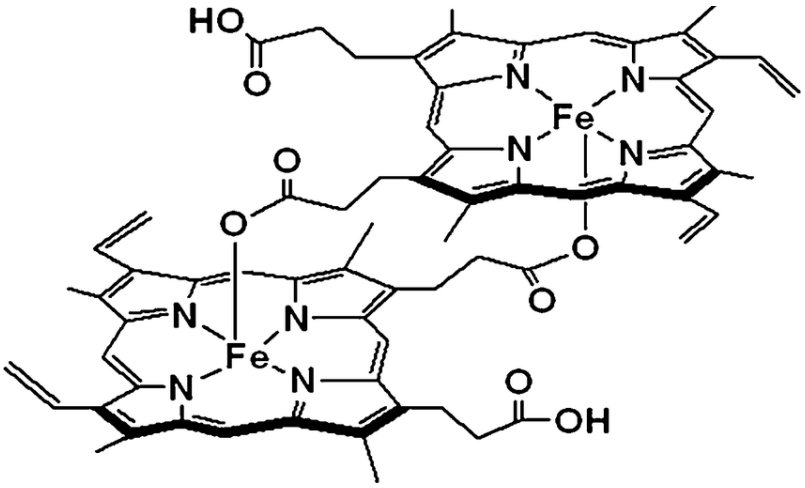

Figure 3: *Chemical structure of HZ showing iron attached to four nitrogen atoms.* Adapted from Carney *et al.* [57].

1.4.3.1 Haemozoin Crystal Structure and Properties

Several studies have been performed on the formation and crystallization of HZ to better understand the parasite's physiology and phenotypic behaviours inside the infected RBC (iRBC). In 1994, scientists Hempelmann and Marques discovered that the haem units present in the HZ crystal dimerize by hydrogen bonding to produce a dimer rather than a polymer, as earlier believed [58]. Further proof that alluded this claim is the geometrical structure of the HZ crystal which has been shown to display slanted end faces with similar angular geometry [42].

To study the parasite's HZ crystal (biogenic) scientists used its synthetic form known as β-hematin to gain insight into its structural composition. Using the X-ray powder diffraction method, β-hematin was found to be centrosymmetric. The surface structure of the different low index faces of the synthetic crystal showed that only its {100}, {010}, {011} faces were relatively flat/smooth. All other faces were uneven and thus unable to develop in a growing HZ crystal [53]. Looking into the growth structure of the HZ crystals the {100} and {010} side faces were seen to be dominant, whereas {011} was less developed and {001} face lesser developed than all others. This centrosymmetric isomeric hematin dimer property of β-hematin has close properties with biogenic HZ crystals which was experimentally confirmed by transmission electron microscopy images and a combination of electron diffraction patterns [42,59].

1.4.3.2 Nucleation of Haemozoin Crystals

The term nucleation also means the formation of HZ crystals in the parasite's DV [53]. Several theories have been propounded as to how HZ crystals are formed. These theories include HZ formation by an autocatalytic process catalysed by enzymes and/or lipids [60], its growth within neutral lipid bodies [61], or HZ nucleation at the membrane–aqueous interface of the digestive vacuole [62].

However, recent studies confirm that HZ nucleates at the inner membrane surface of the DV [53]. This was observed in reconstructed soft X-ray tomograms and electron microscopy images of iRBCs. These images revealed that HZ crystals in the early trophozoite stage lie side by side and near the inner membrane surface of the DV (Figure 4) on the side that takes up a more flattened surface ({100} face). In the trophozoite stage, the HZ crystal was also found to nucleate at different parts of the DV [63,64]. The assembly line of each HZ crystal is formed and grows as hematin dimers are supplied. This occurs simultaneously at different parts of the DV in the trophozoite stage, as earlier mentioned [53,64]. Next, HZ separates itself from the nucleating membrane and keeps growing in the lumen of the DV as the parasite matures [53].

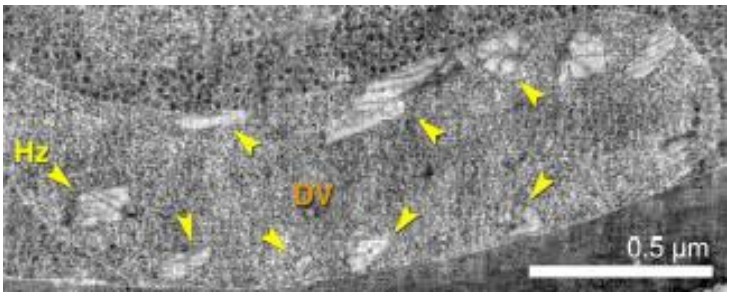

Figure 4: A reconstructed tomographic section of HZ crystals lying side by side at the inner membrane wall of the digestive vacuole of an early stage trophozoite. © 2021 The Authors. ChemMedChem published by Wiley-VCH GmbH (Adapted from Kapishnikov *et al.*) [53].

1.5 Antimalarial Drug Treatment

HZ formation pathway, besides being an essential process for parasite survival, is also the target of most antimalarial drugs. In fact, the inhibition of this pathway has been an effective target for antimalarial drugs, like those of the quinoline family. These drugs truncate dimerization of free haem, thereby hindering HZ formation and exposing the parasites to its toxicity [65–68]. Due to arising cases of drug resistant strains as a result of mutations, more research studies are being centred in understanding better the HZ formation process, since crystals do not undergo mutations.

The release of HZ following the lysis of erythrocytes is linked with the onset of chills and fever, thus several antimalarial drugs target the HZ formation process [69]. Given that the morphology of HZ crystals has been explained earlier, it is important to understand how antimalarials inhibit HZ crystallization within the parasite. Several studies suggest that quinolines amongst other antimalarials bind to haem monomers, as well as the faces of HZ [53,70,71].

Antimalarial drugs can be classified into several families based on their structure and mode of action. They consist of the aryl-amino alcohols (quinine (QN) and mefloquine (MQ)), 4-aminoquinolines (chloroquine (CQ)), endoperoxides (such as artemisinin (ART) and its derivatives), antifolates (pyrimethamine, proguanil, sulfadoxine), naphthoquinones (atovaquone) and 8-aminoquinolines (primaquine (PMQ), tafenoquine) [72]. The family of antimalarial drugs known to target the haem detoxification pathway are the quinolines-based drugs and endoperoxides.

1.5.1 Artemisinin and its derivatives

ART and its derivatives are sesquiterpene lactone compounds containing an endoperoxide bridge essential for drug action [73]. ARTs have a unique mechanism of action from other antimalarial drugs. They have a fast-acting mode of action and are effective in exploiting multiple

pathways to attack the parasite proteins [74]. When ART and its derivatives are ingested, they rapidly modify into DHA [75], which becomes 5-10 times more potent than ART [75]. In the blood, its endoperoxide bridge encounters Fe^{II} from haem produced from the digestion of the host's haemoglobin, and ART becomes activated.

When this occurs, the endoperoxide bond gets cleaved by Fe^{II} and prompts the release of free radicals. These free radicals attack the nucleophilic groups of the parasite's proteins and lipids, leading to cellular damage and finally parasite death. With *P. falciparum* infections, this mechanism of action occurs in the matured intra-erythrocytic stages (late rings, trophozoites, and early schizonts) prior to the formation of merozoites [76]. Recently, it has been suggested that ART might also act in a similar fashion as the quinoline drugs, by inhibiting the formation of HZ [77]. Due to ART short half-life (1 hour), it is administered as a combination therapy with other antimalarial drugs having a longer half-life [74,75].

1.5.2 Quinolines

In the 17th century, the bark of *Cinchona* trees was found to be helpful in the treatment of fevers. QN the key, active substance found in *Cinchona spp*s was discovered and isolated in the 19th century and later utilized as a base for the synthesis of pure compounds with antimalarial activity [53,78]. Due to its potential antimalarial activity, QN became a primary drug for the synthesis of quinolines such as MQ, amodiaquine (AQ), piperaquine (PPQ), PMQ, and CQ. Most quinolines share similar mechanisms of action since they possess a characteristic quinoline ring system related to one another. Although, lumefantrine (LUM) and halofantrine (HF) are also made up of a quinoline ring system they are distinct from each other.

The quinoline family can be further subdivided into two: the aminoquinolines, which comprise CQ, AQ, PPQ, PMQ, and aryl-amino alcohols, comprising of MQ, HF, QN, and LUM. Among these drugs, CQ has been most widely studied and was shown to target the haem detoxification pathway following haemoglobin degradation [79,80].

CQ is a weak base usually deprotonated at physiological pH levels. However, in the acidic environment of the DV, it starts to get di-protonated [81] and forms clusters with hematin dimers of the haem group, truncating them and preventing them from crystalizing into HZ [79,80]. In this regard, the detoxification process is obstructed, and reactive haem accumulates in the DV and may then diffuse [79], becoming harmful to the parasite [79–81].

1.5.2.1 Piperaquine

PPQ is a bisquinoline antimalarial, comprising of two quinoline nuclei joined by a covalent aliphatic or aromatic bond [82]. It was synthesized in the 1960s and became recommended by the Chinese National Malaria Control Programme in 1978, as it was seen to have higher efficacy and tolerance than CQ. This led to the subsequent mass production and distribution of 140 million adult treatment doses [82].

PPQ is slowly absorbed and reaches high plasma concentrations in 5 hours with a longer clearance time of 20 days. Concerning the mechanism of action of PPQ, studies show that PPQ may share a similar drug target with CQ. This implies that it may inhibit the haem-detoxification pathway occurring in the DV [83]. Although it was found to be effective, rising cases of PPQ resistance led to a reduction in its use as monotherapy in the 1980s [82].

Presently, PPQ is used in ACT combination therapy conjugated with DHA (DHA-PPQ) (Figure 5). This combination was formulated to slow down the emergence of *P. falciparum-resistant* strains. In the last two decades, PPQ with the partner drug DHA has been seen to be highly effective in the treatment of uncomplicated malaria infections as well as prophylaxis for re-infection [84]. Myriad clinical trials were performed in malaria endemic countries to assess the efficacy of DHA-PPQ against uncomplicated *P. falciparum* and *P. vivax* malaria. Starting from Asia, 13 trials were conducted including 1,874 patients that received DHA-PPQ as treatment. This trial occurred between 2002 and 2006 and displayed excellent therapeutic outcomes as well as a good safety profile. Trials conducted in China, Cambodia, Laos, Thailand, Vietnam, and Myanmar revealed a 97% cure rate (Kaplan-Meyer derived estimates) within an overall 28-day period [84]. DHA-PPQ was also administered in five other trials including 228 patients in Cambodia, 60 patients in Vietnam, 547 patients in Papua Indonesia, and 268 patients in Afghanistan. These trials affirmed the success achieved in earlier trials with a cure rate higher than 95% [84].

These trials were also done in several African countries on children from 6 months to 10 years of age, with uncomplicated malaria infections. DHA-PPQ studies were carried out to evaluate the safety and therapeutic effects of ACT in these African countries from 2003 to 2009. In total, 6 trials were performed on 252 patients in Rwanda, 426 patients in Uganda, 187 patients in Burkina Faso, and 80 patients in Sudan with uncomplicated malaria infections. Results from these trials were similar to the trials conducted in Asia including 28-day cure rates spanning from 95% in Rwanda to 100% in Sudan [85].

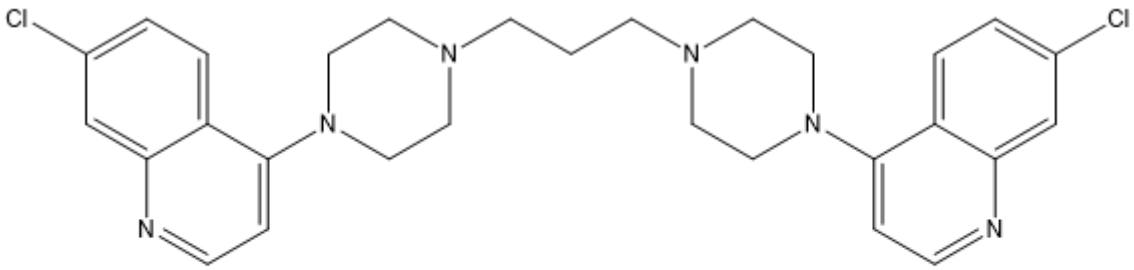

Piperaquine tetraphosphate

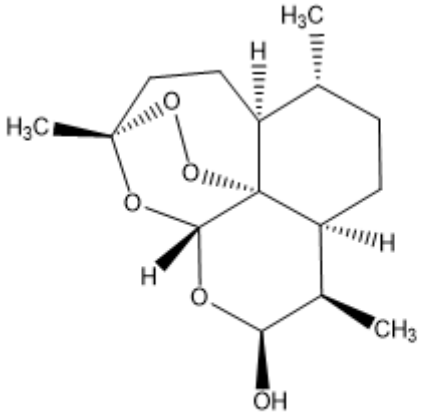

Dihydroartemisin

Figure 5: Schematic diagram of the chemical structure of DHA and PPQ tetraphosphate.

1.5.3 Antimalarial Drug resistance

As earlier stated, a major setback in malaria elimination is the rising resistance to antimalarial drugs. This is seen in several trials using semi-synthetic quinolines amongst other drugs [86]. The need for novel antimalarial drugs is more critical now than ever. However, a better understanding of the mechanism of drug resistance and the factors responsible for it, are required to develop new drugs or new combination therapies.

1.5.3.1 Parasite Resistance to Artemisinin Combination Therapies

For ACTs, cases of prolonged parasite clearance have been correlated with decreased susceptibility to ART reported from the Thailand-Cambodia border and have progressed to other Southeast Asian countries (Thai-Cambodian border and Western Cambodia) [87,88]. Reports reveal that mutations found in the kelch 13 (K13)-propeller protein is linked to this phenomenon [89]. Recent insights into the role of these mutations include the identification of altered kinetics

of parasite intra-erythrocytic development cycle (IDC) [90], and the identification of interaction partners that appear to reduce haemoglobin endocytic traffic in ART resistant parasites [91], leading to reduced formation of Fe^{III} PPIX and consequently less haem:ART adducts during the parasite IDC.

Interestingly, *P. falciparum* resistance to other antimalarial drugs such as quinoline was also initiated in this region before spreading to other parts of the world. Presently, ACT resistance is not yet prevalent in Sub-Saharan Africa, where the burden of malaria infections lies [8]. But taking all these into account, it is important to streamline our focus to the underlying factors responsible for this resistance and the mechanisms by which the parasite develops resistance to antimalarials (such as DHA-PPQ) (90].

1.5.3.2 Dihydroartemisinin-Piperaquine Resistance

DHA-PPQ has emerged to be one of the highly efficient ACT over the last decades as shown by the clinical trials stated earlier. However, in recent years there have been rising concerns as reports of DHA-PPQ *P. falciparum* resistant strains were reported in Cambodia [92,93].

Early concerns were that the mechanism of resistance of PPQ was similar to CQ. Since both are aminoquinolines, PPQ may also target the haem detoxification pathway like CQ. Some studies further confirmed that when *in vitro P. falciparum* parasites were incubated with PPQ, the production of HZ was impeded [94].

In another research conducted from 2009 to 2015 using clinical isolates from Cambodia, results showed an interrelation between the amplification of *pfpm2* and *P. falciparum plasmepsin 3 (pfpm3)* gene cluster on chromosome 14, and de-amplification of an 80-kb region (single copy) of *P. falciparum multidrug resistance transporter 1* (*PfMDR1*). PPQ half-maximal inhibitory concentration (IC_{50}) assays conducted were seen to be increased indicating reduced parasite susceptibility [94]. PPQ survival assays also showed elevated survival rates. Two other studies [95,96] using Cambodian isolates also confirmed an interrelation of PM2 and PM3 copy numbers with PPQ resistance. Plasmepsins are aspartic proteases responsible for the degradation of haemoglobin, and function in synergy with the cysteine proteases. However, the aspartic proteases play critical roles in the haemoglobin degradation process. Therefore, an absence of the plasmepsin enzymes may adversely impact the efficacy of haem formation and the production of HZ [97]. Bonilla *et al.* [98] demonstrated this by studying the impact of triple (*Pfpm1, Pfpm2 and P. falciparum* histoaspartic proteases (Pfhap)) and quadruple (*Plasmodium falciparum plasmepsin*

4 (*Pfpm4*), *Plasmodium falciparum plasmepsin 1* (*Pfpm1), Pfpm2 and Pfhap*) knockout plasmepsin mutants. In this study, the author saw that quadruple-PM knockouts grew slower in standard medium and had a decreased HZ production in comparison to wild type (WT) parasites. Additionally, triple-PM knockouts were also unable to utilize the amino acids formed from the degradation of haemoglobin as effectively as WT parasites, suggesting that the deficiency of these parasite lines may be in the steps following haem release from haemoglobin degradation [98]. Therefore, plasmepsins are not only functional in the cleavage of haemoglobin but also influence haem generation and its transformation into HZ.

1.6 Antimalarial Drug Mediating Transporters

For an antimalarial drug to work effectively, it must gain access to its required site of action. Responsible for this are mediating transporters that carry molecules and ions through membrane barriers to their target site. They perform different physiological roles such as translocating nutrients into cells, efflux of toxic metabolic waste products and foreign substances (such as drugs), as well as producing and maintaining transmembrane electrochemical gradients. Membrane transport proteins execute important roles in the development and replication of the parasite and more importantly in the occurrence of antimalarial drug resistance [99,100].

Although mediating proteins are essential key players in drug metabolism, only a few have been explored and linked with multi-drug resistance phenotypes [99] such as the *PfMDR1* and *P. falciparum* chloroquine resistance transporter (*Pf*CRT).

P. falciparum membrane transport proteins are predicted to be encoded by 144 of the parasite's 5,712 genes, accounting for ~2.5% of the *P. falciparum* genome [101]. However, most are putative transporters which physiological function or link to drug resistance remains unknown. Known polymorphisms in two transporters are thought to alter the parasite's susceptibility to most of the current antimalarial drugs: (i) The CQ resistance transporter *Pf*CRT, member of the drug/metabolite transporter superfamily and (ii) the *PfMDR1*, member of the ATP-binding cassette (ABC) transporters superfamily. They regulate the flux of solutes, into the parasite DV and span its membrane. *Pf*MDR1 mediates entry of xenobiotics into the DV while *Pf*CRT supports their efflux from the DV.

Much less explored as drug resistance players or even as possible drug targets are the ABC transporter, *Pf*MDR2.

1.6.1 *P. falciparum* MDR2

*Pf*MDR2 *was* later discovered, and studies have shown its involvement in heavy metal transport across the membrane. The gene *pfmdr2* encodes for a protein having 10 predicted transmembrane domains along with a single ATP-binding site at the 3' end [102,103]. It is located on chromosome 14 as a single copy and is localized in two sites of the parasite – the plasma membrane and DV membrane [103,104]. In a homology search performed in an earlier study using GenBank sequences, it was seen that the *Pfmdr2* gene had significant homology with an *hmt1* gene found in the fission yeast *Schizosaccharomyces pombe*. It has been discovered that this yeast gene is associated with cadmium resistance and is assumed to be involved in the transport of cadmium-containing complexes. It was further seen that the *hmt1* gene also possessed 10 transmembrane domains and a single ATP binding site [105].

Northern blot analysis of the *Pfmdr2* gene performed by Rosenberg *et al.* revealed that it is expressed in a specific stage (trophozoites) of the parasite's intra-erythrocytic life cycle and not in the ring stage [103]. *Pf*MDR2 western analysis results exposed a protein structure with a band of 110 kDa. (103). Earlier studies show that there is no change in the *Pfmdr2* expression or gene copy, in drug-resistant parasites in comparison to drug-sensitive parasites. Nevertheless, due to its proximity to the *hmt1* gene, it may have an essential role in heavy metal resistance in the malaria parasite [103,105].

A metabolic pathway of *P. falciparum* that is inadequately understood is its method of heavy metal homeostasis. Heavy metals are characterized as metals having a density above 5 g/cm^3. Amongst the 90 naturally occurring metal elements, there are 53 heavy metals. Of these heavy metals, 20 are accessible to living things, a fewer are essential, and the rest may be present in cells due to their broad distribution in diverse ecosystems. Although heavy metals may be essential to parasites, when present in concentrations above specific levels they become toxic to cells. Therefore, organisms have evolved diverse mechanisms for the homeostasis of these metals including *P. falciparum* [105].

Interestingly, a study performed in 2006 confirmed that *Pfmdr2* gene was responsible for the efflux of heavy metals [105]. In this study, cadmium was used as heavy metal due to the ubiquitous systems present in organisms to tackle it. In various organisms, cadmium depletes glutathione and protein-bound sulfhydryl groups [105,106], leading to the production of reactive oxygen species such as hydroxyl radicals, superoxide, and hydrogen peroxide. This causes DNA damage as well as other cellular imbalances.

Due to the sensitivity of the *P. falciparum* natural habitat (intra-erythrocytic phase) to oxidative stress, this heavy metal is especially applicable to the parasite. With its exposure to cadmium, the mechanisms with which it uses for homeostasis can be characterized and the role of *PfMDR2* protein in the process [103]. What differentiated heavy metal-sensitive parasites from their resistant counterparts was the presence of a stop codon that rendered the gene and its encoding protein inactive. This led to the accumulation of heavy metals in the parasite's cytoplasm.

After characterization of *PfMDR2* at DNA, RNA, and protein levels, it was found that the WT sensitive line carried a mutated *Pfmdr2* gene. A TGA nonsense mutation found in this line inactivated the protein and led to the accumulation of heavy metals thus hindering normal cellular functions. However, after culturing this WT sensitive line in the presence of cadmium, it evolved to become resistant and the TGA nonsense mutation reverted to a TGT cysteine codon. Consequently, this reversion facilitated the efflux of heavy metals because of the replacement of the complete length of the protein product. This concept was further proven with four other strains, all of which were found to be resistant to heavy metal and carried the TGT codon at the same position. Therefore, the concept of parasite resistance in relation to *PfMDR2* overexpression or gene amplification is eliminated by several studies including this. The accumulation of heavy metals in the WT cadmium sensitive line can be a result of protein absence due to its cellular degradation [103).

In a more recent study, it was found that mutations in *k13,* more particularly to the 3D7 strain (whose genetic background is ubiquitous in parts of Southeast Asia) is related to a strong set of molecular markers, of which nonsynonymous mutations in *Pfmdr2* and *Pfcrt* were identified among other genes [107]. Additionally, although the part *Pf*MDR2 plays are yet to be understood in parasite resistance, other studies have also found its relation to antifolates resistance and tolerance to heavy metals as earlier mentioned [108]. Since it has been identified that *Pf*k13 mutation (found in artemisinin resistant strains) is associated with the *mdr2* gene, this suggests that it may be involved in any of the pathways between haemoglobin degradation and HZ formation.

1.7 Current Tools for Malaria Diagnosis

For over a century, microscopy has remained the "gold standard" for malaria detection and has helped in fostering malaria diagnosis and treatment, nevertheless, it has had its own limitations. For accurate analysis, well-trained personnel are needed to correctly decipher Giemsa-stained blood smears [109]. Mass production of RDTs have improved the diagnostic process of

the disease but are less sensitive than microscopy and unable to quantify infection [110,111]. Other novel diagnostic tools such as polymerase chain reaction (PCR) and flow cytometry have proven to produce more effective results [112,113]. However, there is still an urgent need for a cheap, inventive, highly sensitive, and easy-to-use diagnostic device that can detect viable parasites. Furthermore, diagnostic tests that can reveal specific phenotypic features concerning parasite specie, strain, and uncover drug resistant strains which is the role of this research thesis, will be helpful towards personalized malaria treatment.

1.7.1 Properties of Haemozoin that Makes It an Attractive Target for Malaria Diagnosis

The HZ crystal has several unique properties, including optical birefringent, photoacoustic and magnetic properties that have made it an attractive natural biomarker for novel malaria diagnostic methods [114,115].

Birefringence is the ability of a transparent and molecularly ordered material to refract light in two rays (or several rays), each adopting slightly different paths [116]. HZ forms bright birefringent granules under polarized light in a red-yellow colour [116]. This optical property of HZ enables it to be easily observed under polarized light up to a detection limit of 30 parasites/μL of blood [117,118].

The photoacoustic property of the HZ has also been explored in its detection and quantification [115]. The photoacoustic effect is the generation of pressure waves from a sample after illuminating it with varying intensities of light [119,120]. These intensities create acoustic vibrations at different frequencies, producing a specific photoacoustic spectrum of the sample according to its absorptions [119]. This photoacoustic spectrum formed can then be measured using detectors (such as photodetectors and ultra-sound transducers) (Figure 6), thus proving detailed information about the sample, even in deep layers of tissue [119,121]. Due to the distinct molar extinction coefficients between haemoglobin and HZ at specific spectral bands, the optical absorption of healthy and iRBCs varies [122,123]. This suggests that iRBCs and healthy RBCs generate varying photoacoustic spectra. This was observed in the results of an *in-silico* computer simulation carried out by Saha *et al.* [119]. Results demonstrated that the intra-erythrocytic stage of the malaria parasite can be identified using the photoacoustic effect generated from samples illuminated with the right optical wavelengths. The authors also observed that as parasites mature,

the amplitude of photoacoustic signals reduces at 434 nm and rises at 700 nm of incident illumination [119].

Nuclear magnetic resonance (NMR) technique has the potential of bringing an effective solution to the present challenge - effective diagnosis in malaria-endemic regions. The NMR machine is an innovative technology consisting of a permanent magnet that creates 0.5 T static magnetic field in a benchtop NMR console and has been explored in malaria diagnosis [109,124]. The detection relates to the molecular dynamic difference between healthy and malaria infected blood due to the presence of HZ, a nanocrystallite lattice of haem dimers with paramagnetic properties, unique to the parasite. Over the years, it has been adapted to be portable, easy to handle, and requiring a little amount of blood (5μL). Furthermore, studies have proven it to be more sensitive and efficient than microscopy and RDTs [124]. This is an important reason why further exploring the NMR as a diagnostic tool in characterizing the malaria parasite's phenotypic features will be the focus of this dissertation.

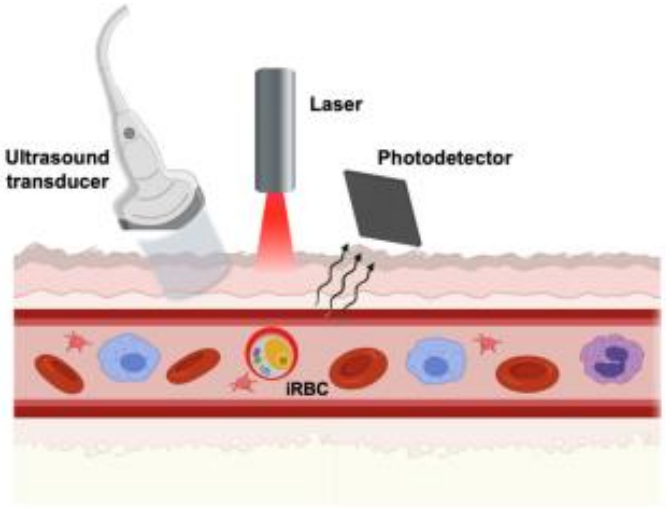

Figure 6: Schematic demonstration of the photoacoustic method for malaria detection. The technique adopts an incident laser, photodetectors for recognition of the optical spectra and an ultrasound transducer that identifies waves generated by the high temperature in the sample. The image is not to scale. Adapted from Vitoria *et al.* [115].

In the intra-erythrocytic stage, malaria parasites consume about 75% of the host's cell haemoglobin. Free haem toxic in nature is released from this process from HZ crystals that are found in the DV as earlier mentioned.

The HZ's unique magnetic property among other properties has become an attractive target and a good biomarker towards exploiting new tools for malaria diagnosis for researchers

[114,125]. Karl *et al.* [126] and Peng *et al.* [127] invented a novel technique for the rapid and sensitive diagnosis of *P. falciparum*- iRBCs with the use of ^{1}H-nuclear magnetic resonance relaxometry (MRR). This technique depends on the detection of HZ crystals that are released by parasites in the host RBCs. HZ is an excellent biomarker due to its large paramagnetic susceptibility. Physiologically, RBCs possess diamagnetic properties, however, with the presence of HZ crystals in iRBCs, magnetic diagnostic devices can easily capture a change using the relaxation time constant (longitudinal (R_1) and transverse (R_2) water relaxation rate constants) [109]. With this technique, further studies were carried out using the MRR method to differentiate the three morphological stages of the parasite, including rings, trophozoites, and schizonts [109]. To distinguish these developmental stages, assessment of modifications in the relaxation rate constants occurring within iRBCs were performed [115,124). As mentioned earlier, HZ crystals deposited in iRBCs increase as the cycle progresses from early to later stages, making the paramagnetic susceptibility of these cells more noticeable. This leads to major changes in the bulk magnetic susceptibility of the iRBCs and consequently confers measurable changes in the MRR of nearby protons [124]. Additionally, results obtained by Gregorio *et al.* [109], showed a direct proportional relationship between high water proton transverse relaxation rate constants (R_2) and the applied magnetic field. This can imply that essential insights can be gotten from the existence and concentration of HZ within iRBCs and consequently the intra-erythrocytic stage the parasites are in.

1.7.2 Principle of the Nuclear Magnetic Resonance

All objects have ions, and all ions have nuclei which can be positively or negatively charged. When these randomly aligned ions are excited by a magnetic field, they take up an aligned orientation (upward or downward) (Figure 7). This is also applied to iRBCs, because of the bulk change from diamagnetic (Fe^{2+}, haemoglobin) to paramagnetic magnetic property (Fe^{3+}, haemozoin). The unpaired iron ions present in the iRBCs, align in the presence of a magnetic field. The time it takes for an excited iron to go back to a randomly aligned state can be measured in time-domain by two relaxation times, the transverse relaxation time/spin-spin relaxation time constant (T_2) and the longitudinal relaxation time/spin-lattice relaxation time constant (T_1). Studies reveal that as parasites grow in iRBCs these relaxation times decrease due to increased HZ deposition [109]. Thus, in high parasite infections and the intermediate and late intra-erythrocytic stages, higher paramagnetic susceptibility is conferred to iRBCs which is seen in a fall in T_1 and T_2

[109,124]. $A_{baseline}$ratio (A-ratio) is defined as the ratio between T_1 and T2 (T_1/T_2) that reveals the dynamic changes that occur along the developing stages or increasing parasitaemia. In NMR, T_2 values drop more rapidly than T_1 because it takes shorter time to revert to equilibrium state (M_0), resulting in the formation of A-ratio. A-ratio values increase with increasing concentration of HZ in a cell, which can be often seen in mature parasites or high parasitaemia infections.

In 2020, a more recent research study was carried out utilizing the inexpensive benchtop-sized NMR spectrometer. In this study, different haemoglobin derivative phenotypes were characterized using two-dimensional magnetic resonance relaxation times for the first time. This meant that the relaxation times T_1 and T_2 (transverse relaxation time) were considered simultaneously [128]. In this study, he was successful in characterizing their specific phenotypic expressions [128].

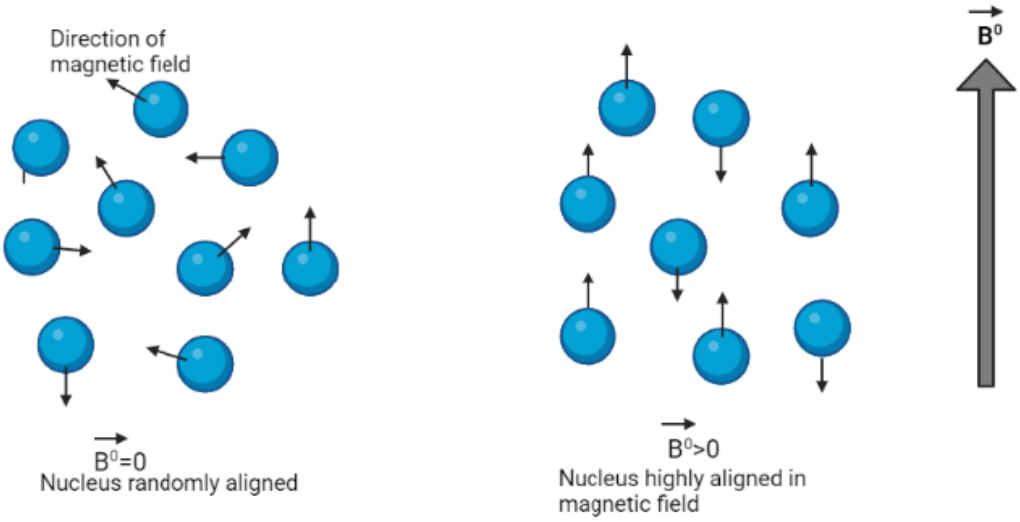

Figure 7: Schematic diagram demonstrating ions in their equilibrium state and highly aligned ions when excited by a magnetic field. Created with BioRender.com.

In another study carried out in diabetes mellitus that same year using the point of care NMR system, important discoveries were further made. The NMR technique was successful in obtaining clinical information on the oxidative stress levels of diabetes mellitus patients using the concentration of haem (Fe^{3+}) (as seen in malaria) and other redox states of haemoglobin contained in their blood samples [129]. This research is a follow-up study from the first two dimensional (2D) "molecular fingerprint" study performed by Peng *et al.* [128].

Since the HZ formation pathway is crucial to parasite survival and has become the target for many anti-malarial drugs including present therapies, we will disclose unique patterns capable to distinguish parasite stage and concentration as a means towards precision medicine [130].

1.7.3 Deep phenotyping using low-field NMR

Despite considerable indirect evidence pointing towards the relation between Hz formation and drug response, direct evidence remains elusive. We are still missing deep genetic and biochemical understanding that better define the relationship between drug action and resistance.

Haemoglobin uptake and concomitant HZ formation are intricately linked with drug response. Microscopic detection of HZ formation in the iRBC serves as diagnostic feature, but the distinct mechanic, optic, acoustic and magnetic features of the iRBC, promoted by the HZ crystals have been insufficiently explored. A recent review describes sensing technologies of HZ [115] with potential to provide molecular insights into the mechanism of drug action/resistance. Molecular characterisation of HZ might provide opportunities to improve our understanding of the genes involved in this process or drug action.

Haemoglobin, abundant in healthy uninfected RBC, is diamagnetic whereas the HZ crystallites are paramagnetic. As parasite maturation across the IDC stages correlates with HZ increases in size and quantity, the iRBC alters the low-spin diamagnetic state (Fe^{2+}, baseline uninfected RBC) into a high-spin paramagnetic state (Fe^{3+}, HZ). A shift towards HZ moiety thus yields distinct T_1 and T_2 relaxation time constants obtained with low-field NMR. This sensitive technology, with high capacity for the identification of the presence of paramagnetic substances, should thus have the capacity to capture distinct NMR spectra of iRBC throughout the parasite IDC and any disturbance in the HZ pathway promoted by drugs. Di Gregorio *et al.*, using infected RBCs treated with DHA and CQ, detected alterations in the slope of relaxation rate (1/T2) and their involvement in Hz degradation [109]. Moreover, Sienkiewicz had shown using multi-frequency high field electron paramagnetic resonance that the spectra obtained for Hz correspond to a high spin Fe^{3+}(S=5/2) [131]. The small but significant hyperfine interactions from the electron-nuclear coupling allows enormous information to be mapped out. Dr. Weng Kung, using the same principle, has proven this technology to detect phenotypic variation in haemoglobinopathies [128]. Therefore, applying innovative spectroscopy might detect the disturbance in the HZ pathway promoted by drugs or genetic alterations as discussed by Veiga and Peng [130]. The true challenge is to obtain

meaningful information from this atypical phenotype, which could possibly be resolved exploring the parasite under a controlled genetic background.

CHAPTER 2

RESEARCH OBJECTIVES

The intra-erythrocytic stage of the malaria parasite evolves from early ring forms to trophozoites and schizonts within 48 hours, depending on haemoglobin as source of amino acid. However, the parasite's survival during these stages is dependent on the detoxification process of haem to the formation of insoluble HZ crystals. These crystals are present in all stages of the intra-erythrocytic phase, conferring specific magnetic changes to the iRBCs. This change from diamagnetic (uninfected RBCs) to paramagnetic (iRBCs) properties can then be detected with high sensitivity by magnetic resonance. Early studies reveal that the NMR spectroscopy is sensitive to detect as few as 10 parasites/μL of iRBCs [7]. Malaria is the leading cause of morbidity globally, particularly in tropical and sub-tropical regions affecting the quality of living in these regions, mostly children and pregnant women who are more susceptible complications that may arise from the presenting symptoms (e.g., anaemia) of malaria. Nevertheless, the path towards malaria elimination has been hindered by drug resistance and ineffective conventional diagnostic tools. To tackle these issues, we are further exploiting the low-field NMR technology to detect novel phenotypic features of the intra-erythrocytic stages of WT parasite strains and mutant lines utilizing the dynamic changes that occur in the pathways between haemoglobin degradation and HZ formation. Therefore, we hypothesize in this study that the NMR-based technology is a promising tool for malaria detection and its ultra-sensibility towards disturbance of haem species in the cell might contribute to unveil the unresolved haem detoxification pathway players. Being that most of the present drugs interfere somehow with this biological pathway, the capture of specific NMR fingerprint could deliver precision malaria medicine that can be used in a POC setting. Having this in mind, this master thesis had the following specific objectives:

1) Characterize the different intra-erythrocytic morphological stages of the parasite using NMR spectroscopy (in the time-domain T_1 and T_2).

2) Using ultra-sensitive time-domain NMR to explore the possible role of *Pf*MDR2, a heavy metal transporter, and plasmesins, aspartic proteases, in the natural balance of the haem species present in the iRBCs.

CHAPTER 3

MATERIALS AND METHODS

3.1 Study 1: Time-domain NMR characterization of wild type parasites

In collaboration with the International Iberian Institute of Nanotechnology (INL), *P. falciparum* parasites were measured using the bench-top NMR spectrometer previously designed by our group.

3.1.1 *P. falciparum* culture

Asexual intra-erythrocytic *P. falciparum* Dd2 (a multidrug resistant strain) parasites were grown in human RBCs in malaria culture medium (MCM) – [RPMI 1640 (Gibco) with 2 mM L-glutamine, 25 mM HEPES, 0.25% Albumax II (Life Technologies), 0.2% $NaHCO_3$, 200 μM hypoxanthine, and 0.25 μg/mL gentamycin] in a regulated atmosphere of 5% O_2/5% CO_2/90% N_2 maintained in an incubator at 37°C. Parasites in T_{25} flasks were cultured at 4% haematocrit in 5 mL of MCM. Plates for drug susceptibility assays were maintained in a hypoxia chamber (Billups-Rothenberg, Inc., CA, USA). Medium changes were carried out daily – unless in specific cases – and the wellbeing, stage and parasitaemia of the cultures monitored regularly by optical microscopy of Giemsa-stained blood smears.

3.1.2 Synchronization of *P. falciparum* culture

Synchronization of *P. falciparum* life cycle was performed by extrapolating late schizont stages using the progression time of *P. falciparum* parasites (rings (0-24 hours), trophozoites ((12-16 hours) and schizonts (8 hours)). With the formation of early rings, the cultures were synchronized by adding 5% Sorbitol (Sigma Aldrich) and incubating for 15 minutes at 37 °C. The culture was then washed and resuspended in MCM. About 20 hours later (towards the end of the ring stage) the cultures were synchronized again, to kill other stages. The synchronization process was repeated several times till the parasites were highly synchronized. At this step, the cultures were grown until late schizonts were formed, confirmed by the formation of merozoites. After about 3 hours, microscopy was repeated to confirm the formation of early rings and a final tight synchronization was done. Prior to the commencement of a new cycle of NMR measurements (Figure 8), synchronization was performed on rings (slack synchronized parasites). When more tight synchronized parasites were required, several synchronizations were done, and the cultures were timely synchronized again 0-3 hours rings post-invasion (tight synchronized parasites).

Figure 8: Bench-top setup NMR system, with a PCB (printed circuit board) probe, a micro coil for sample detection. Capillaries are placed into the coil with the end containing concentrated iRBCs. Adapted from Peng *et al.* INL laboratory protocol, NMR setup with a capillary tube containing concentrated blood at one end.

3.1.3 *P. falciparum* growth analysis

P. falciparum growth was determined by optical microscopy or by flow cytometry.

For microscopy analysis, few drops of blood were added onto a glass slide to make a thin smear. The thin smear was fixed with 100% methanol and stained with 10% Giemsa's azur eosin methylene blue solution (Merck) for 15 minutes. Parasitaemia was determined by counting the number of parasitized RBCs per total RBC counted per field.

For flow cytometry analysis, 15 µL of 4% haematocrit culture of *P. falciparum* were incubated with 40 µL of staining solution [2X SYBR Green I (Applied Biosystems) and 1.6 µM MitoTracker Deep Red (Applied Biosystems)] for 30 minutes at 37 °C. Together with the incubated cells, 300 µL of 1X phosphate buffered saline (PBS) were added into test tubes and analysed in the LSRII flow cytometer (BD Biosciences). SYBR Green I stains DNA of parasitized cells and MitoTracker stains mitochondrial membrane potential of living parasites. Data obtained was analysed using FlowJo software (TreeStar). Gate was performed on the SYBR Green I and MitoTracker positive cells, giving the accurate parasitaemia against the total number of cells.

3.1.4 Dilution of *P. falciparum* culture

The culture was diluted with RBCs to obtain 0.01, 0.1 and 1% parasitaemia. For this, after counting the number of parasitized cells by optical microscopy or flow cytometry, *P. falciparum* iRBCs were diluted to obtain 0.01, 0.1 and 1% parasitaemia at 4% haematocrit, according to equation $C_1V_1 = C_2V_2$. Based on the calculation a set volume of parasitized RBCs was obtained and diluted in a specific volume of media and blood to achieve a required parasite concentration.

Calculation: (To obtain 1% parasitemia)

Given that: $C_1V_1 = C_2V_2$

C_1= 4.7

V_1=?

C_2= 1

V_2= 5 mL (MCM)

V_1= (1×5)/4.7 =1.06 mL (set volume of parasitized RBCs)

1.06 mL +3.9 mL (set volume of MCM (5 mL of MCM – 1.06 mL))

Blood: Calculations were made to obtain 4% haematocrit (315.2 µL of blood was obtained).

3.1.5 *P. falciparum* sample preparation for time-domain NMR detection

Prior to NMR detection, blood samples were washed three times with 1X PBS at 1500 rpm for 5 minutes. Following this, samples were transferred into a heparinised micro-capillary tube (Fisherbrand™,Thermo Fisher Scientific, USA). Three capillaries were made for each dilution (prepared as explained in 2.1.4), and sealed with plasticine (Cristoseal®, Krakerler Scientific Inc., USA). The tubes were centrifuged using a Sorvall Legend Micro 21 microcentrifuge (Thermo Fisher Scientific, USA) at 6000 xg for 1 minute. The length of sedimented blood in the capillary tube was measured using a ruler to ensure it was within 5-6 mm, to fit the length of the NMR coil suggested to improve detection sensitivity (Figure 8) [124]. Each tube was then loaded into the NMR coil at the sedimented iRBC band for detection.

3.1.6 NMR measurement

The ^{1}H NMR measurements of iRBCs were carried out at resonance frequency of 21.65 - 21.76 Hz within the NMR device at the International Iberian Laboratory (INL) as demonstrated by Peng *et al.* [124]. T_2 relaxation time was characterized by standard Carr-Purcell-Meiboom-Gill (CPMG) train pulse (80 microsound (μs) of inter-echo time) comprising of 12,000 echoes and 32 scans, to achieve average signal, and was processed by Prospa 3.12 software (Magritek, New Zealand). In addition, exponential and real time fit were used to obtain T_2 relaxation time. The recycle delay was set to 2 seconds, to allow all the spins sufficient time to revert to thermal equilibrium state. T_1 relaxation time was characterized using standard inversion recovery method with additional CPMG detection, often adopted for T_1 measurement in an inhomogeneous magnetic environment. For T_1 detection, CPMG pulse with echo-time of 500 μs comprising of 64 echoes were carried out 4 times along with delay times between two extremes. Minimum and maximum gap between 180- and 90- pulse consisting of 'minimum delay' of 1 ms and 'maximum delay' of 4000 ms, respectively, were used. The inter-measurement time was set to 2 seconds.

3.1.7 NMR phenotypic assay

Tight synchronized and slack synchronized cultures were characterized, using different approaches (Figure 9).

For slack synchronized cultures, different parasitaemia for a particular stage were measured on different days. For each day, three capillaries were prepared for the parasitaemia to be measured on that day. The three capillaries for that parasitaemia were read consecutively at each time point over a period of 8-12 hours (8-12 measurements).

For tightly synchronized cultures, early ring forms were obtained at 0-6 hours post invasion, counted, diluted, and transferred to capillaries. Three capillaries for each parasitaemia were prepared. Each capillary for every parasitaemia were measured consecutively at every time point. Each parasitaemia had a minimum of three measurements.

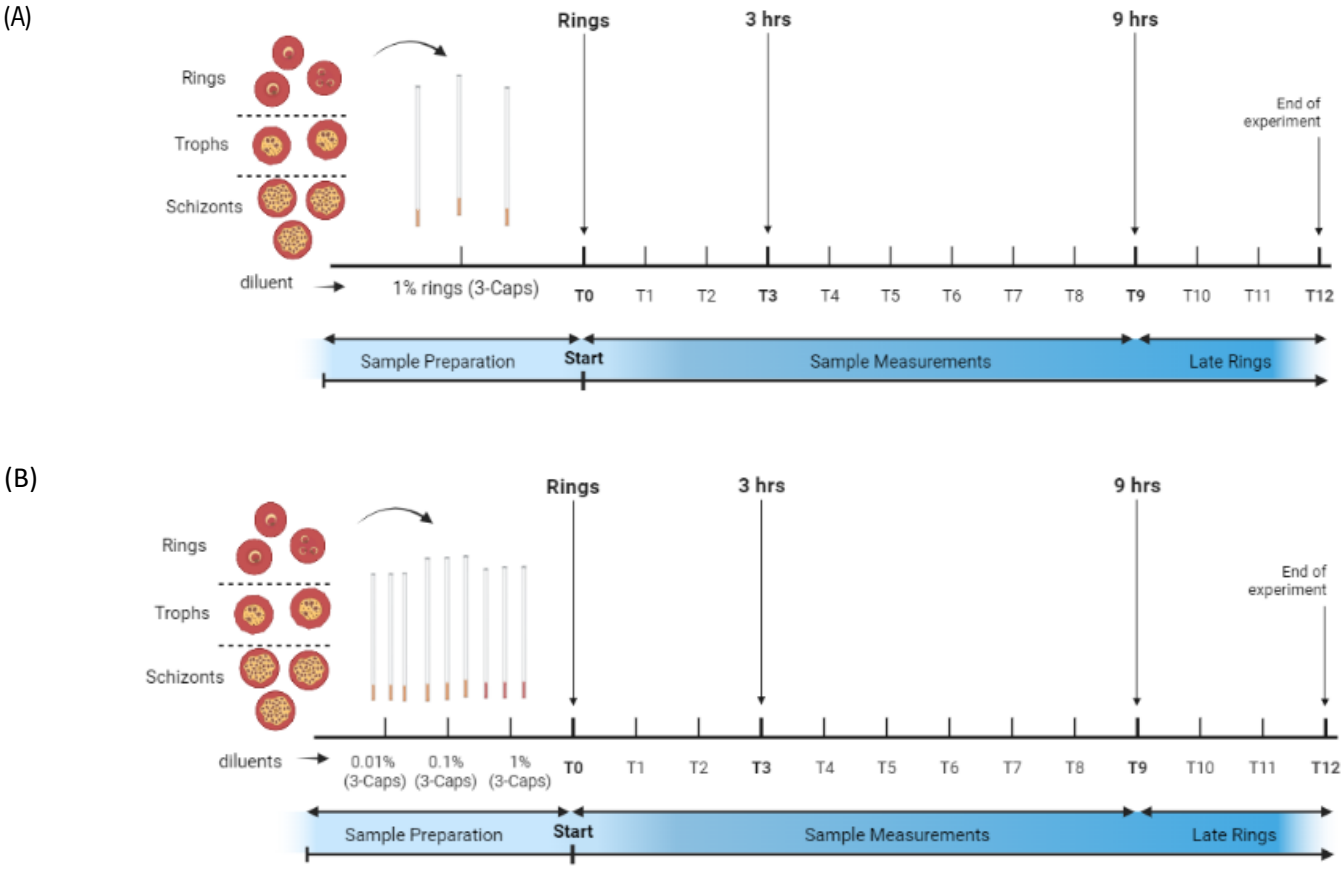

Figure 9: Schematic diagram of sample preparation and NMR measurement process. (A) Slack synchronized cultures of rings, different parasitaemia (e.g., 1% as shown above) collected into three capillaries on different occasions. (B) Tight synchronized cultures of rings collected into nine capillaries, three capillaries for each diluent Created by Biorender.

3.1.8 Statistical Analysis

The data from NMR measurements were analysed and plotted with OriginPro software (2018 version). The Statistic test used were calculated in GraphPad Prism 7 using One-way Anova, Sidak multiple comparison tests (for comparing 3 parameters) and two-tailed Mann-Whitney-U test for comparing two parameters.

3.2 Study 2: Phenotypic features of the *P. falciparum* MDR2 transporter

P. falciparum pfmdr2 knockout (KO) parasites has previously been attempted in the laboratory lacking confirmation of the gene editing event. Cryopreserved unconfirmed *Pf*MDR2 knockout (KO) parasites were thawed using NaCl gradient (comprising of 12% NaCl, 1.6% NaCl and 0.9% NaCl + 0.2% dextrose). Cryopreserved cultures were left to thaw and transferred to 50 mL falcons. For every 1 mL of thawed blood 0.2 mL of 12% NaCl was added drop by drop while mixing at the same time and the falcon

was left to stand for 5 minutes. About 10 mL of 1.6% NaCl for every 1 mL of original thawed blood was added using the same process. The same volume and procedure were carried out for 0.9% NaCl + 0.2% dextrose and the cultures were centrifuge at 1500 rpm for 5 minutes. The supernatant generated was discarded and the iRBCs pellet resuspended in MCM and maintained under standard conditions.

The KO parasite lines were constructed using the selection-linked integration (SLI) system into Dd2 and 3D7 WT parasite lines. Other member of our group had previously performed the construction of the plasmid, its transfection into the parasite and selection of parasites. Parasites were first exposed to 2.5 nM WR99210 to select parasites with episomal plasmid. Prior to my study, the parasites were at the second selection drug Geneticin (G418 (Sigma)) to select parasites with the integrated plasmid (containing the KO *pfmdr2* gene).

After a few days of parasite culture, *Pf*MDR2 KO parasites culture was able to expand to 1% parasitaemia so G418 (200 µg/mL diluted in MCM) was added and maintained under standard conditions (as previously described in section 2.1.1). G418 culture medium was changed daily to maintain the cultures for weeks until an experiment is to be undertaken.

3.2.1 Genomic DNA Isolation

Genomic DNA (gDNA) was isolated from the *pfmdr2* KO parasites using the NZY Tissue gDNA Isolation Kit (Nzytech), following the guidelines provided by the manufacturer.

Prior to the start of the protocol the Stuart SBH130D block heater was set at 56° C. Following this, 25 µL of Proteinase K solution was added to 200 µL of iRBCs in a microcentrifuge tube. This mixture was combined with 200 µL of buffer NL*, mixed vigorously by vortex and incubated at 56°C for 10 – 15 minutes in the block heater (Stuart SBH130D). The heated solution and 210 µL of 100 % ethanol were mixed by vortex and transferred into a NZYSpin Tissue column placed in a 2 mL collection tube.

The setup was centrifuged for 1 minute at >11,000 xg and flow through discarded. The step was repeated when 500 µL of buffer NW1 and 600 µL of NW2 were dispensed into the column. Following this, the NZYSpin Tissue Column was placed back into a collection tube and centrifuged for 2 minutes at >11,000 xg. To elute the DNA, the column was placed in a clean microcentrifuge tube and 30 µL of buffer NE was added directly in the membrane column and then incubated at room temperature and centrifuge for 2 minutes. The gDNA product was stored at -20°C.

3.2.2 Genotyping *of P. falciparum Pf*MDR2 KO parasites

Edited-parasite lines were genotyped for *pfmdr2* KO confirmation by polymerase chain reaction (PCR) followed by gel electrophoresis. PCR was adopted to verify *pfmdr2* mutant and WT cultures (Figure 10). To accomplish this, primers in the 5', 3' region and WT (control) were used as described in the Table 1 and Figure 11 below, to confirm plasmid integration in the *pfmdr2* mutant parasites. The reaction condition used is presented accordingly in Table 2.

Following PCR, agarose gel electrophoresis was used to confirm the amplified DNA of the mutant parasites. Agarose gels were made by combining agarose with 1X Tris-acetate-EDTA (TAE) buffer [20 mM acetic acid, 1mM EDTA, 40 mM Tris (pH 7.6)) at a final concentration of 1%. The agarose gel was heated until brought to a boil and then cooled under running water to a temperature of about 50°C. NZYTech GreenSafe Premium was added into the mixture, so the DNA bands can be visualized later under ultraviolet light. The gel was then poured into a horizontal gel cast and left to solidify at room temperature. To determine the molecular weight of the bands, GeneRuler™ 1kb DNA Ladder (Thermo Scientific) was used. All gel electrophoresis were carried out in an electrophoresis machine at constant 100V in 1X TAE buffer. Images of the gel were taken using Gel Doc™ EZ System (Bio-Rad).

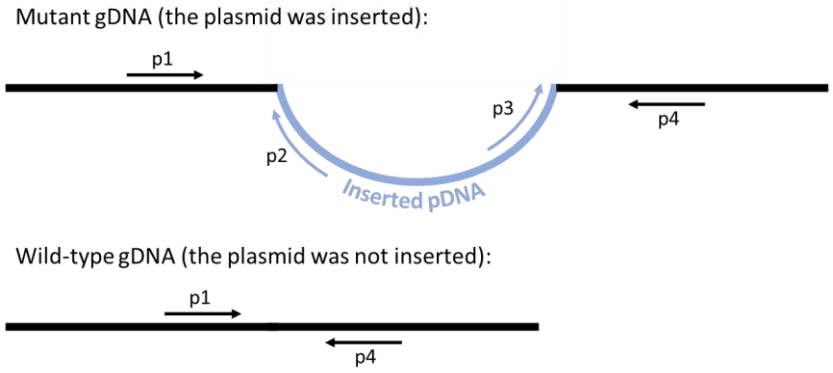

Figure 10: PCR strategy of primers used for verifying mutant and WT parasites.

Table 1: Primer sequence and PCR strategy for mutant and WT parasites confirmation.

Reaction	Primer sequence (5' → 3')	PCR strategy
5'	P1 – CCGGTATCTTAGTTATATTG	95°C – 3 min; 35 cycles: 95°C – 30 sec, 60°C – 30 sec, 72°C – 30 sec; 72°C – 10 min; 4°C – ∞
	P2 – CTTGTTGAATTAGATGGTG	
3'	P3 – TATCTTTATAGTCCTGTCG	
	P4 – TATATTTAGGTTGGGCATC	
WT	P1 – CCGGTATCTTAGTTATATTG	
	P4 – TATATTTAGGTTGGGCATC	

Table 2: Reaction condition used in the confirmation PCR.

Reaction	
5'	100 µM of each primer, 2 U of NZYTaq II Green Master Mix (Supreme), 7µL of endo-toxin free water and 1 µL of DNA sample in a total volume of 20µL.
3'	100 µM of each primer, 2 U of NZYTaq II Green Master Mix (Supreme), 7µL of endotoxin-free water and 1 µL of DNA sample in a total volume of 20µL..
WT	100 µM of each primer, 2 U of NZYTaq II Green Master Mix (Supreme), 7µL of endo-toxin free water and 1 µL of DNA sample in a total volume of 20µL.
Control	100 µM of each primer, 2 U of NZYTaq II Green Master Mix (Supreme), 7µL of endo-toxin free water and 1 µL of endo-toxin free H_2O sample in a total volume of 20µL.

3.2.3 Construction of *Pf*MDR2 KO parasites

3.2.3.1 Plasmid DNA isolation from E. coli competent cells

Plasmid DNA (pDNA) was obtained from the recombinant *Escherichia coli* competent cells using the NZYMaxiprep™ Kit following the manufacturer's guidelines. The Maxiprep technique was designed for large-scale generation of pDNA quantities of up to 500 µg. Using this technique, we obtained plasmid DNA concentrations ranging from 1556.9 ng/ µL to 2602.1 ng/ µL. First, *E. coli* competent cells containing the *pfmdr2* gene were expanded into 400 mL lysogeny broth (LB) liquid media [10 g/L bacto-tryptone, 5 g/L yeast extract and 10 g/L NaCl] with the appropriate antibiotic. The cells were cultured in a shaking incubator at 37 °C overnight. The *E. coli* cell culture, grown overnight was collected by

centrifugation at 4000 rpm for 15 minutes. The cell pellet produced from this process was resuspended in 12 mL of NML1-EF solution containing Rnase and vortexed vigorously. To the resuspended cell solution, 12 mL of NML2-EF buffer was added and mixed gently by inverting the tube 6 – 8 times. The solution was then incubated at room temperature for 2 – 3 minutes. Next 12 mL of pre-cooled buffer was added to the suspension and the lysate formed was mixed gently by inverting the tube for 6 – 8 times again. The suspension and lysate were incubated on ice for 5 minutes. After this, the lysate formed was separated from the suspension using a wet filter and the wet filter transferred onto a NZYMaxi-EF Column. The column was washed a couple of times following the manufacturer's instructions and the flow through discarded.

To elute the pDNA from the column, 15 mL of NMEL-EF buffer was dispensed into the NZYMaxi-EF Column. The eluate was then collected in a clean tube, precipitated (by adding 11 mL of room-temperature isopropanol), and centrifuged at 4000 rpm for 1 hour 30 minutes at 4°C. After carefully discarding the supernatant, 5 mL of 70% (room-temperature) and centrifuged at 4000 rpm for 30 minutes. Ethanol was carefully removed from the tube and the cell pellet was left to air dry in an aseptic environment. The cell pellet was then resuspended in Cytomix [10 mM/L K_2HPO_4/KH_2PO_4, 120 mM/L KCl, 0.15 mM/L $CaCl_2$, 5 mM/L $MgCl_2$, 25 mM/L HEPES, 2 mM/L EGTA, adjusted with 10 M/L KOH to pH 7.6]. After separating plasmid DNA, the concentration and purity were measured using NanoDrop™ 1000 spectrophotometer (Thermo Scientific).

3.2.4 *P. falciparum* transfection

Parasitized erythrocytes were electroporated with the pDNA extracted from the *E. coli* cells. Parasitized RBCs (at 4% haematocrit) were transfected with 50 µg of pDNA. To this mixture, pure cytomix solution was added and transferred to a Gene Pulser®/MicroPulser™ Electroporation Cuvette. The Cuvettes were placed in a Gene Pulser Xcell™ (BioRad) electroporator, and an electric pulse at 0.31 kV with capacitance of 950 µfD was allowed to pass through the cells. This technique is utilized to create pores in the membrane of the cells allowing the pDNA to be incorporated. After the electroporation procedure, the parasites were washed in 3 mL of MCM and transferred to a 50 mL falcon, to which gas was added. The falcon was placed in an incubator for an hour, for the cells to recover. After an hour, the resuspended supernatant was aspirated and 5 mL of MCM added. This mixture was transferred to T_{25} flasks and maintained under normal conditions as earlier described. To generate a *Pf*MDR2 KO line, plasmids were transfected into both 3D7 and Dd2 *P. falciparum* strains.

3.2.5 *P. falciparum* selection

The transfected cultures were maintained until parasites re-emerged (about 2 weeks). Parasitaemia of the cultures was monitored daily till they reached an adequate parasitaemia (≥1%). Then, the KO cultures were selected with 2.5 nM WR99210, an antifolate drug that selects for parasites with the presence of h*dhfr*, present in our plasmid (strategy construction presented in Figure 11). WR99210 was added to the culture daily (for 5 days) until no living parasites were seen under the microscope. Usually, after several days we observe a re-emergence of resistant parasites, however, in our case there was no re-appearance of parasites. Thus, we were unable to achieve episomally integrated mutant parasites.

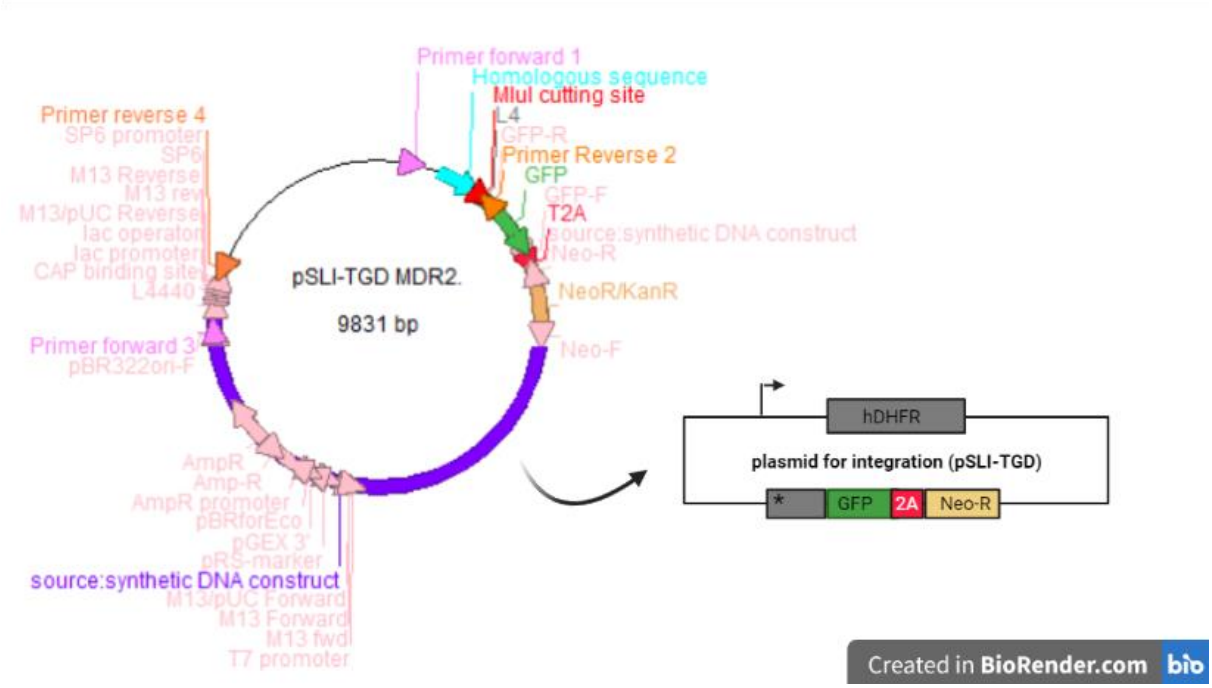

Figure 11: Gene editing strategy used in the construction of *Pf*MDR2 mutant parasites. pSLI-TGD containing *pfmdr2* gene (which is the homologous sequence) was constructed and inserted into the parasite genome along with a green fluorescence protein (GFP) FP, a skip peptide (2A) and Neomycin-R (which confers resistance to G418). The resistant marker – hDHFR incorporated into mutated parasites were selected with WR99210.Adapted from Addgene, Created with BioRender.com.

3.2.6 Drug susceptibility assays

*Pf*MDR2 drug susceptibility assays were carried out in flat-bottom 96 well plates in 200 µL of MCM at 1% haematocrit and 0.4% starting parasitaemia. Drug plates were prepared prior to an assay with descending concentrations – two-fold dilution in each successive well – of chloroquine, dihydroartemisinin, piperaquine, pyrimethamine, pyronardine, desethylamodiaquine, mefloquine and lumefantrine with initial concentrations of 1000 nM, 50 nM, 400 nM, 100 nM, 90 nM,1000 nM, 200 nM

and 50 nM respectively. As positive growth control two wells were left without any drug exposure. After 72 hours, parasitaemia was measured in the fluorimeter as explained in 2.3.1.

3.3 Study 3: Phenotypic features of the *P. falciparum* plasmepsins

3.3.1 Haem Fractionation Assay

Haem fractionation assay [132] was performed on tightly synchronized parasites (as described in 2.1.2) at 0–3-hour post-invasion rings stage. In this assay, previously constructed and characterized edited-parasite lines with an extra copy of *pfpm2* and the hybrid of the PM 1 and PM 3 genes *(pfpm3-1)* were used [133]. Parasitaemia of the cultures were obtained by optical microscopy or flow-cytometry. Cultures prepared were maintained in T_{25} flasks at 2% haematocrit and parasitaemia of 0.7%.

Following this, samples were collected at two time-points of parasite culture: 0 and 32 hours. At each time point, 2 mL of iRBCs (0.7% starting parasitaemia) were collected from each culture in aliquots and centrifuge at 1500 rpm for 5 minutes. The resuspended supernatant was aspirated and combined with 1800 µL of 1X PBS and 200 µL of 1% saponin, agitated and incubated at 37°C for 2 minutes to lyse the iRBCs. Following this, centrifugation was performed on the mixture at 2000 rpm for 15 minutes. The supernatant generated was removed and the pellets formed were washed twice with 500 µL of 1X PBS and centrifuged at 3000 rpm for 7 minutes. At the last time, the supernatant was discarded, resuspended in 100 µL of 1X PBS and stored at - 4°C.

Haemoglobin, free haem, and HZ were obtained at 3 respective phases of the fractionation process. In the first phase, thawed samples were mixed with 50 µL of water and sonicated for 5 minutes in a SONOREX SUPER ultrasound bath (Bandelin). The pellets generated were combined again with water and 0.2M HEPES buffer (pH – 7.5) and centrifuge at 3600 rpm for 20 minutes.

The resuspended supernatant was transferred into Eppendorfs and 50 µL of 4% sodium dodecyl sulphate (SDS) was added, sonicated for 5 minutes, and incubated at 37°C for 30 minutes. The resulting mixture was combined with 50 µL each of NaCl (0.3 M) and 25% pyridine (in 0.2 M HEPES buffer). From this solution, 200 µL was taken and kept aside, marking the completion of the haemoglobin fractionation phase. Thus, we moved on to separate free haem.

The free haem fractionation phase began with resuspending pellets (obtained from the above protocol) in 50 µL each of water and SDS (at 4%). They were then sonicated for 5 minutes and incubated

at 37°C for 30 minutes to stabilize free haem. Next the solutions were combined with 50 µL each of HEPES (0.2M), NaCl (0.3 M) and 25% pyridine, centrifuge for 5 minutes and transferred to other Eppendorfs. The solutions were further diluted by adding water to a final volume of 400 µL, thus marking the completion of the free haem fractionation phase.

To obtain HZ, pellets containing HZ (obtained from the haem fractionation phase) were resuspended in 50 µL of 0.3 M NaOH and sonicated for 15 minutes. The resulting mixture was then incubated at 37°C for 30 minutes. Following this, 50 µL of HEPES (0.2 M), HCl (0.3 M), 25% pyridine and 150 µL of water were added to the incubated mixture and transferred to new Eppendorfs.

After these procedures, the samples were transferred to a 96-well plate and analysed, using a Varioskan® Flash fluorimeter (Thermo Scientific) and SkanIt™ software to determine the concentration of haemoglobin, free haem and HZ ratio in WT and mutant parasites. The fluorimeter was set at an excitation wavelength of 485 nM, emission wavelength of 530 nM and an excitation bandwidth of 12 nM with a measurement time of 100 ms. Results obtained were calculated in Microsoft Excel Spreadsheet software and graphically analysed in GraphPad Prism 7.0.

Calculation Used:

To obtain Total Absorbance (Abs) = Abs of hb + Abs of free haem + Abs of HZ

To obtain fractionation (%) = (Abs fraction÷Abs total) ×100

To Normalize at 32 hours (T32) = %fractionation at T32/% fractionation at T0 (for haemoglobin, free haem and HZ) for mutant and WT parasites.

CHAPTER 4

RESULTS

4.1 Phenotyping infected red blood cells through relaxometry spectroscopy

Given the powerful analytical capacity of Nuclear magnetic resonance (NMR) in obtaining detailed information about the structure, dynamics, reaction state, and chemical environment of molecules and knowing that along the parasite cycle haemoglobin decreases as HZ increases, attaining its maximum content in the later stages, we have characterized the life cycle of *P. falciparum* using T_1-T_2 relaxometry spectroscopy.

To achieve this, we applied two approaches:

- Slack synchronized cultures to track and compare the behavioral patterns of the intracellular stages along time;
- Tight synchronized cultures to determine changes that occur at specific intracellular stage and parasite concentration.

4.2 Time-domain iRBC characterization of slack synchronized parasites

Slack synchronized *P. falciparum* iRBCs samples were taken with parasites at different morphological stages (rings (0-18 hours), trophozoites (18-36 hours), and schizonts (36-48 hours)) and at different parasitemia (0.01%, 0.1%, and 1%). Each sample, prior to being measured, was collected into three capillaries to create technical replicates and then measured over time. This implies that each of the three capillaries was measured consecutively to create many sample readings. Each morphological stage at a particular parasitemia was read consecutively for 8-12 hours using the three capillaries as technical replicates (Figure 12). It is important to emphasize that these concentrations were measured for a period of 6-12 hours on different days. With this procedure, we derived T_1-T_2 readings as the parasite progressed

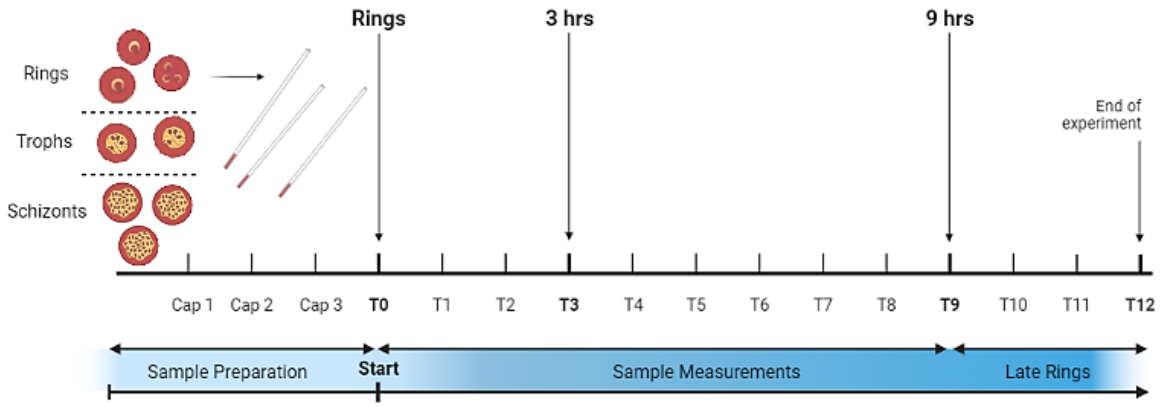

Figure 12: Schematic diagram representing sample preparation and characterization of rings collected in three capillaries. The three capillaries were read at time points T0 to T12 corresponding to 0h to 12h,respectively. This procedure was performed for rings at 0.01%, 0.1%, and 1% and for trophs and schizonts as well. Created by BioRender.com

through its morphological stages in real-time. T_1-T_2 readings were obtained using Carr-Purcell-Meiboom-Gill (CPMG) pulse sequence and inversion recovery by CPMG, respectively.

Results from slack synchronized cultures indicate that T_1 of RBCs infected with parasites at ring stage, reduced with increasing parasite concentration (Figure 13A); we observed that we had significantly higher T_1 readings ($P < 0.005$) at 0.01% parasite concentration than at 1%, where we obtained the shortest relaxation time. T_2 readings (Figure 13B), however, showed a slight fluctuation with an increase at 0.1% and a further significant decrease at 1% ($P < 0.0001$). Consequently, this caused fluctuations in A-ratio, which is the ratio of T_1 asnd T_2 relaxation times and increases with increasing parasitaemia and parasite maturity. A-ratio readings (Figure 13C) reduced at 0.1% parasitemia and increased again at 1% ($P < 0.0001$), due to fluctuations in T_2. Each parasitemia of rings was measured on different days resulting in several biological replicates. Moreover, in order to minimize error due to small sample size , a particular parasitaemia was measured more than once on different days which created different biological replicates with divergent A-ratio values. This may be the reason we did not see a consistent trend in the increase of A-ratio across each parasitemia at this stage.

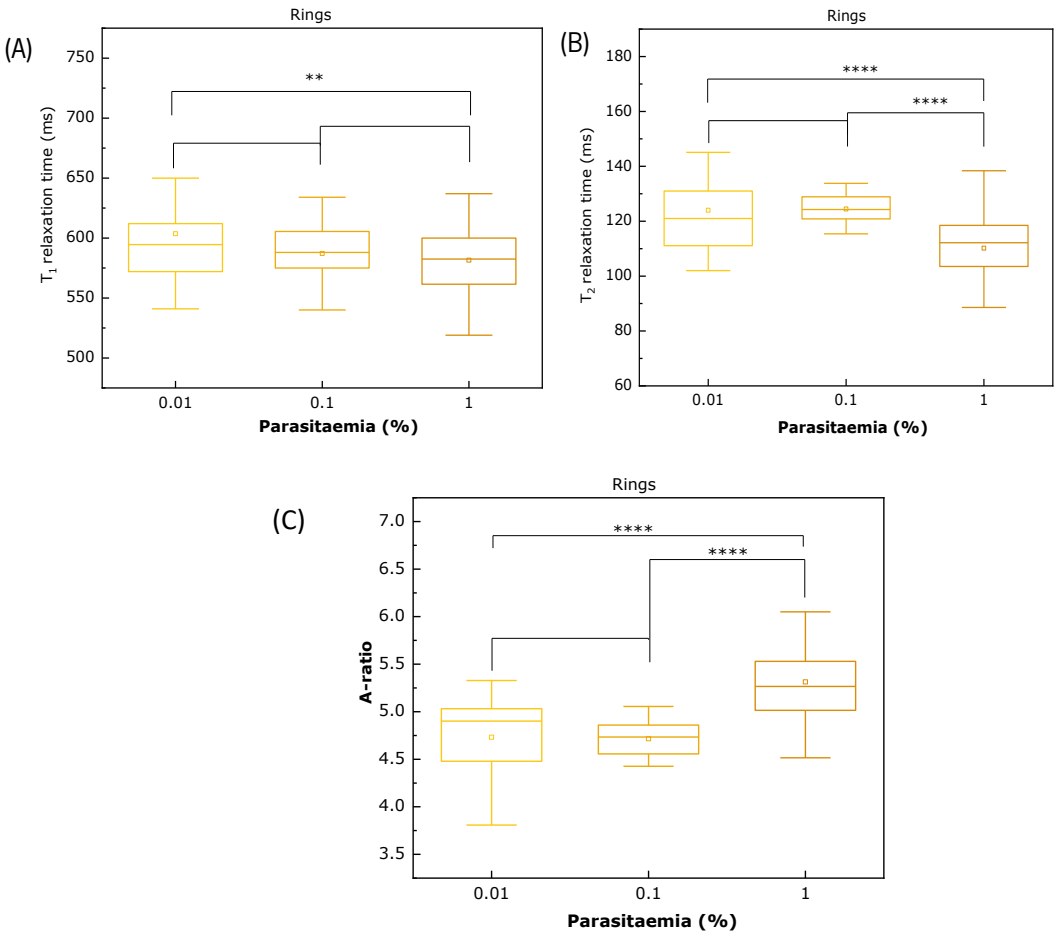

Figure 13: Time tracking T_1, T_2, and A-ratio readings of asynchronous rings across varying parasite concentration (0.01, 0.1, 1 %). **** ($P < 0.0001$), ** ($P < 0.05$), bars with no astericks represent non-significant P values.

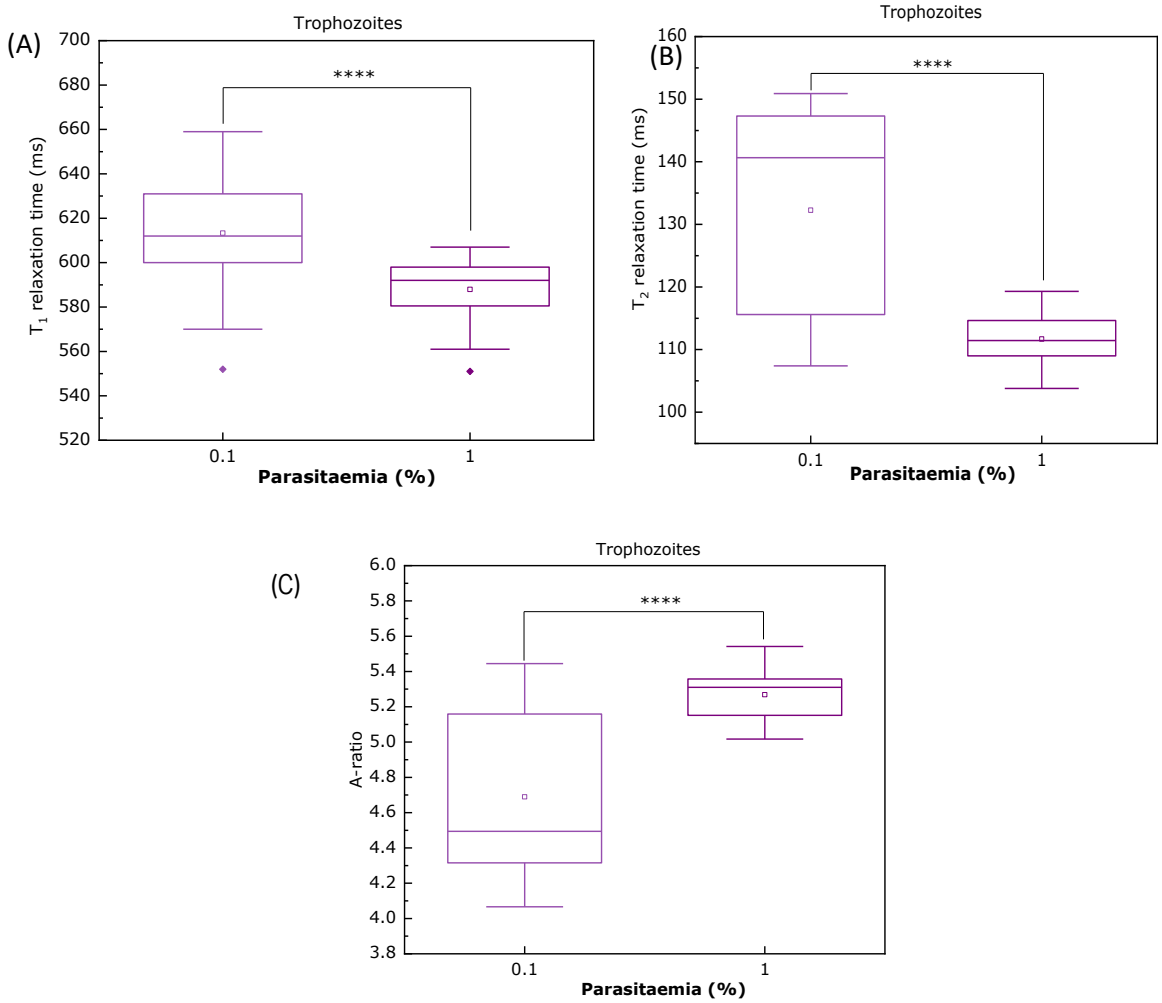

Figure 14: Image of Time tracking T_1-T_2 and A-ratio measurements of asynchronized Trophozoite stages across 0.01,0.1 and 1 % parasitemia. **** ((P> 0.0001), bars with no asterick represent non-significance).

The iRBC with parasites at the schizont stage, were characterized in the time-domain at 0.01% and 1% parasitemia (Figure 15). T_1 and T_2 readings obtained at this stage reflected similar results with trophozoites (Figure 14). However, it was a different case with A-ratio which was seen to decrease with increasing parasitemia.

The rationale behind this is that, at the trophozoite stage, A-ratio readings increased with increasing parasitemia, because again T_2 relaxation time reduced faster than T_1 relaxation time. T_2 is tissue-specific and decays faster than the time T_1 takes to recover and revert back to M_0. However, at the schizont stage, we saw that T_1 readings reduced slightly faster than T_2 and resulted in a decreased A-ratio value at an higher parasitaemia.

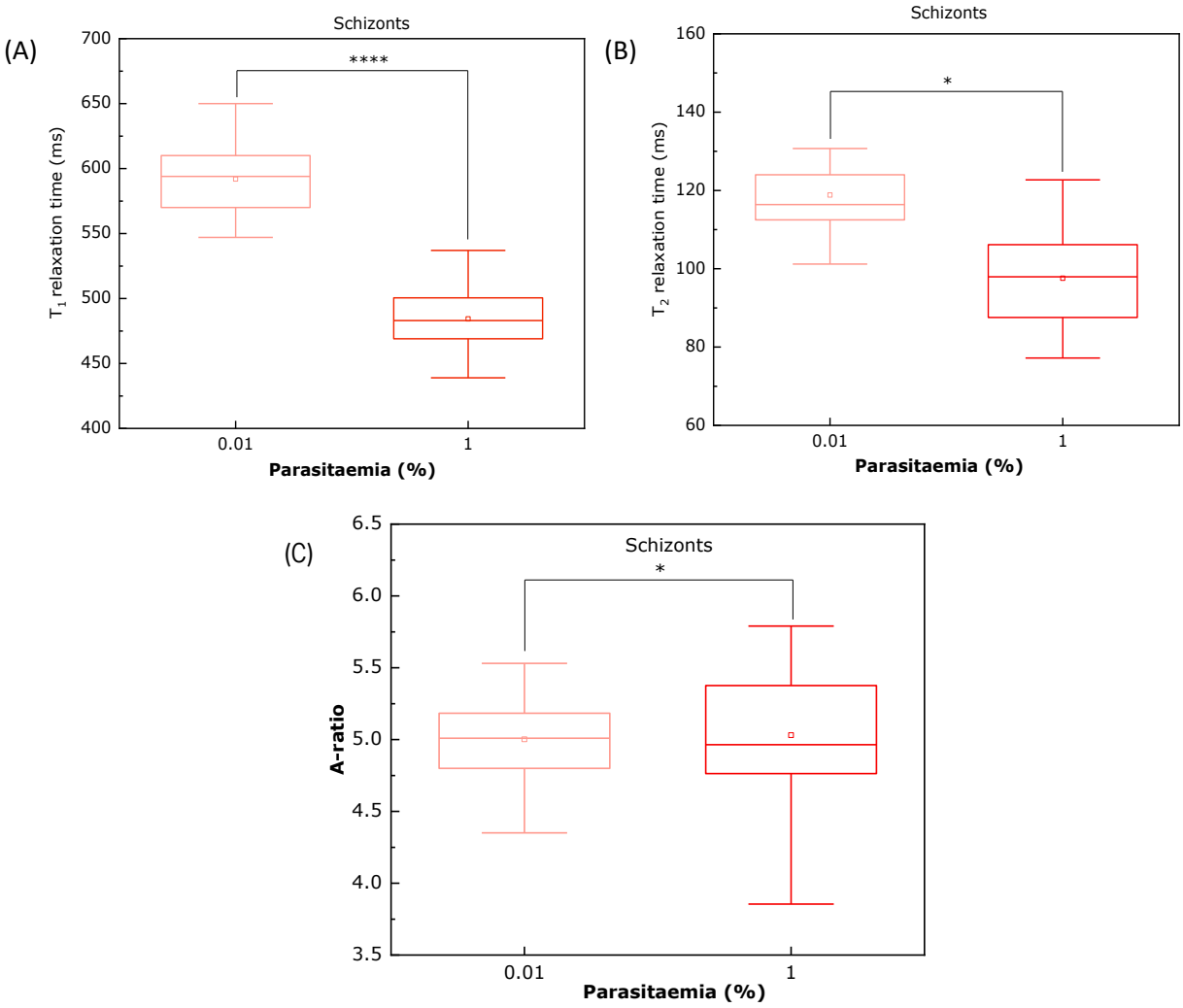

Figure 15: Time tracking T_1, T_2 and A-ratio readings of asynchronous schizonts stages at 0.01 and 1% parasite concentration. **** ($P < 0.0001$), * ($P < 0.05$).

To identify how T_1, T_2, and A-ratio vary between each intracellular stage we analyzed the stages at 1% parasitemia (Figure 16). Interestingly, we detected a behavioral pattern specific to each stage which reflected in T_1, T_2, and A-ratio values. T_1 displayed a slight increase from rings to trophozoites and then decreased rapidly at the schizont stage. This made, the A-ratio higher at the trophozoite stage since they are more metabolically active than early rings. A-ratio values, showed the same behavior pattern with T_1 relaxation time, which may be due to several reasons. To determine what specifically happened we analyzed the triplicate reading of all the timepoints (about 8-16 hours) for each parasite (Figure 17).

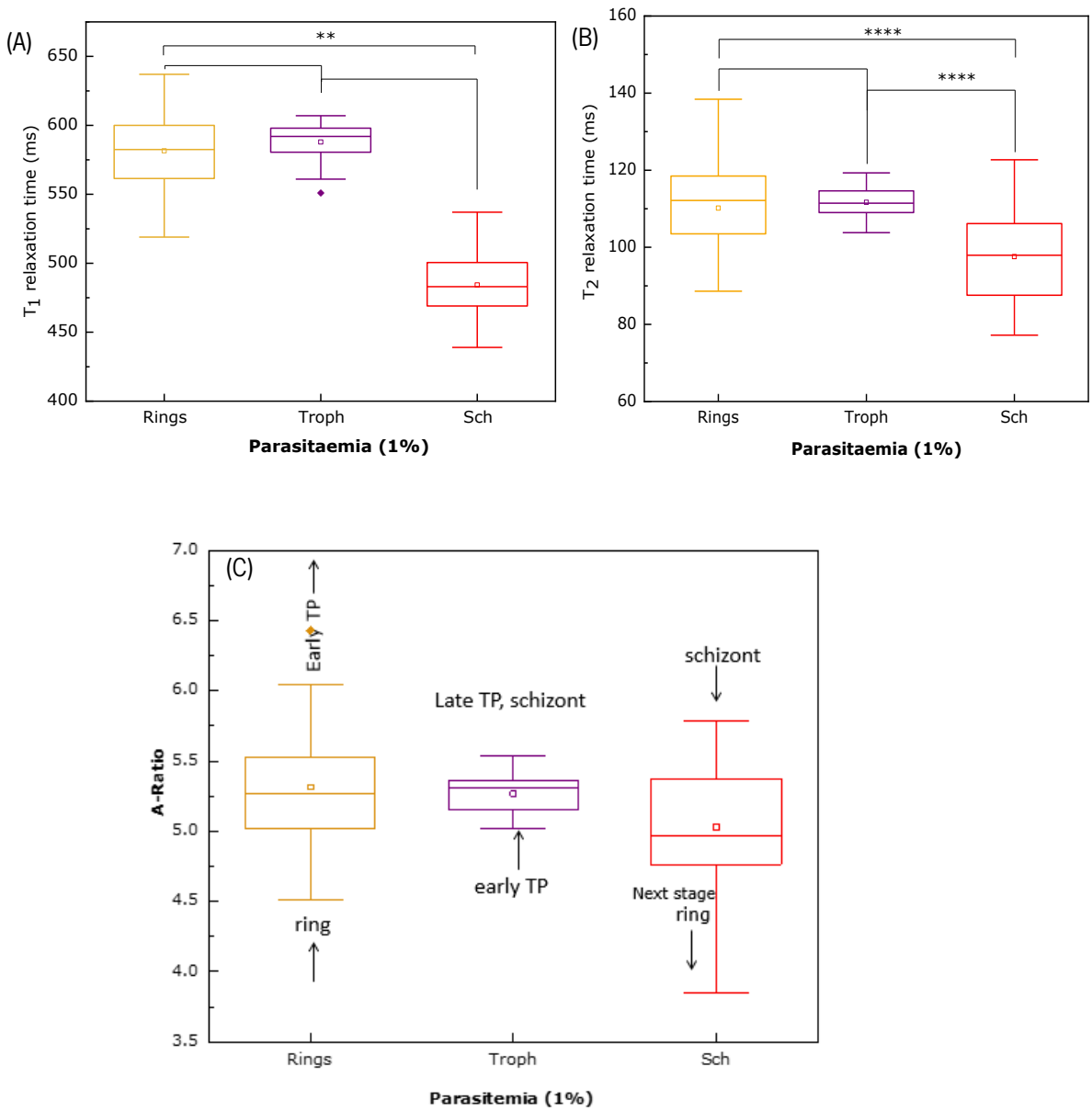

Figure 16: A-ratio values showing the behavioral pattern of the intra-erythrocytic stage at 1% parasitemia. **** ($P < 0.0001$), ** ($P < 0.005$).

In order to determine the impact of the magnetic field on the parasite cycle progression, we measured each capillary over time. This time-tracking method enabled us to detect differences at each level, as each capillary is exposed to a magnetic field over time. Here we analyzed the A-ratio values of the 8 -12 measurements of the triplicates over time ranging from 8-16 hours this was performed for all the stages at 1%.

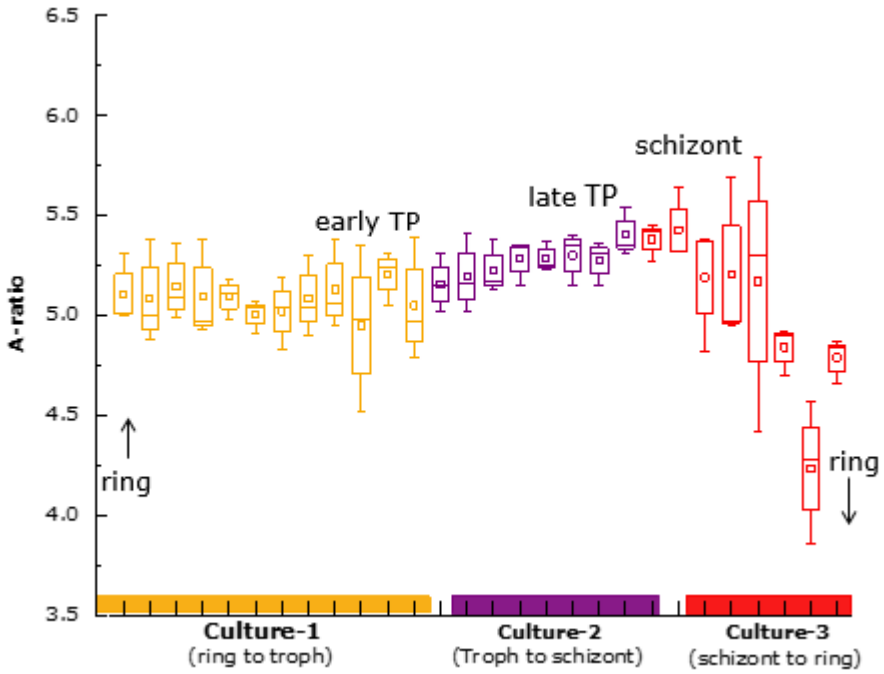

Figure 17: Reflects the progression of the intra-erythrocytic cycle over time. Starting from A-ratio readings of iRBCs at ring stage to schizonts and back to early rings.

Using this method we identified an undulating pattern across the stages (Figure 17), which gives an insight into what transpires across each stage of the intra-erythrocytic cycle. We could deduce that the A-ratio is almost constant during the ring stage, increasing in the trophozoite stages reaching a peak at the schizont stage, and then falls towards the ending hours of characterization. This pattern mirrors what occurs at the intracellular level of parasites, where the ring stage marks the initiation of haemoglobin degradation, and the trophozoite and schizont stages are characterized by increased accumulation of haem and formation of HZ crystals. This implies that with increased concentration of denatured haemoglobin and HZ, A-ratio readings increased at trophozoite and schizont stages. This analysis also gives an answer to why the mean value of A-ratio always fell at the schizont stage, being the most metabolically active. Thus as schizonts mature into late schizonts, and form merozoites in the iRBCs prior to an invasion, the cells lyse releasing HZ and other cellular contents into extra-cellular space, thereby neutralizing HZ concentration and the paramagnetic susceptibility conferred by the infected cells. This revelation re-enforces the uncomprising nature of the magnetic property of HZ in reflecting the physiological changes happening intra-cellularly before a new cycle begin.

4.3 Time-domain iRBC characterization of tight synchronized parasites

The same characterization regarding T_1, T_2, and A-ratio using NMR spectrometry was performed for tight synchronized *P. falciparum* Dd2 parasites. This approach was undertaken in order to

characterize haemoglobin/free haem/HZ ratios at different time points. Given that we obtained fluctuations in the measurements of slack synchronized parasites, here we optimized the protocol to reduce errors due to haemoglobin, free haem and HZ ratios. Tightly synchronized cultures were used, and measurements were taken at specific time-points, including rings at 0-6 hours, trophozoites at 25-30 hours, and schizonts at 36-40 hours. In addition, serial dilutions were made from the same culture to obtain the different parasite concentrations, thereby reducing the chances of errors as a result of multiple biological replicates.

4.3.1 Early intra-erythrocytic stage

T_1-T_2 readings of all stages were extrapolated using CPMG pulse sequence and inversion recovery by CPMG respectively. As observed in Figures 18A and 18B, T_1 and T_2 decreased with increase in parasitemia at the ring stage, however reduction was only observed between 0.01 and 1% parasitaemia ($P < 0.05$). Furthermore, it was seen that T_2 relaxation time reduced more rapidly than T_1 relaxation time resulting in an increase in A-ratio (Figure 18C). This trend demonstrated, that T_2 reduced more rapidly than T_1 as parasitemia increased.

4.3.2 Later intra-erythrocytic stages

In the trophozoite stage, we measured the same parasitemia levels as with the ring stages and compared T_1-T_2 values across (Figure 19). T_1-T_2 readings from the trophozoite stages showed reduced relaxation times between 0.01% and 0.1% but, there was a slight increase in T_1-T_2 relaxation times at 1% parasitemia.

This implies that trophozoite readings were not consistent with that of rings. We see there is an increase in A-ratio between 0.01% and 0.1% but again a decrease in A-ratio at 1% parasitemia. The trophozoite stage of *P. falciparum* is characterized by higher metabolic activities, leading to a higher accumulation of denatured haemoglobin as well as a higher concentration of HZ crystals. This could be identified by the general reduced T_1 and T_2 readings (across parasitemia) of trophozoites in comparison to rings. However, the inconsistency displayed at 1% parasitemia may be due to technical fault. Since capillaries at 1% were the last to be measured at each time point any unnecessary delay due to technical difficulty may lead to increased errors at the final measurements, therefore, increasing the mean of T_1 and T_2 values.

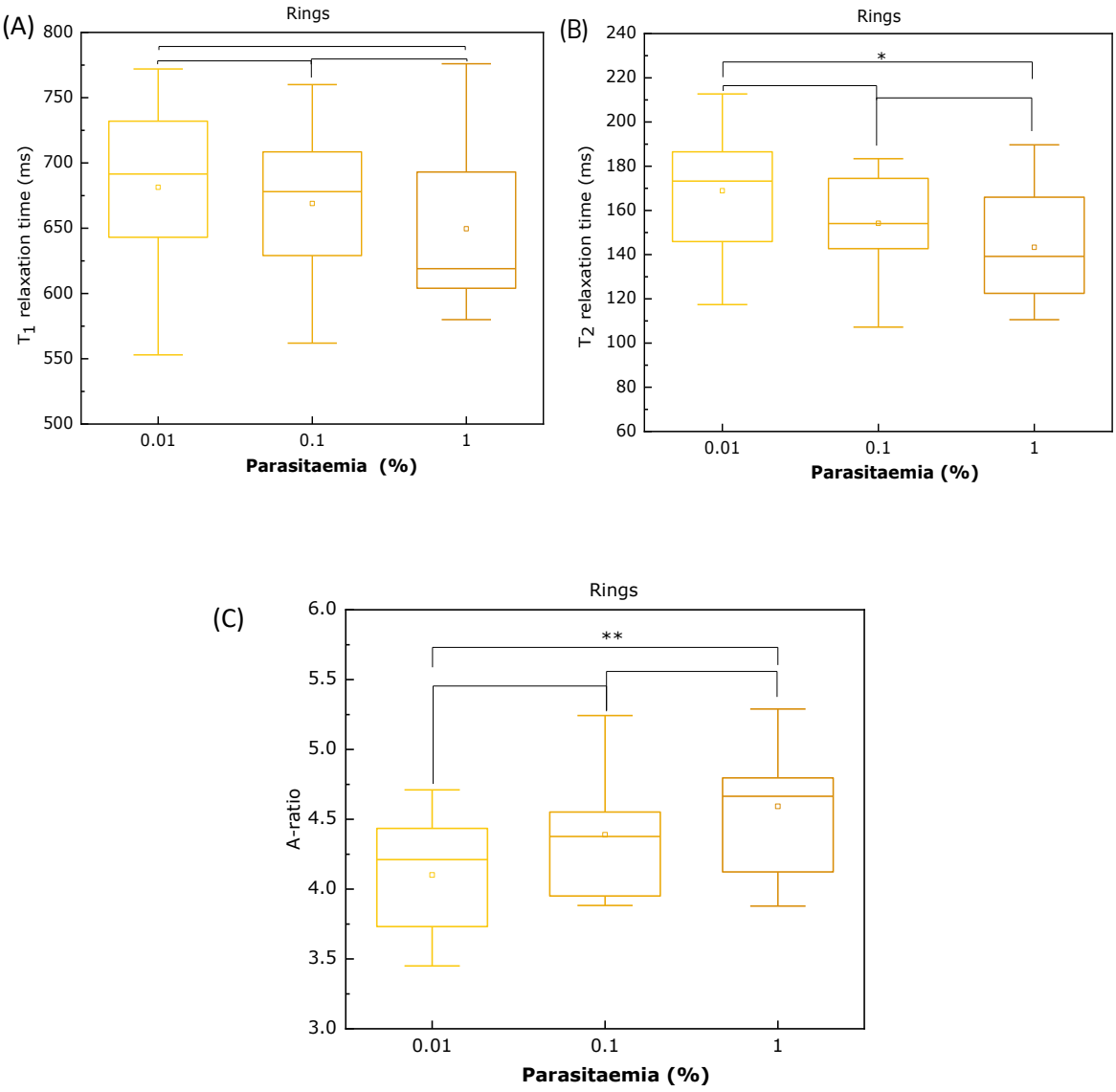

Figure 18: Rings across parasitemia (0.01, 0.1, 1 %) showing (a) Transverse and (b) Longitudinal relaxation time and (c) A-ratio Synchronized cultures. * ($P < 0.05$), ** ($P < 0.005$), bars with no asterick represents non-significant P value).

The schizont stage is the last morphological stage of the intra-erythrocytic cycle, before a new phase begins (Figure 20). At this stage, high levels of metabolic activity transpire within iRBCs as well as higher concentrations of haem conversion (to HZ crystals).

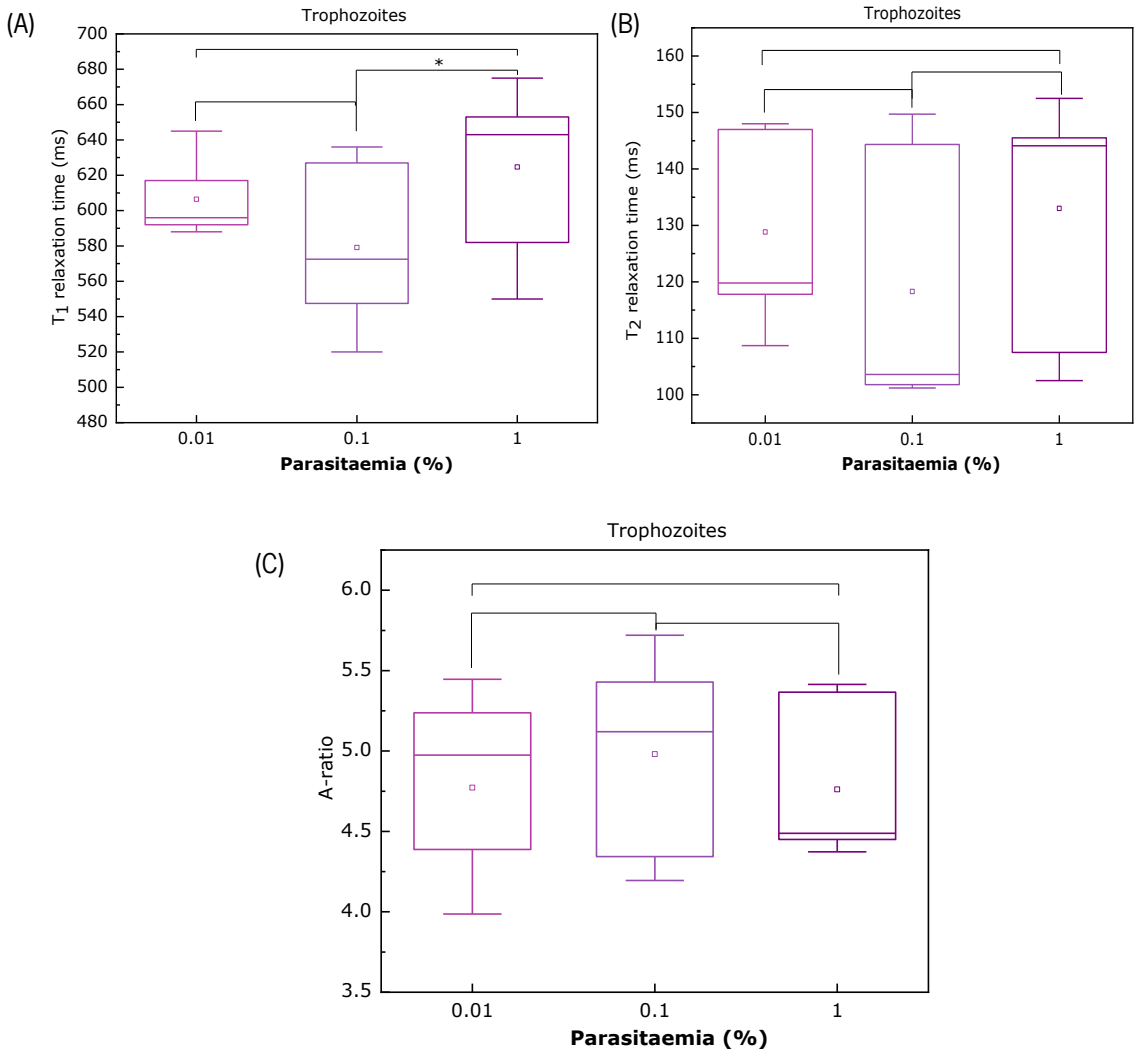

Figure 19: Image of T_1-T_2 and A-ratio measurements of Trophozoite stages across 0.01,0.1 and 1 % parasitemia. * ($P < 0.05$), bars with no asterick represents with non-significant *P* value.

NMR readings of the schizont stage as demonstrated in Figure 20C, reflected contrary A-ratio results. Findings from our study reflected increased relaxation times (T_1 and T_2) with increasing parasitemia. Furthermore, T_2 relaxation time increased more rapidly than T_1 leading to a consistent decrease in A-ratio across increasing parasite concentrations. These results were quite unique as they directly contrasted results from the other stages.

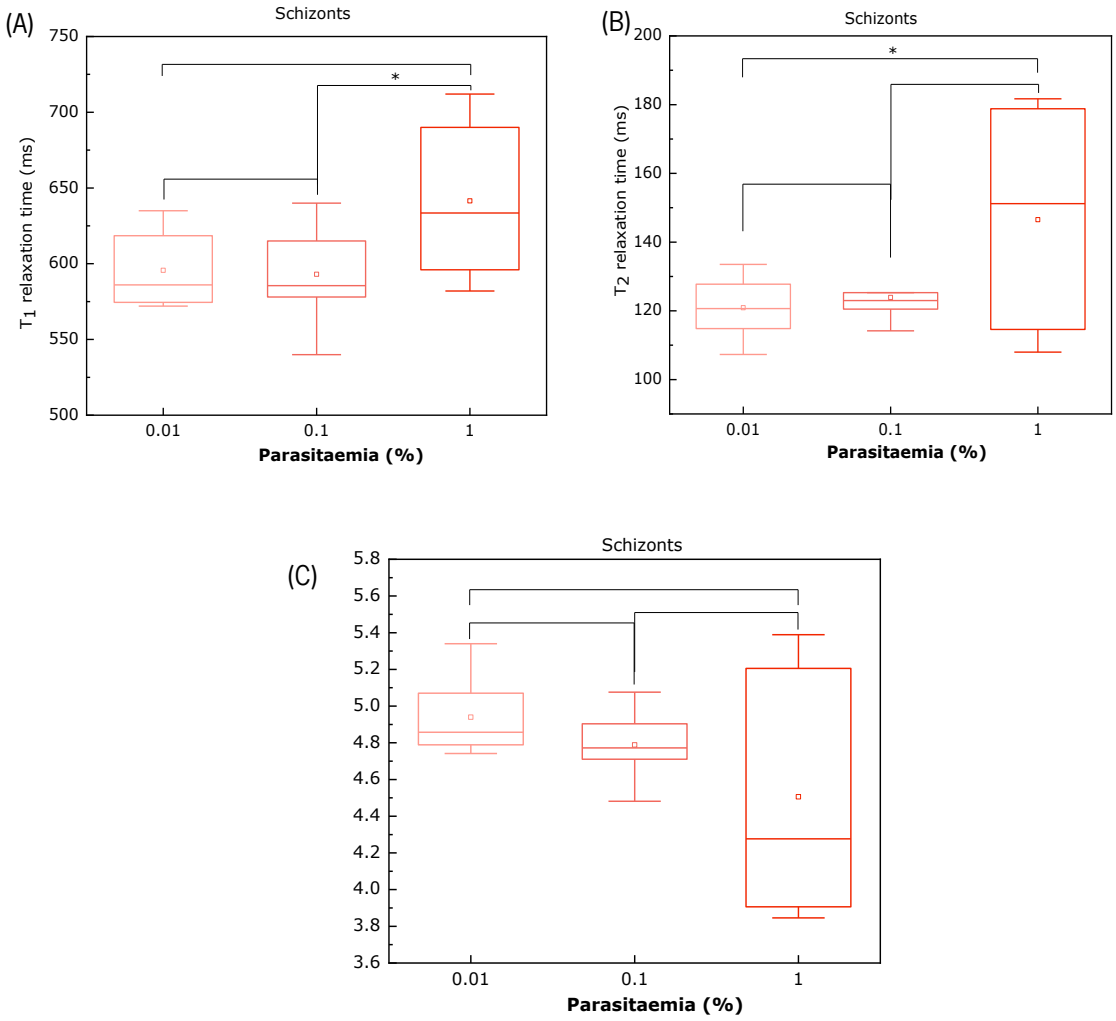

Figure 20: T_1, T_2, and A-ratio readings of Schizonts across different parasitemia (0.01, 0.1, and 1 %). * ($P < 0.05$), bars with no asterick represents with non-significant *P* value.

To understand the dynamics across the intra-erythrocytic stages, at different parasitemia, we exploited T_1 and T_2 readings of rings, trophozoites, and schizonts at 0.01, 0.1, and 1% parasitemia. With these readings, we could see what occurs as the parasite matures by directly comparing each stage with the same parasitemia.

First, we characterized rings, trophozoites, and schizonts at a parasite concentration of 0.01% as demonstrated in Figure 21. With the progression of the lifecycle from rings to trophozoites and schizonts, both T_1 and T_2 decreased, the decrease being more evident from ring to trophozoites ($P < 0.05$ and $P < 0.0005$ respectively) as well as rings to schizonts ($P < 0.0005$ for both T_1 and T_2). This is quite identical to results we identified from asynchronous schizonts at 1% (Figure 17). The increase in T_1 and T_2 readings may be due to the increase in haem production from the degradation of haemoglobin. As the parasite matures from rings to trophozoites, it becomes more metabolically active and poses more

oxidative stress to the iRBCs. However, as parasites grow into schizonts and further into late schizonts the fall in T_1 and T_2 readings may be due to RBC lysis and release of HZ extracellularly. Taking these two approaches into account, we see that the increase in HZ formation confers paramagnetic susceptibility to iRBCs and that it is easily detected by the NMR. The A-ratio values also exhibited this pattern across the stages (Figure 21C).

The same graphical analysis was performed for 0.1% and 1% parasitemia across each morphological stage.

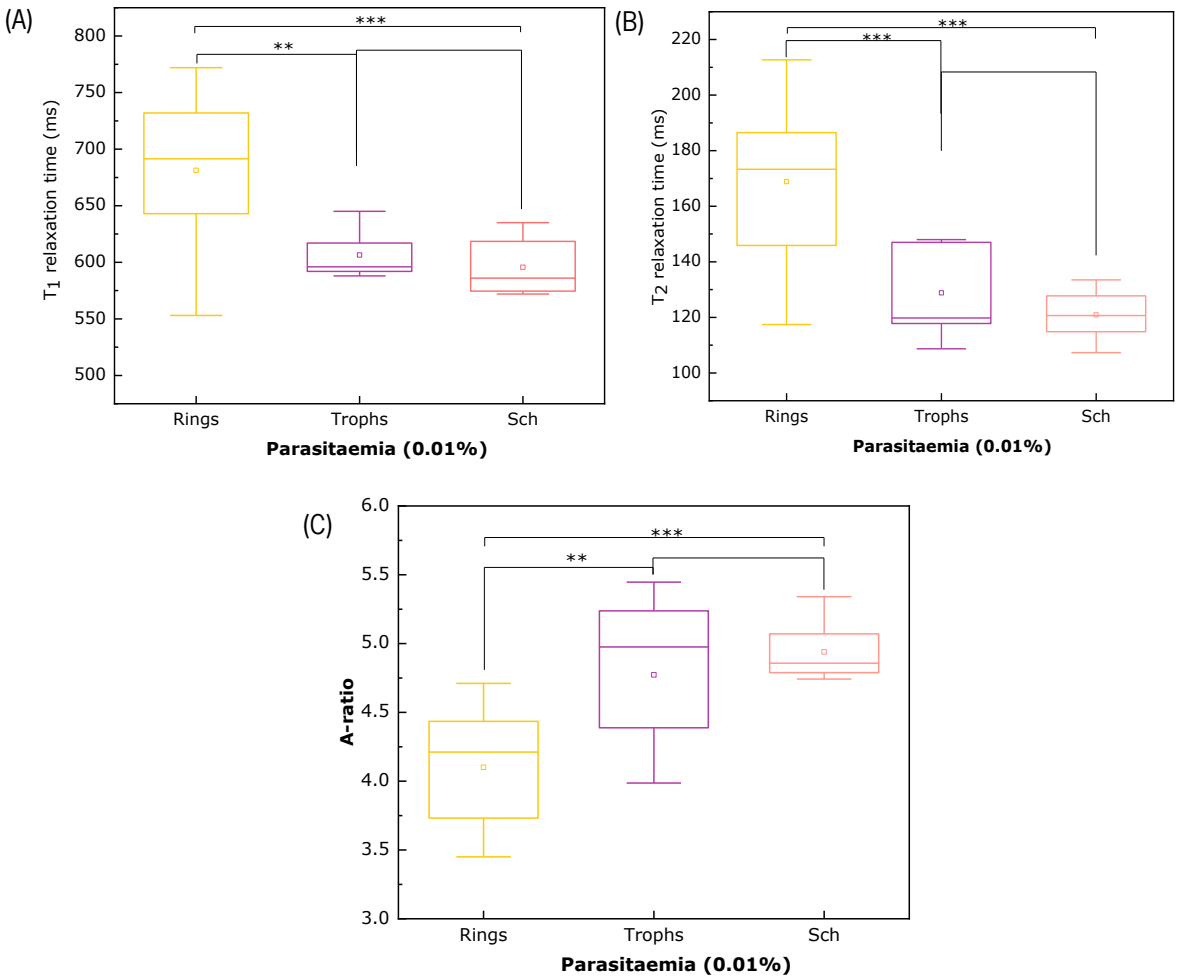

Figure 21: T_1, T_2 and A-ratio readings across *P.falciparum* intra-erythrocytic stages at 0.01% parasitemia.*** ($P < 0.0005$), ** ($P < 0.005$), bars with no asterick represents with non-significant *P* value.

At 0.1% parasitemia, we identified significantly decreased T_1 and T_2 relaxation times between rings and trophozoites ($P < 0.0001$), and a slight increase between trophozoites and schizonts (Figure 22). A-ratio values also reflected a significant increase as rings progressed to trophozoites ($P < 0.0005$) quite identical to readings from 0.01% parasitaemia (Figure 22C).

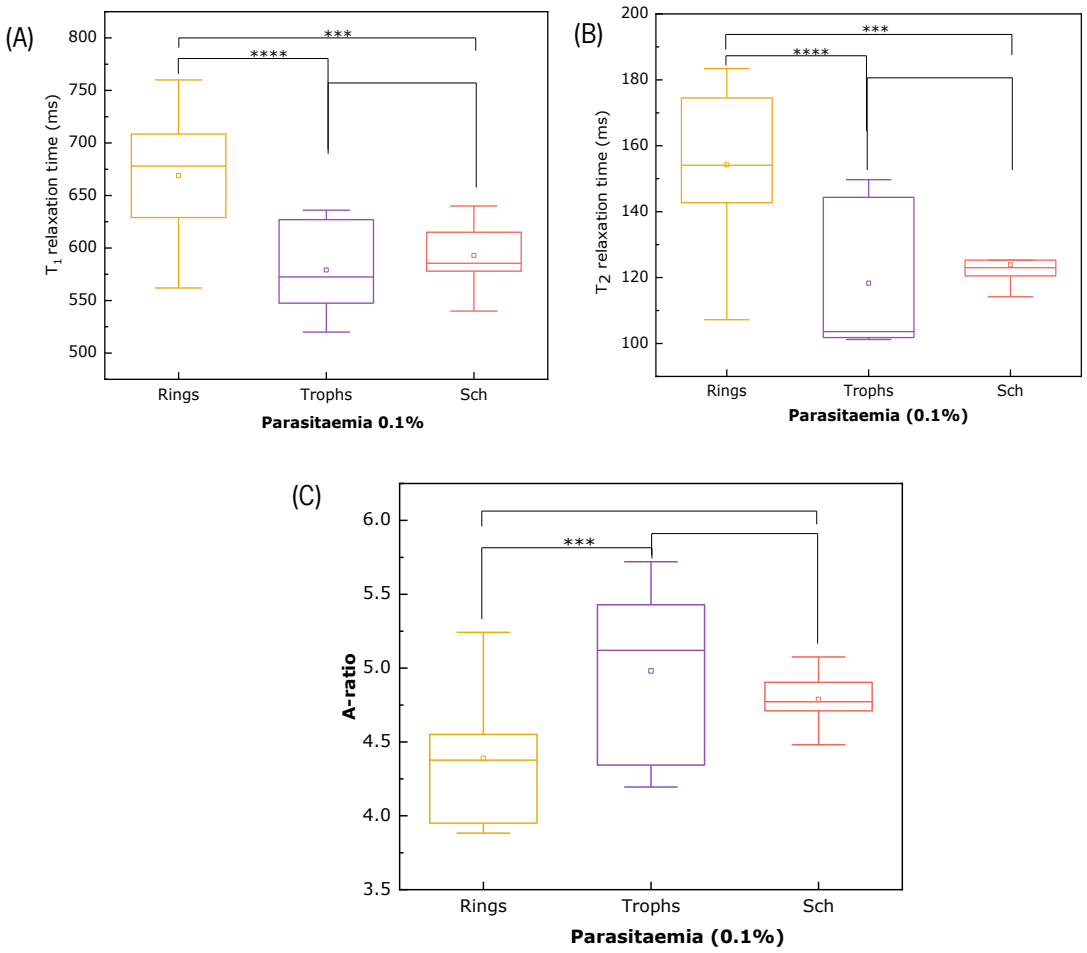

Figure 22: T_1, T_2 and A-ratio readings across *P.falciparum* intra-erythrocytic stages at 0.1% parasitemia. *** ($P < 0.0005$), bars with no asterick represents with non-significant *P* value.

When parasites at 1% concentration were analyzed, similar T_1 results with those of 0.01 % and 0.1% were also obtained. As shown in Figure 23, there was a reduction in T_1 readings of rings and trophozoites however, an increase in T_2 readings was detected with parasites at the schizont stage.

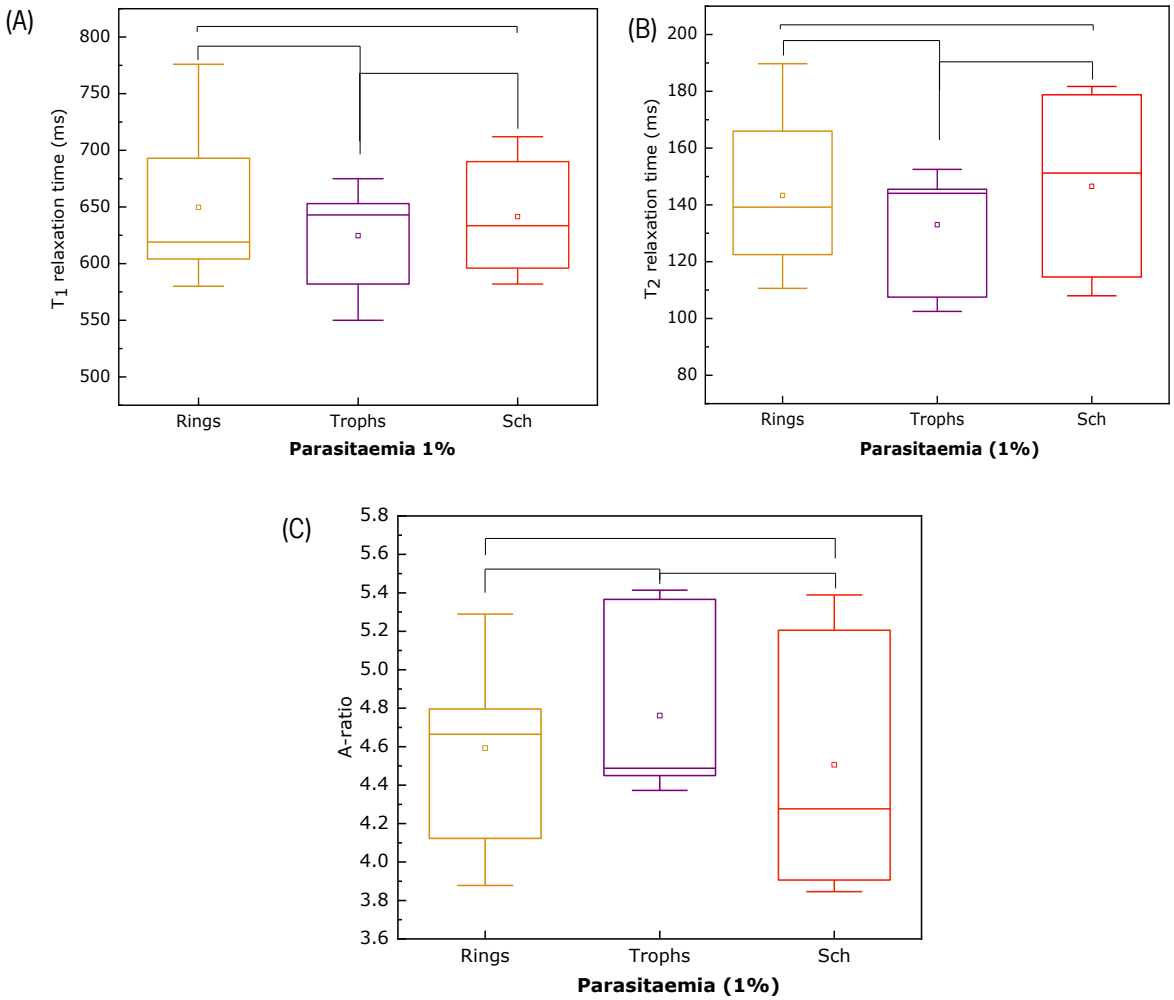

Figure 23: T_1, T_2 and A-ratio readings across *P.falciparum* intra-erythrocytic stages at 1% parasitemia. Bars with no asterick represents with non-significant *P* value.

4.4 Understanding the role of *Pf*MDR2 in the physiology of *P. falciparum* parasites

Transporter proteins are important to carry out several physiological functions and drug responses, but from the predicted 144 transporters in the parasite genome, most of their physiological function or link to drug resistance remains unknown [101]. That is the case of the *pfmdr2* gene whose function in the intracellular events of the malaria parasite is yet to be adequately understood. *Pf*MDR2 is a transporter present in the parasite's DV membrane and is associated with the efflux of heavy metals in parasites [103]. As Fe^{3+} is a heavy metal and previous work with *Pf*MDR2 KO lines, reported it to be sensitive to heavy metal rich environments, we questioned about the role of this transporter, and if it could be involved in the haemoglobin degradation to HZ formation pathway, altering the NMR profile [103].

Our group had previously commenced work in the construction of a *Pf*MDR2 KO parasite line aiming to study its functions in the intra-erythrocytic phase of development and its role in drug resistance, *in vitro*. The genetic strategy to construct the KO line was based on the SLI system [134], which uses a plasmid (pSLI-TGD; addgene #85791) with a promorterless targeting region (in this case the *pfmdr2* locus), fused to a green fluorescent protein (GFP) and linked to an additional selectable marker, neomycin (confers resistance to G418), that is separated by a skip peptide 2A as illustrated in Figure 24 [134]. The plasmid also contains the expression of *hDHFR* gene that confers resistance to the antifolate WR99210. In this approach, when single-crossover integration occurs into the targeted *locus*, the selectable marker is expressed, but not fused to the target, allowing integration selection. The *pfmdr2* gene comprises 3072 bp and is highly enriched in A and T, which is difficult for its amplification. For the construction of KO, only part of the *pfmdr2* sequence (466 bp) was used, after amplification from Dd2 WT strain. Selection of KO parasites needs two rounds of selection promoted by two drug resistance markers. A first selection with WR99210 allows the selection of parasites that contains the plasmid but not integrated in the genome of the parasite. A second round of selection is done with G418 that selects for single cross over event integration at the *pfmdr2* locus. These two rounds of selection were previously done and herein proceed to confirmation of the editing event. *P. falciparum* Dd2 culture that went through transfections protocol with the constructed pSLI-MDR2 plasmid and that went through two rounds of selection with WR99210 and G418, were thawed. When parasitaemia reached 1%, cultures were maintained under G418 selection for two cycles. Parasites were able to grow under G418 pressure indicating the successful integration of the plasmid and therefore assumed to be *Pf*MDR2 KO parasites.

A preliminary IC50 assay was conducted to evaluate if the *pfmdr2* KO alters parasites susceptibility to CQ, DHA, PPQ, pyrimethamine, pyronaridine, desethylamodiaquine, MQ and LMF, since most of these drugs' mechanism of action are somehow related with the haemoglobin degradation to HZ formation pathway. Although the concentrations of pyrimethamine and MQ do not seem suitable, results in Figure 24 suggest that *pfmdr2* KO does not alter the susceptibility to the tested drugs. This result does not corroborate with previous reports in the literature demonstrating an effect in *Pf*MDR2 in modulating drug response [135].

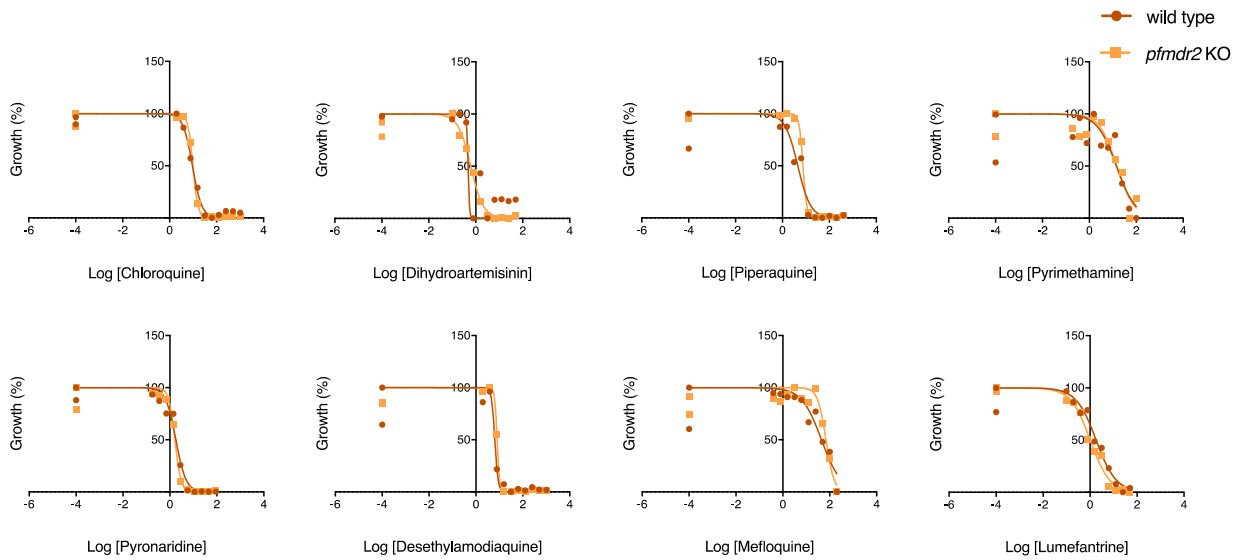

Figure 24: Graphical representation of *in vitro* IC50 assays carried out on *pfmdr2* KO parasites. Mean±SEM IC50 values are represented for chloroquine, dihydroartemisinin, piperaquine, pyrimethamine, pyronaridine, desethylamodiaquine, mefloquine, lumefantrine. At least three assays were performed for each drug.

Therefore, following, the Dd2 recombinant lines maintained at G418 pressure, was genotyped for integration confirmation with three sets of reactions: the 5' (851 bp), 3' (624 bp) and WT (837 bp; meaning WT culture and control of no integration). *P. falciparum* Dd2 WT strain and a Dd2 recombinant line with integration of pSLI in another gene were used as negative controls for integration and one with no DNA as control of the PCR reaction. Figure 25 demonstrates that no amplification was observed for the 5' nor 3' reactions at the constructed Dd2 *pfmdr2* KO line, while a correct band was observed for the WT reaction and in the edited line in another gene and in the negative controls for integration.

This result indicates that the plasmid for KO of *pfmdr2* was not integrated in the parasite genome in the targeted *locus*. Nevertheless, the culture was resistant to G418, suggesting that, most likely, the plasmid integrated somewhere else in the parasite genome and expression of neomycin resistance gene happened using a promoter elsewhere in parasite genome.

Several aliquots previously frozen were genotyped, and the same result was observed, concluding that all previous work was unsuccessful to construct a *pfmdr2* gene KO Dd2 line.

The plasmid designed and used for transfection was further subjected to mapping confirmation through restriction enzymes and Sanger sequencing. The restriction map and sequencing confirmed successful plasmid design further used to repeat transfection into *P. falciparum* Dd2 strain. After several transfection attempts, parasites were unable to grow under WR99210 revealing the unsuccessful expression of the plasmid episomaly. These results and the defined master thesis time, precluded this

study to move on with further phenotypic characterization including impact into drug response and haem species balance through haem fractionation assays and low-field NMR characterization.

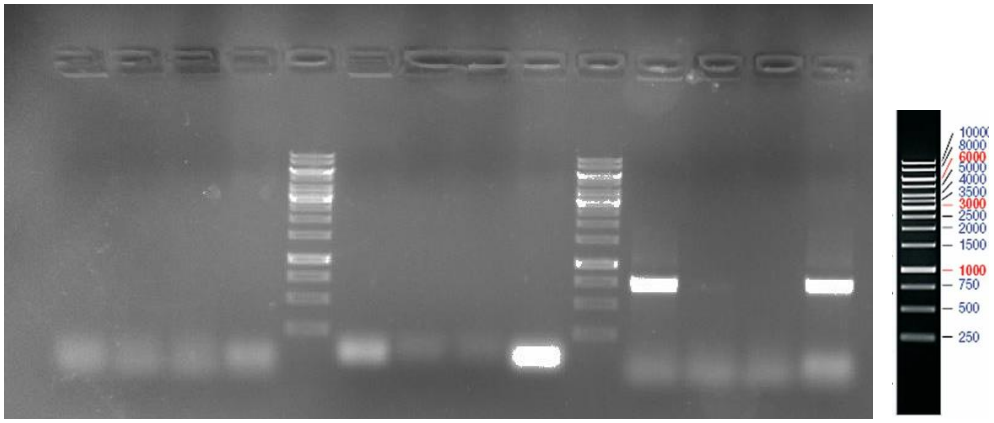

Figure 25: PCR results for confirmation of *pfmdr2* KO. Gel electrophoresis results indicating no amplification of the 5' nor 3' reactions at the constructed Dd2 *pfmdr2* KO line, while a correct band was observed for the WT reaction and in the edited line in another gene and in the negative controls for integration.

4.3 Plasmepsins impact into the balance of the haem species

Belonging to the family of aspartic proteases, plasmepsins are a sub-group of proteins known to play critical physiological roles in the degradation of haemoglobin. Plasmepsin I, II and III are found in the DV and are involved in cleaving haemoglobin into peptides [49]. However, these proteins are also involved in antimalarial drug resistance specifically to PPQ [92,95]. Studies [92,95] show that *pfpm2* and *pfpm3* genes gain an extra copy and *pfmdr1* transporter gene is de-amplified in PPQ resistant strains. Previous conducted studies by our group also confirmed this amplification.

As a follow up study from this research, our goal was to better understand how the plasmepsin proteins influence the concentration of haemoglobin, free haem, and HZ in the developmental stages of *P. falciparum*. To accomplish this, we used recombinant strains previously constructed in the lab containing plasmepsin gene copy number amplification and compared with its WT strain that just harbours one copy of the gene. In physiological conditions, plasmepsins aid the parasite in cleaving haemoglobin especially in metabolically active stages (such as trophozoites). With this understanding, we performed haem fractionation assay to determine what transpires in overly expressed plasmepsin parasites in comparison to WT parasites. Following the haem fractionation protocol, we obtained highly synchronized iRBCs at different time points (0 and 32 hours).

Results displayed in Figure 26 demonstrate that at 32 hours, WT parasite had the lowest concentration of haemoglobin than overexpressed plasmepsin parasite lines, while PM2 parasite had the

highest amounts of haemoglobin. Free haem concentrations were far higher in Dd2^{attb} parasites than the mutant strains, being that it cleaved more haemoglobin. PM3-1 parasite line possessed substantial amounts of free haem than the other mutant line - PM2, implying that the cleaved haemoglobin transformed successfully into free haem. When we analysed the HZ concentration of these parasites at 32 hours, we identified that the hybrid PM3-1 parasites possessed the lowest amount of HZ. PM2 parasites had the highest concentration of HZ, superseding the other parasites.

Furthermore, general comparison of parasites at 32 hour revealed higher amounts of free haem and HZ than parasites at 0 hour, this is understandable since at 32 hours trophozoites are more metabolically active than early ring forms.

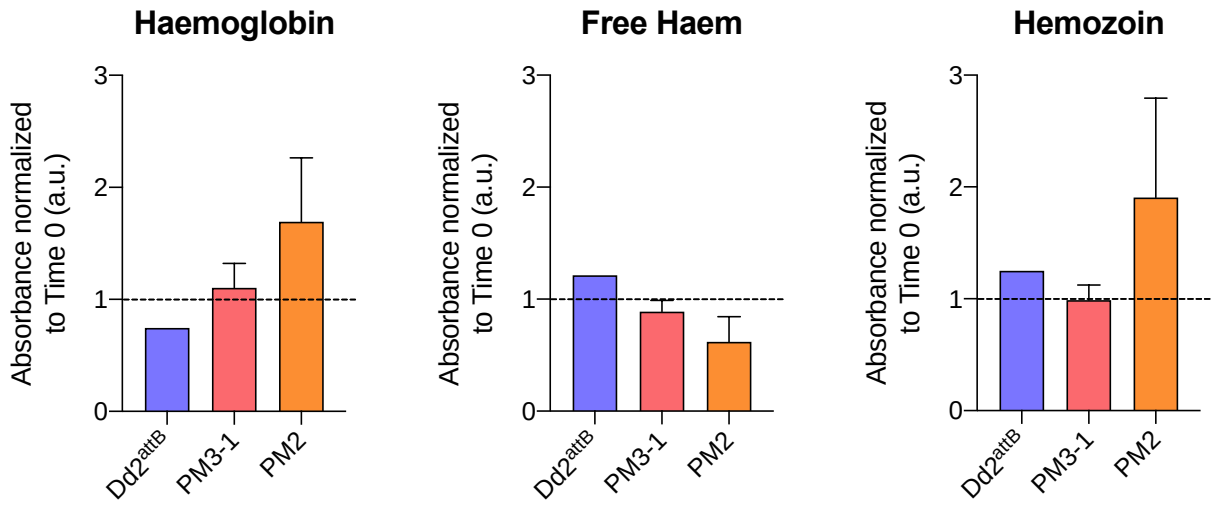

Figure 26: Graphical Analysis of Haem fractionation assay showing ratio of haemoglobin, free haem and HZ between different parasite lines at 32 hours.

CHAPTER 5

DISCUSSION

5.1 Phenotyping infected red blood cells through relaxometry spectroscopy

Malaria is the leading cause of morbidity globally, particularly in tropical and subtropical regions, where asymptomatic and low parasitaemia infections are prevalent. In these regions, many individuals carry the infections without presenting symptoms due to acquired immunity. These types of infections cannot be detected by current standard field diagnostics such as optical microscopy (limit of detection - 50 parasites/μL) and rapid diagnostic test (limit of detection - 100-200 parasites/μL) since in many cases the parasites are at a lower density. Nevertheless, infections like this cause malaria to thrive, as uninfected mosquitos get the parasite's gametocyte from infected carriers and pass it on to uninfected individuals [18]. Thus, instigating further transmission of the disease, and if left untreated may progress to severe complications. Moreover, these carriers without developing any symptoms of the infection, may cause imported malaria, or transmit the infection through blood transfusion, or organ transplant [136–140].

Effective diagnostic tools, that can identify these cases are critically needed as this facilitates the prevention of malaria transmission in endemic regions as well as internationally. Such infections can then be treated early, thus bringing us a step closer to global malaria elimination. In addition to this, a system that is capable of immediately identifying a parasite strain is crucial to stop the spread of drug resistance, an essential goal of this research. The NMR, however, has proven to be a reliable and sensitive tool for the detection of low-density malaria infections. In fact, our group has previously explored the potential of NMR for malaria diagnosis and obtained a sensitivity level of as few as 10 parasites/μL of iRBCs [124].

MRR is a diagnostic tool that measures the relaxation rate of the water content of cells/tissues by obtaining spin-echoes of the water content within their environment. It incorporates conventional NMR spectroscopy along with an MRI system. By using MRR, two-dimensional T_1 and T_2 relaxation readings provide visualization and identification, of the intermediate redox states and transient dynamic pathways of the blood specimen.

This strategy was applied to categorize diabetic patients into different oxidative sub-groups (in association with their glycaemic index) using whole blood samples. Redox homeostasis is a vital physiological phenomenon needed in regulating the balance between surrounding antioxidant and oxidative stress-inducing activities. Before oxidative stress occurs, there is a transfer of electrons leading to the creation of oxidized products. This oxidized product is more stable and can be easily measured by proton NMR relaxometry. Different techniques have been used to identify the redox properties of blood utilizing either optical or magnetic properties of Fe^{2+} present in haemoglobin. In this study, detection of reactive oxygen species (ROS) was done by quantifying the combined redox state of Hb/plasma by direct characterization of the H^1 relaxation states of the water content in blood samples using MRR. This method

proved successful in obtaining crucial clinical information on the oxidative stress levels of the patients; as haemoglobin in the blood exists in different redox states including Fe^{2+}, Fe^{3+} (as seen in malaria) and Fe^{4+}. Free haem (Fe^{3+} protoporphyrin IX) is a major contributor of oxidative stress also present in malaria infections and has lethal effects on both DNA/protein and iRBCs.

Considering this study, we applied the same principle to malaria. We utilized a low-cost benchtop NMR spectrometer system, to further explore the intra-erythrocytic cycle of the malaria parasite using the HZ formation pathway as a target. HZ is a paramagnetic biomarker that elicits specific signals with changes in parasite concentration and physiology. This magnetic change is mediated greatly by the transfer of electrons and a change in the redox state of RBCs from a low-spin diamagnetic state of haem (Fe^{2+}) into a high-spin paramagnetic state of HZ (Fe^{3+}).

With this, we are able to create a proof of concept by matching certain signals to certain parameters of the parasite, be it the stage or concentration level of the parasite. HZ crystals are also known to display unique intrinsic magnetic and optical properties, making them a more attractive target for developing novel diagnostic tools.

The intra-cellular stage of *P. falciparum* is characterized by increased haemoglobin concentration at the ring stage in comparison to other stages. However, as the parasites mature haemoglobin reduces and there is an increase in free haem and HZ crystals, this makes the ratio of haemoglobin: free haem: HZ change as the parasite life cycle progresses. Due to these changes, we can see a characteristic phenotype for each of the stages using the NMR.

- Herein, we used both slack synchronized and tightly synchronized *P. falciparum* WT parasites cultured in RBCs. Proton measurements of T_1 and T_2 relaxation times based on the bulk water present in the samples were made, while A-ratio values expressed the dynamic change between T_1 and T_2 values. Several samples of slack synchronized cultures were measured at each morphological stage to identify phenotypic and physiological differences across each stage. First, we time-tracked triplicates of each stage to detect specific differences along time (8-16 hours). Next, we compared time-tracked measurements of all the stages to determine the phenotypic differences across time and between each developmental stage.
- For synchronized parasites, measurements were performed at specific points to study the relative dynamic changes that occur through each intracellular stage.

Several research studies have exploited the large paramagnetic susceptibility of the HZ to study the maturation stages of the malaria parasite [124,127]. This was done by examining changes in the transverse relaxation rate constant ($R_2=1/T_2$) of ^{1}H-water resonance [109,124]. One of such study was by

Di Gregorio *et al.* [109], where they utilized both transverse and longitudinal relaxation rate constant ($R_1=1/T_1$) of ^{1}H-water resonance. Using four different stages of parasite infection (rings, early trophozoites, late trophozoites and schizonts) they characterized the changes that occurred as the parasites progressed from one stage to another. Here, they identified low R_1 values as the cycle progressed from ring to early trophozoite stage, however upon passing to the late morphological stages R_1 values were seen to increase. R_2 values were also seen to increase with increased parasite maturation. This occurred because of changes in the water exchange rate across cellular membranes.

Comparing this finding to that from the DM study [129], T_1 and T_2 relaxation times were seen to reduce with increasing protein oxidative damage. This is due to restricted mobility of bulk water proton as oxidative damage increased (in the DM patients). Although these two studies used different parameters the DM study validates the findings from Gregorio *et al.* This is because R_1 and R_2 are inversely related to T_1 and T_2 respectively, therefore Gregorio *et al.* [109] detected an increase in the relaxation rate constants with increasing parasite maturity, whereas findings from the DM study showed decreased relaxation times [109,129].

Bringing this knowledge back home, we identified very few similarities between these two studies and the results we obtained from our slack synchronized cultures. This is expected as Gregorio *et al.* used highly synchronized parasite cultures. However, with the use of synchronized cultures we identified more similar measurement patterns. To further exploit the sensitivity of the NMR at different dilutions of each stage we analysed T_1, T_2 readings of ring cultures at 0.01%, 0.1% and 1% parasitaemia.

Here we obtained similar readings with Peng *et al.,* where different dilutions of iRBCs were used to determine the limit of detection of the MRR. This technique was performed by measuring the transverse relaxation rate constant (R_2) across ascending parasite concentrations. Findings from this study showed a spike in R_2 values with an increase in parasite concentration, similar to some of our findings [124]. At the ring stage, we identified reduced T_1 and T_2 readings when parasitaemia levels increased attesting to the sensitive nature of the NMR. Furthermore, Gregorio *et al.* identified an increase in T_1 and T_2 relaxation times at different parasitaemia in late ring and trophozoite stages. This is because the water exchange rate across the RBC membrane decreases by 50% 24-28 hours post invasion in RBCs. Although we had similar findings with this study at the ring stage, when the parasites passed onto the trophozoite stage we identified inconsistent T_1, T_2 readings across parasitaemia, this may be due to technical faults or the need for more samples to be characterized at the trophozoite stage. In addition, Gregorio *et al.* suggested that essential changes that occur in the water exchange rate across membranes of iRBCs have a

characteristic behaviour for each intracellular stage of the malaria parasite. This was seen when we characterized slack synchronized parasite cultures of all morphological stages across time using A-ratio.

With each sample having a total of 8-12 measurements (about 8-12 hours), we noticed a plateau at the beginning of the ring stage, a slight decrease as we progressed and then a spike as rings passed to early trophozoites, late trophozoites and schizont, however toward the end of the schizont stage we saw another fall in A-ratio which may be an indication of the initiation of a new cycle of early rings.

To further understand why this occurs we need to get back to the basis by which NMR identifies iRBCs, which is due to the presence of HZ. T_1 and T_2 measurements deliver essential information on the presence of HZ in iRBCs and the intra-erythrocytic stage of the parasite. With increased parasite concentration we saw a decrease in T_1 and T_2 readings (rings). This is essential since only ring stages are seen under the microscope in the field. Reason being that, in most cases only ring forms flow in blood vessels, iRBCs containing the later stages are sequestered to the walls of the vessels hindering them from flowing freely. This implies that with the NMR we can determine the concentration of the infection due to the rise in the amount of HZ present in the iRBCs. When we analysed T_1 and T_2 readings of tight synchronized cultures across parasite maturation we also identified a reduction between rings and trophozoite stages at 0.01 and 0.1 percent parasitaemia, due to increase in the amount of HZ. However, as trophozoite matured into schizonts we identified a slight increase in T_1, T_2 readings and a slight decrease in A-ratio values. This may be due to a reduction in the concentration of HZ as schizonts start to form new merozoites, setting the stage for a new cycle of early rings. Furthermore, as the iRBCs lyse, they release HZ extra-cellularly contributing to a reduced intra-cellular content of HZ and consequently a reduction in the H1bulk paramagnetic susceptibility of the cells. So, although, we see an increase in A-ratio at the start of the schizont stage, towards the final hours of its characterization we see a drop in A-ratio values, this therefore contributes to a fall in the mean value of schizonts in relation to trophozoites. Since HZ possess high paramagnetic susceptibility, we see the NMR detects this reduction in HZ concentration as a result of a new invasion and the formation of a new cycle. In our study overall, we identified an inversely proportional relationship between high T_1 and T_2 readings with applied magnetic field.

Reliable diagnostic tools are necessary to identify early infections and administer the right prescription of drugs for treatment. Over-prescription and mis-prescription of antimalarial drugs is avoided with the use of proper and effective diagnostic tools. Furthermore, detection of early infections is important to curtail the transmission of parasites to other individuals in the community.

5.2 Understanding the role *Pf*MDR2 in the physiology of *P. falciparum* parasites

Since we were unable to obtain *Pf*MDR2 mutant parasites by pSLI selection system, we may be successful if we change the genetic engineering strategy. Most of the molecular cloning procedures in our laboratory utilized this system, however presently the CRISPR-Cas 9 system is being integrated in some of our laboratory procedures to optimize these procedures. Therefore, using the CRISPR-Cas 9 system may improve the success rate of getting gene edited parasites. If proven successful, future work with these recombinant lines may contribute to the understanding of *Pf*MDR2 natural function and their role in drug response. Furthermore, we will be able to characterize any other distinctive phenotype in these mutant lines using several *invitro* techniques. Since it was shown in a particular study [107] that mutations in *k13,* in the 3D7 strain is connected to a strong set of molecular markers such as nonsynonymous mutations in *Pf*MDR2 on chromosome 14, we may be able to identify these distinctive features utilizing these *invitro* techniques. In another study [141], it was identified that mutations in p*fmdr2* gene on chromosome 13 was associated with [142] sulphadoxine resistance. This implies that *Pf*MDR2 may be involved in the transport of organic anions such as folates as identified for *Pf*MRP1[142]. Therefore, we can determine the function of *pfmdr2* mutations in sulphadoxine resistance using drug susceptibility assays or other *invitro* techniques.

After performing these *invitro* experiments, we can characterize *Pf*MDR2 parasites using time domain (T_1 and T_2) NMR to identify distinct phenotypic features from the WT strains we characterized earlier. This will help us determine specific functions the *Pf*MDR2 protein play at specific stages in the parasite life cycle owing to its ability to transport heavy metals from the food vacuole. Interestingly we may identify distinct T_1 and T_2 relaxation readings due to higher/lower paramagnetic susceptibility of these parasites.

5.3 Plasmepsins impact into the balance of the haem species

Plasmepsins I, II and III have been identified to play an essential role in cleaving haemoglobin moieties of intracellular parasites into peptides. However, a gain of an extra copy of the *plasmepsin* gene have been shown to generate PPQ resistance. In this research, we performed the haem fractionation assay to determine what occurs at early rings and late trophozoites stages in plasmepsin overexpressed and WT parasites. Here we saw that the WT lines cleaved more haemoglobin than mutant lines at the late trophozoite stage. This was unexpected, since an extra gain in the copy number of the plasmepsin gene would make the protein cleave far higher amounts of haemoglobin than usual. Consequently, we obtained increased concentrations of free haem, formed as by product in comparison to mutant parasites.

In general, haemoglobin concentrations were much lower at 32 hours than at 0 hour. This is because, as the rings develops into trophozoites more haemoglobin is ingested [50]. In an earlier study, it was detected that the highest amount of degradation occurred at the trophozoite stage, of which we identified in this assay. Additionally, among the proteases, the aspartic proteases accounted for 60-80% of globin degradation activity [143]. Although PM3-1 and PM2 parasites had high concentrations of haemoglobin and free haem, when we analysed HZ at 32 hours, we saw PM2 parasites had high concentrations of HZ than WT and PM3-1 parasites. Conclusively, mutant parasites cleaved less haemoglobin than the WT, interestingly, we extracted higher amounts of HZ (PM2) at 32 hours than WT parasites at 32 hours. However, these results should be taken with caution, as more assays need to be performed to obtain more accurate data.

Relating this finding to the results we obtained from NMR measurements of WT parasites, we see some similarities between. In early ring forms and low parasite concentrations, where haemoglobin concentrations are higher, we see a reduced paramagnetic susceptibility demonstrated in relatively lower A-ratio. However, in the trophozoite stage and at relatively higher concentration of parasites, we saw a rise in A-ratio value, although the case was different in schizonts where we saw a fall. This was due to a dynamic reduction in the paramagnetic susceptibility of the samples due to the formation of early ring forms at the terminal hours of measurement. This in turn increased the mean of A-ratio. This was further confirmed when we performed time-tracking NMR characterization across the whole cycle, where we saw a peak at the schizont stage and then a fall at the 10th-12th hours of measurements.

With this understanding, time domain NMR could be used to characterize plasmepsin mutant parasites. Further studies using this technique, will shed light into possible novel phenotypic features that could detect these changes in the parasite. These phenotypic features in comparison to control WT parasites could be studied and hopefully distinct phenotypic patterns along the developmental stages can be identified. Hypothesizing from haem fractionation results, we may see higher A-ratio values at trophozoite and schizonts stages in comparison to their WT counterparts. This will be due to the high paramagnetic susceptibility conferred by higher concentrations of free haem and HZ crystals. With these results we can create a more robust proof of concept that can be implemented in the future for diagnosing specific resistant parasite strains such as PPQ mutant strains, from susceptible ones.

CHAPTER 6

FINAL REMARKS AND FUTURE PERSPECTIVES

Despite the milestones we seem to have crossed in the field of malaria, there are still myriads of questions to explore that may bring lasting solutions to the problems we are facing in malaria diagnosis and treatment. Taking the essential natural biomarker - HZ for example, it has been studied at the microscopic level and has been utilized as an attractive target for treatment. Apart from its optic characteristic, it has magnetic, photo-acoustic, electrical properties to name just a few. These properties can be further exploited and adopted for field diagnostics, providing more specific and sensitive information than the current field diagnostics. In this research, we exploited further the magnetic property of HZ in studying the dynamic changes in the IDC stages. With this knowledge we were able to predict or validate what transpires in the maturing parasite in respect to its physiological condition, growth, and metabolism along a life cycle. This reveals that an in-depth study of the magnetic property of HZ, using different strains, species and parasite concentration can provide a standard phenotypic pattern that can be channelled into diagnosis and treatment at POC. In our study, we characterized the Dd2 WT strains along the IDC stages at 0.01, 0.1 and 1% using T1, T2 and A-ratio. In the future we hope to characterize antimalarial drugs that block specific processes in the parasites to better understand the haemoglobin to HZ formation pathways.

Additionally, drug resistant strains can be studied, and comparisons can be made with WT strains. We attempted to go deep into this using a controlled genetic background for *Pf*MDR2 KO parasites and plasmepsin gene copy number amplification parasites. Although, during the time of this thesis, we were not able to characterize these parasites with the NMR to determine their specific behavioural patterns in comparison to WT parasites, we know it will be an interesting subject to explore. The phenotypic patterns obtained from studying these mutant parasites can be used on the field in the future to diagnose a resistant parasite strain to an anti-malarial drug, of which an alternative anti-malarial drug can be prescribed, thus fostering effective treatment and a proof of concept towards precision malaria medicine.

Mutant lines of understudied parasite genes and proteins that have been hypothesized to be involved in drug resistance, targeting the haemoglobin - HZ formation pathway can be exposed for its role into drug modulation. These mutant lines can then be NMR characterized to identify changes in their paramagnetic properties. Gregorio *et al.* was successful in doing this using WT parasite strains [109]. The mode of action of these drugs can be investigated in WT strains and mutant lines to determine their underlying mechanism of resistance. Fluctuations in temperature and the need for a stable power source are major limitations of the NMR that can be adapted to field settings however, it is an excellent research tool that can be adopted for malaria studies to solve the problems the world is facing in malaria diagnosis and drug therapy, thereby taking us a step closer to global malaria elimination.

CHAPTER 7

REFERENCES

1. WHO. Word Malaria Report 2021. Word Malaria report Geneva: World Health Organization. (2021). Licence: CC. 2021. 2013–2015 p.

2. WORLD HEALTH ORGANIZATION. WORLD MALARIA REPORT 2019. WORLD HEALTH ORGANIZATION; 2019.

3. Yang GG, Kim D, Pham A, Paul CJ. A meta-regression analysis of the effectiveness of mosquito nets for malaria control: The value of long-lasting insecticide nets. Int J Environ Res Public Health. 2018 Mar 19;15(3).

4. Bhatt S, Weiss DJ, Cameron E, Bisanzio D, Mappin B, Dalrymple U, et al. The effect of malaria control on Plasmodium falciparum in Africa between 2000 and 2015. Nature. 2015 Oct 8;526(7572):207–11.

5. Pryce J, Richardson M, Lengeler C. Insecticide-treated nets for preventing malaria. Vol. 2018, Cochrane Database of Systematic Reviews. John Wiley and Sons Ltd; 2018.

6. Aidoo M, Incardona S. Ten Years of Universal Testing: How the Rapid Diagnostic Test Became a Game Changer for Malaria Case Management and Improved Disease Reporting. Am J Trop Med Hyg. 2022;106(1):29.

7. Froeschl G, Saathoff E, Kroidl I, Berens-Riha N, Clowes P, Maboko L, et al. Reduction of malaria prevalence after introduction of artemisinin-combination-therapy in Mbeya Region, Tanzania: results from a cohort study with 6773 participants. Malar J. 2018;17(1):1–11.

8. Balikagala B, Fukuda N, Ikeda M, Katuro OT, Tachibana SI, Yamauchi M, et al. Evidence of artemisinin-resistant malaria in Africa. New England Journal of Medicine. 2021;385(13):1163–71.

9. Noedl H, Se Y, Schaecher K, Smith BL, Socheat D, Fukuda MM. Evidence of artemisinin-resistant malaria in western Cambodia. New England Journal of Medicine. 2008;359(24):2619–20.

10. Wongsrichanalai C, Meshnick SR. Declining artesunate-mefloquine efficacy against falciparum malaria on the Cambodia–Thailand border. Emerg Infect Dis. 2008;14(5):716.

11. Sachs J, Malaney P. The economic and social burden of malaria. Nature. 2002;415(6872):680–5.

12. Malaria no more UK. Malaria: Bad for business.

13. TO C. Business and Malaria: A Neglected Threat? 2006;

14. Boutayeb A. The impact of infectious diseases on the development of Africa. Handbook of disease burdens and quality of life measures. 2010;1171.

15. Nieuwenhof M. MVIP Malawi Ntchisi District Hospital Davie Banda Nurse in malar. Geneva; 2016.

16. Preiser P, Kaviratne M, Khan S, Bannister L, Jarra W. The apical organelles of malaria merozoites: host cell selection, invasion, host immunity and immune evasion. Microbes Infect. 2000;2(12):1461–77.

17. Riehle MM, Markianos K, Niaré O, Xu J, Li J, Touré AM, et al. Natural malaria infection in Anopheles gambiae is regulated by a single genomic control region. Science (1979). 2006;312(5773):577–9.

18. Sato S. Plasmodium—a brief introduction to the parasites causing human malaria and their basic biology. J Physiol Anthropol [Internet]. 2021;40(1):1. Available from: https://doi.org/10.1186/s40101-020-00251-9

19. Gilles HM, Warrell DA. Bruce-Chwatt's essential malariology. Edward Arnold (Publisher) Ltd.; 1996.

20. Hartmeyer GN, Stensvold CR, Fabricius T, Marmolin ES, Hoegh S v, Nielsen H v, et al. Plasmodium cynomolgi as cause of malaria in tourist to Southeast Asia, 2018. Emerg Infect Dis. 2019;25(10):1936.

21. Singh B, Daneshvar C. Human infections and detection of Plasmodium knowlesi. Clin Microbiol Rev. 2013;26(2):165–84.

22. Frischknecht F, Matuschewski K. Plasmodium sporozoite biology. Cold Spring Harb Perspect Med. 2017;7(5):a025478.

23. Amino R, Thiberge S, Martin B, Celli S, Shorte S, Frischknecht F, et al. Quantitative imaging of Plasmodium transmission from mosquito to mammal. Nat Med. 2006;12(2):220–4.

24. Prudêncio M, Rodriguez A, Mota MM. The silent path to thousands of merozoites: the Plasmodium liver stage. Nat Rev Microbiol. 2006;4(11):849–56.

25. Touray MG, Warburg A, Laughinghouse A, Krettli AU, Miller LH. Developmentally regulated infectivity of malaria sporozoites for mosquito salivary glands and the vertebrate host. J Exp Med. 1992;175(6):1607–12.

26. Baptista V, Costa MS, Calçada C, Silva M, Gil JP, Veiga MI, et al. The future in sensing technologies for malaria surveillance: a review of hemozoin-based diagnosis. ACS Sens. 2021;6(11):3898–911.

27. Sturm A, Amino R, van de Sand C, Regen T, Retzlaff S, Rennenberg A, et al. Manipulation of host hepatocytes by the malaria parasite for delivery into liver sinusoids. Science (1979). 2006;313(5791):1287–90.

28. Gerald N, Mahajan B, Kumar S. Mitosis in the human malaria parasite Plasmodium falciparum. Eukaryot Cell. 2011;10(4):474–82.

29. Venugopal K, Hentzschel F, Valkiūnas G, Marti M. Plasmodium asexual growth and sexual development in the haematopoietic niche of the host. Nat Rev Microbiol. 2020;18(3):177–89.

30. Josling GA, Llinás M. Sexual development in Plasmodium parasites: knowing when it's time to commit. Nat Rev Microbiol. 2015;13(9):573–87.

31. Tadesse FG, Meerstein-Kessel L, Gonçalves BP, Drakeley C, Ranford-Cartwright L, Bousema T. Gametocyte sex ratio: the key to understanding Plasmodium falciparum transmission? Trends Parasitol. 2019;35(3):226–38.

32. Bennink S, Kiesow MJ, Pradel G. The development of malaria parasites in the mosquito midgut. Cell Microbiol. 2016;18(7):905–18.

33. Ngwa CJ, Rosa TF, Pradel G. The biology of malaria gametocytes. IntechOpen Rijeka, Croatia; 2016.

34. Sinden RE, Hartley RH. Identification of the meiotic division of malarial parasites. J Protozool. 1985;32(4):742–4.

35. Siciliano G, Costa G, Suárez-Cortés P, Valleriani A, Alano P, Levashina EA. Critical steps of Plasmodium falciparum ookinete maturation. Front Microbiol. 2020;11:269.

36. Araki T, Kawai S, Kakuta S, Kobayashi H, Umeki Y, Saito-Nakano Y, et al. Three-dimensional electron microscopy analysis reveals endopolygeny-like nuclear architecture segregation in Plasmodium oocyst development. Parasitol Int. 2020;76:102034.

37. Vaughan JA. Population dynamics of Plasmodium sporogony. Trends Parasitol. 2007;23(2):63–70.

38. Smith RC, Jacobs-Lorena M. Plasmodium–mosquito interactions: a tale of roadblocks and detours. In: Advances in insect physiology. Elsevier; 2010. p. 119–49.

39. Zhou G, Kohlhepp P, Geiser D, del Carmen Frasquillo M, Vazquez-Moreno L, Winzerling JJ. Fate of blood meal iron in mosquitoes. J Insect Physiol. 2007;53(11):1169–78.

40. Marinkovic M, Diez-Silva M, Pantic I, Fredberg JJ, Suresh S, Butler JP. Febrile temperature leads to significant stiffening of Plasmodium falciparum parasitized erythrocytes. American Journal of Physiology-Cell Physiology. 2009;296(1):C59–64.

41. Mohandas N, An X. Malaria and human red blood cells. Med Microbiol Immunol. 2012;201(4):593–8.

42. Weissbuch I, Leiserowitz L. Interplay between malaria, crystalline hemozoin formation, and antimalarial drug action and design. Chem Rev. 2008;108(11):4899–914.

43. Coronado LM, Nadovich CT, Spadafora C. Malarial hemozoin: from target to tool. Biochimica et Biophysica Acta (BBA)-General Subjects. 2014;1840(6):2032–41.

44. Krogstad DJ, Schlesinger PH, Gluzman IY. Antimalarials increase vesicle pH in Plasmodium falciparum. J Cell Biol. 1985;101(6):2302–9.

45. Klonis N, Tan O, Jackson K, Goldberg D, Klemba M, Tilley L. Evaluation of pH during cytostomal endocytosis and vacuolar catabolism of haemoglobin in Plasmodium falciparum. Biochemical Journal. 2007;407(3):343–54.

46. Krugliak M, Zhang J, Ginsburg H. Intraerythrocytic Plasmodium falciparum utilizes only a fraction of the amino acids derived from the digestion of host cell cytosol for the biosynthesis of its proteins. Mol Biochem Parasitol. 2002;119(2):249–56.

47. Ginsburg H. Some reflections concerning host erythrocyte-malarial parasite interrelationships. Blood Cells. 1990;16(2–3):225–35.

48. Esposito A, Tiffert T, Mauritz JMA, Schlachter S, Bannister LH, Kaminski CF, et al. FRET imaging of hemoglobin concentration in Plasmodium falciparum-infected red cells. PLoS One. 2008;3(11):e3780.

49. Moura PA, Dame JB, Fidock DA. Role of Plasmodium falciparum digestive vacuole plasmepsins in the specificity and antimalarial mode of action of cysteine and aspartic protease inhibitors. Antimicrob Agents Chemother. 2009;53(12):4968–78.

50. Francis SE, Sullivan Jr DJ, Goldberg and DE. Hemoglobin metabolism in the malaria parasite Plasmodium falciparum. Annual Reviews in Microbiology. 1997;51(1):97–123.

51. Bozdech Z, Llinás M, Pulliam BL, Wong ED, Zhu J, DeRisi JL, et al. The transcriptome of the intraerythrocytic developmental cycle of Plasmodium falciparum. PLoS Biol. 2003;1(1):e5.

52. Gluzman IY, Francis SE, Oksman A, Smith CE, Duffin KL, Goldberg DE. Order and specificity of the Plasmodium falciparum hemoglobin degradation pathway. J Clin Invest. 1994;93(4):1602–8.

53. Kapishnikov S, Hempelmann E, Elbaum M, Als-Nielsen J, Leiserowitz L. Malaria pigment crystals: The achilles' heel of the malaria parasite. ChemMedChem. 2021;16(10):1515–32.

54. Ferreira CM, Stiebler R, Saraiva FM, Lechuga GC, Walter-Nuno AB, Bourguignon SC, et al. Heme crystallization in a Chagas disease vector acts as a redox-protective mechanism to allow insect reproduction and parasite infection. PLoS Negl Trop Dis. 2018;12(7):e0006661.

55. Hempelmann E, Egan TJ. Pigment biocrystallization in Plasmodium falciparum. Trends Parasitol. 2002;18(1):11.

56. Hempelmann E. Hemozoin biocrystallization in Plasmodium falciparum and the antimalarial activity of crystallization inhibitors. Parasitol Res. 2007;100(4):671–6.

57. Carney CK, Fricke M, Harry SR, Imai H, Kniep R, Sato K, et al. Biomineralization I: Crystallization and Self-Organization Process. Vol. 270. Springer; 2006.

58. Hempelmann E, Marques HM. Analysis of malaria pigment from Plasmodium falciparum. J Pharmacol Toxicol Methods. 1994;32(1):25–30.

59. Buller R, Peterson ML, Almarsson O, Leiserowitz L. Quinoline binding site on malaria pigment crystal: a rational pathway for antimalaria drug design. Cryst Growth Des. 2002;2(6):553–62.

60. Egan TJ. Haemozoin formation. Mol Biochem Parasitol. 2008;157(2):127–36.

61. Egan TJ. Recent advances in understanding the mechanism of hemozoin (malaria pigment) formation. J Inorg Biochem. 2008;102(5–6):1288–99.

62. Kapishnikov S, Berthing T, Hviid L, Dierolf M, Menzel A, Pfeiffer F, et al. Aligned hemozoin crystals in curved clusters in malarial red blood cells revealed by nanoprobe X-ray Fe fluorescence and diffraction. Proceedings of the National Academy of Sciences. 2012;109(28):11184–7.

63. Kapishnikov S, Weiner A, Shimoni E, Schneider G, Elbaum M, Leiserowitz L. Digestive vacuole membrane in Plasmodium falciparum-infected erythrocytes: Relevance to templated nucleation of hemozoin. Langmuir. 2013;29(47):14595–602.

64. Kapishnikov S, Weiner A, Shimoni E, Guttmann P, Schneider G, Dahan-Pasternak N, et al. Oriented nucleation of hemozoin at the digestive vacuole membrane in Plasmodium falciparum. Proceedings of the National Academy of Sciences. 2012;109(28):11188–93.

65. Monti D, Vodopivec B, Basilico N, Olliaro P, Taramelli D. A novel endogenous antimalarial: Fe (II)-Protoporphyrin IXα (heme) inhibits hematin polymerization to β-hematin (malaria pigment) and kills malaria parasites. Biochemistry. 1999;38(28):8858–63.

66. Ziegler J, Linck R, Wright DW. Heme aggregation inhibitors antimalarial drugs targeting an essential biomineralization process. Curr Med Chem. 2001;8(2):171–89.

67. Agrawal R, Tripathi R, Tekwani BL, Jain SK, Dutta GP, Shukla OP. Haem polymerase as a novel target of antimalarial action of cyproheptadine. Biochem Pharmacol. 2002;64(9):1399–406.

68. Solomon VR, Haq W, Srivastava K, Puri SK, Katti SB. Synthesis and antimalarial activity of side chain modified 4-aminoquinoline derivatives. J Med Chem. 2007;50(2):394–8.

69. Kwiatkowski D, Bate CAW, Scragg IG, Beattie P, Udalova I, Knight JC. The malarial fever response—pathogenesis, polymorphism and prospects for intervention. Ann Trop Med Parasitol. 1997;91(5):533–42.

70. Buller R, Peterson ML, Almarsson O, Leiserowitz L. Quinoline binding site on malaria pigment crystal: a rational pathway for antimalaria drug design. Cryst Growth Des. 2002;2(6):553–62.

71. Noland GS, Briones N, Sullivan Jr DJ. The shape and size of hemozoin crystals distinguishes diverse Plasmodium species. Mol Biochem Parasitol. 2003;130(2):91–9.

72. Gelband H, Panosian CB, Arrow KJ. Saving lives, buying time: economics of malaria drugs in an age of resistance. 2004;

73. Meunier B, Robert A. Heme as trigger and target for trioxane-containing antimalarial drugs. Acc Chem Res. 2010;43(11):1444–51.

74. Antoine T, Fisher N, Amewu R, O'Neill PM, Ward SA, Biagini GA. Rapid kill of malaria parasites by artemisinin and semi-synthetic endoperoxides involves ROS-dependent depolarization of the membrane potential. Journal of antimicrobial chemotherapy. 2014;69(4):1005–16.

75. Tilley L, Straimer J, Gnädig NF, Ralph SA, Fidock DA. Artemisinin action and resistance in Plasmodium falciparum. Trends Parasitol. 2016;32(9):682–96.

76. Geary TG, Divo AA, Jensen JB. Stage specific actions of antimalarial drugs on Plasmodium falciparum in culture. Am J Trop Med Hyg. 1989;40(3):240–4.

77. Ribbiso KA, Heller LE, Taye A, Julian E, Willems A v, Roepe PD. Artemisinin-Based Drugs Target the Plasmodium falciparum Heme Detoxification Pathway. Antimicrob Agents Chemother. 2021;65(4):e02137-20.

78. Pelletier PJ, Caventou JB. Recherches chimiques sur les quinquinas. Crochard; 1820.

79. Wellems TE, Plowe C v. Chloroquine-resistant malaria. J Infect Dis. 2001;184(6):770–6.

80. Combrinck JM, Mabotha TE, Ncokazi KK, Ambele MA, Taylor D, Smith PJ, et al. Insights into the role of heme in the mechanism of action of antimalarials. ACS Chem Biol. 2013;8(1):133–7.

81. Olliaro P. Mode of action and mechanisms of resistance for antimalarial drugs. Pharmacol Ther. 2001;89(2):207–19.

82. Basco LK, Ringwald P. In vitro activities of piperaquine and other 4-aminoquinolines against clinical isolates of Plasmodium falciparum in Cameroon. Antimicrob Agents Chemother. 2003;47(4):1391–4.

83. Ross LS, Dhingra SK, Mok S, Yeo T, Wicht KJ, Kümpornsin K, et al. Emerging Southeast Asian PfCRT mutations confer Plasmodium falciparum resistance to the first-line antimalarial piperaquine. Nat Commun. 2018;9(1):1–13.

84. Gargano N, Cenci F, Bassat Q. Antimalarial efficacy of piperaquine-based antimalarial combination therapies: facts and uncertainties. Tropical Medicine & International Health. 2011;16(12):1466–73.

85. Mohamed AO, Abdel Hamid MM, Mohamed OS, Elkando NS, Suliman A, Adam MA, et al. Efficacies of DHA–PPQ and AS/SP in patients with uncomplicated Plasmodium falciparum malaria in an area of an unstable seasonal transmission in Sudan. Malar J. 2017;16(1):1–6.

86. Noreen N, Ullah A, Salman SM, Mabkhot Y, Alsayari A, Badshah SL. New insights into the spread of resistance to artemisinin and its analogues. J Glob Antimicrob Resist. 2021;27:142–9.

87. Amaratunga C, Sreng S, Suon S, Phelps ES, Stepniewska K, Lim P, et al. Artemisinin-resistant Plasmodium falciparum in Pursat province, western Cambodia: a parasite clearance rate study. Lancet Infect Dis. 2012;12(11):851–8.

88. Dondorp AM, Nosten F, Yi P, Das D, Phyo AP, Tarning J, et al. Artemisinin resistance in Plasmodium falciparum malaria. New England journal of medicine. 2009;361(5):455–67.

89. Ariey F, Witkowski B, Amaratunga C, Beghain J, Langlois AC, Khim N, et al. A molecular marker of artemisinin-resistant Plasmodium falciparum malaria. Nature. 2014;505(7481):50–5.

90. Heller LE, Roepe PD. Quantification of free ferriprotoporphyrin IX heme and hemozoin for artemisinin sensitive versus delayed clearance phenotype Plasmodium falciparum malarial parasites. Biochemistry. 2018;57(51):6927–34.

91. Birnbaum J, Scharf S, Schmidt S, Jonscher E, Hoeijmakers WAM, Flemming S, et al. A Kelch13-defined endocytosis pathway mediates artemisinin resistance in malaria parasites. Science (1979). 2020;367(6473):51–9.

92. Amaratunga C, Lim P, Suon S, Sreng S, Mao S, Sopha C, et al. Dihydroartemisinin–piperaquine resistance in Plasmodium falciparum malaria in Cambodia: a multisite prospective cohort study. Lancet Infect Dis. 2016;16(3):357–65.

93. Saunders DL, Vanachayangkul P, Lon C. Dihydroartemisinin–piperaquine failure in Cambodia. New England Journal of Medicine. 2014;371(5):484–5.

94. Mukherjee A, Gagnon D, Wirth DF, Richard D. Inactivation of plasmepsins 2 and 3 sensitizes Plasmodium falciparum to the antimalarial drug piperaquine. Antimicrob Agents Chemother. 2018;62(4):e02309-17.

95. Bopp S, Magistrado P, Wong W, Schaffner SF, Mukherjee A, Lim P, et al. Plasmepsin II–III copy number accounts for bimodal piperaquine resistance among Cambodian Plasmodium falciparum. Nat Commun. 2018;9(1):1–10.

96. Witkowski B, Duru V, Khim N, Ross LS, Saintpierre B, Beghain J, et al. A surrogate marker of piperaquine-resistant Plasmodium falciparum malaria: a phenotype–genotype association study. Lancet Infect Dis. 2017;17(2):174–83.

97. Chugh M, Sundararaman V, Kumar S, Reddy VS, Siddiqui WA, Stuart KD, et al. Protein complex directs hemoglobin-to-hemozoin formation in Plasmodium falciparum. Proceedings of the National Academy of Sciences. 2013;110(14):5392–7.

98. Bonilla JA, Bonilla TD, Yowell CA, Fujioka H, Dame JB. Critical roles for the digestive vacuole plasmepsins of Plasmodium falciparum in vacuolar function. Mol Microbiol. 2007;65(1):64–75.

99. Klaassen CD, Aleksunes LM. Xenobiotic, bile acid, and cholesterol transporters: function and regulation. Pharmacol Rev. 2010;62(1):1–96.

100. Borges-Walmsley MI, McKEEGAN KS, Walmsley AR. Structure and function of efflux pumps that confer resistance to drugs. Biochemical Journal. 2003;376(2):313–38.

101. Martin RE. The transportome of the malaria parasite. Biological Reviews. 2020;95(2):305–32.

102. Zalis MG, Wilson CM, Zhang Y, Wirth DF. Characterization of the pfmdr 2 gene for Plasmodium falciparum. Mol Biochem Parasitol. 1993;62(1):83–92.

103. Rosenberg E, Litus I, Schwarzfuchs N, Sinay R, Schlesinger P, Golenser J, et al. pfmdr2 confers heavy metal resistance to Plasmodium falciparum. Journal of Biological Chemistry. 2006;281(37):27039–45.

104. Peel SA. The ABC transporter genes of Plasmodium falciparum and drug resistance. Drug resistance updates. 2001;4(1):66–74.

105. Ortiz DF, Kreppel L, Speiser DM, Scheel G, McDonald G, Ow DW. Heavy metal tolerance in the fission yeast requires an ATP-binding cassette-type vacuolar membrane transporter. EMBO J. 1992;11(10):3491–9.

106. Steffens JC, Hunt DF, Williams BG. Accumulation of non-protein metal-binding polypeptides (gamma-glutamyl-cysteinyl) n-glycine in selected cadmium-resistant tomato cells. Journal of Biological Chemistry. 1986;261(30):13879–82.

107. Volkman SK, Herman J, Lukens AK, Hartl DL. Genome-wide association studies of drug-resistance determinants. Trends Parasitol. 2017;33(3):214–30.

108. Miotto O, Amato R, Ashley EA, MacInnis B, Almagro-Garcia J, Amaratunga C, et al. Genetic architecture of artemisinin-resistant Plasmodium falciparum. Nat Genet. 2015;47(3):226–34.

109. di Gregorio E, Ferrauto G, Schwarzer E, Gianolio E, Valente E, Ulliers D, et al. Relaxometric studies of erythrocyte suspensions infected by Plasmodium falciparum: a tool for staging infection and testing anti-malarial drugs. Magn Reson Med. 2020;84(6):3366–78.

110. Grimberg BT, Grimberg KO. Hemozoin detection may provide an inexpensive, sensitive, 1-minute malaria test that could revolutionize malaria screening. Expert Rev Anti Infect Ther. 2016;14(10):879–83.

111. Weissbuch I, Leiserowitz L. Interplay between malaria, crystalline hemozoin formation, and antimalarial drug action and design. Chem Rev. 2008;108(11):4899–914.

112. Berry A, Benoit-Vical F, Fabre R, Cassaing S, Magnaval JF. PCR-based methods to the diagnosis of imported malaria. Parasite. 2008;15(3):484–8.

113. Shapiro HM, Apte SH, Chojnowski GM, Hänscheid T, Rebelo M, Grimberg BT. Cytometry in malaria—a practical replacement for microscopy? Curr Protoc Cytom. 2013;65(1):11–20.

114. Baptista V, Peng WK, Minas G, Veiga MI, Catarino SO. Review of Microdevices for Hemozoin-Based Malaria Detection. Biosensors (Basel). 2022;12(2):110.

115. Baptista V, Costa MS, Calçada C, Silva M, Gil JP, Veiga MI, et al. The future in sensing technologies for malaria surveillance: a review of hemozoin-based diagnosis. ACS Sens. 2021;6(11):3898–911.

116. Lawrence C, Olson JA. Birefringent hemozoin identifies malaria. Am J Clin Pathol. 1986;86(3):360–3.

117. Butykai A, Orbán A, Kocsis V, Szaller D, Bordács S, Tátrai-Szekeres E, et al. Malaria pigment crystals as magnetic micro-rotors: key for high-sensitivity diagnosis. Sci Rep. 2013;3(1):1–10.

118. Pirnstill CW, Coté GL. Malaria diagnosis using a mobile phone polarized microscope. Sci Rep. 2015;5(1):1–13.

119. Saha RK, Karmakar S, Roy M. Computational investigation on the photoacoustics of malaria infected red blood cells. PLoS One. 2012;7(12):e51774.

120. Rosecwaig A. Photoacoustic and Photoacoustic Spectroscopy. Wiley Interscience, New York; 1983.

121. Balasubramanian D, Mohan Rao C, Panijpan B. The malaria parasite monitored by photoacoustic spectroscopy. Science (1979). 1984;223(4638):828–30.

122. Catarino SO, Félix P, Sousa PJ, Pinto V, Veiga MI, Minas G. Portable device for optical quantification of hemozoin in diluted blood samples. IEEE Trans Biomed Eng. 2019;67(2):365–71.

123. Silva I, Lima R, Minas G, Catarino SO. Hemozoin and hemoglobin characterization by optical absorption towards a miniaturized spectrophotometric malaria diagnostic system. In: 2017 IEEE 5th Portuguese Meeting on Bioengineering (ENBENG). IEEE; 2017. p. 1–4.

124. Peng WK, Kong TF, Ng CS, Chen L, Huang Y, Bhagat AAS, et al. Micromagnetic resonance relaxometry for rapid label-free malaria diagnosis. Nat Med. 2014;20(9):1069–73.

125. Zimmerman PA, Howes RE. Malaria diagnosis for malaria elimination. Curr Opin Infect Dis. 2015;28(5):446–54.

126. Karl S, Mueller I, St Pierre TG. Considerations regarding the micromagnetic resonance relaxometry technique for rapid label-free malaria diagnosis. Vol. 21, Nature Medicine. Nature Publishing Group; 2015. p. 1387.

127. Peng WK, Chen L, Han J. Development of miniaturized, portable magnetic resonance relaxometry system for point-of-care medical diagnosis. Review of Scientific Instruments. 2012;83(9):095115.

128. Peng WK, Ng TT, Loh TP. Machine learning assistive rapid, label-free molecular phenotyping of blood with two-dimensional NMR correlational spectroscopy. Commun Biol. 2020;3(1):1–10.

129. Peng WK, Chen L, Boehm BO, Han J, Loh TP. Molecular phenotyping of oxidative stress in diabetes mellitus with point-of-care NMR system. NPJ Aging Mech Dis. 2020;6(1):1–12.

130. Veiga MI, Peng WK. Rapid phenotyping towards personalized malaria medicine. Malar J. 2020;19(1):1–5.

131. Sienkiewicz A, Krzystek J, Vileno B, Chatain G, Kosar AJ, Bohle DS, et al. Multi-frequency high-field EPR study of iron centers in malarial pigments. J Am Chem Soc. 2006;128(14):4534–5.

132. Combrinck JM, Fong KY, Gibhard L, Smith PJ, Wright DW, Egan TJ. Optimization of a multi-well colorimetric assay to determine haem species in Plasmodium falciparum in the presence of anti-malarials. Malar J. 2015;14(1):1–14.

133. Silva M, Calçada C, Teixeira M, Veiga MI, Ferreira PE. Multigenic architecture of piperaquine resistance trait in Plasmodium falciparum. Lancet Infect Dis. 2020;20(1):26–7.

134. Spielmann T, Birnbaum J, Flemming S, Reichard N, Soares AB, Mesén-Ramírez P, et al. Selection linked integration (SLI) for endogenous gene tagging and knock sideways in Plasmodium falciparum parasites. 2017;

135. van der Velden M, Rijpma SR, Russel FGM, Sauerwein RW, Koenderink JB. PfMDR2 and PfMDR5 are dispensable for Plasmodium falciparum asexual parasite multiplication but change in vitro susceptibility to anti-malarial drugs. Malar J. 2015;14(1):1–7.

136. Monge-Maillo B, López-Vélez R. Migration and malaria in Europe. Mediterr J Hematol Infect Dis. 2012;4(1).

137. Pulvirenti J, Musso M, Fasciana T, Cascio A, Tricoli MR, Oliveri N, et al. Transfusion-Transmitted Malaria of Plasmodium malariae in Palermo, Sicily. In: Healthcare. MDPI; 2021. p. 1558.

138. Verra F, Angheben A, Martello E, Giorli G, Perandin F, Bisoffi Z. A systematic review of transfusion-transmitted malaria in non-endemic areas. Malar J. 2018;17(1):1–14.

139. Rodriguez M, Tome S, Vizcaino L, Fernandez-Castroagudin J, Otero-Anton E, Molina E, et al. Malaria infection through multiorgan donation: an update from Spain. Liver Transplantation. 2007;13(9):1302–4.

140. Rosso F, Agudelo Rojas OL, Suarez Gil CC, Lopez Vargas JA, Gómez-Mesa JE, Carrillo Gomez DC, et al. Transmission of malaria from donors to solid organ transplant recipients: A case report and literature review. Transplant Infectious Disease. 2021;23(4):e13660.

141. Martinelli A, Henriques G, Cravo P, Hunt P. Whole genome re-sequencing identifies a mutation in an ABC transporter (mdr2) in a Plasmodium chabaudi clone with altered susceptibility to antifolate drugs. Int J Parasitol. 2011;41(2):165–71.

142. Dahlström S, Veiga MI, Mårtensson A, Björkman A, Gil JP. Polymorphism in PfMRP1 (Plasmodium falciparum multidrug resistance protein 1) amino acid 1466 associated with resistance to sulfadoxine-pyrimethamine treatment. Antimicrob Agents Chemother. 2009;53(6):2553–6.

143. Yayon A, Waa JA vande, Yayon M, Geary TG, Jensen JB. Stage-Dependent Effects of Chloroquine on Plasmodium falciparum In Vitro 1. J Protozool. 1983;30(4):642–7.